Diplomarbeit

Cross Section Database for Neutral Sodium Beam Plasma Edge Diagnostics

Ausgeführt am Insitut für Allgemeine Physik

der Technischen Universität Wien

unter der Anleitung von:

Ao.Univ.Prof. Dr. Friedrich Aumayr

Mag. Dorian Bridi

durch

Katharina Igenbergs

Hermanngasse 11/7

A-1070 Wien

9. Mai 2007

εξ ων δε η γενεσις εστι τους ουσι,
και την φθοραν εις ταυτα γνεσθαι
κατα το κρεων διδοναι γαρ αυτα δικην
και τισιν αλληλοις της αδικιας
κατα την του χρονου ταξιν

Anfang und Ursprung
der seienden Dinge
ist das Apeiron
(das grenzenlos Unbestimmbare).
Darin finde auch ihr Untergang statt,
gemäß ihrer Schuldigkeit.
Denn sie zahlen einander gerechte Strafe
und Buße für ihre Ungerechtigkeit
nach der Zeit Anordnung.

Anaximander
⋆ 610 BC, † 546 BC

Abstract

In recent years, the developments in fusion plasma physics have been very promising and gradually paving the way for a nuclear fusion power plant. The detailed knowledge of the plasma edge region is critical for further engineering and scientific developments. In this plasma edge region, the electron density can be measured very precisely by injecting a beam of neutral atoms into the plasma, detecting the intensities of certain emission lines spectroscopically, and recursively calculating the plasma density profile. In the past, there have been promising experiments to test the feasibility of active neutral beam diagnostics. The use of diagnostic Li and He beams has been studied extensively. Developing this technique further, this diploma thesis now focuses on the use of neutral sodium atoms in active neutral beam diagnostics.

An extensive cross section database has been constructed. The collision processes of interest that were included in the database are electron-impact target excitation, electron-impact target ionization, proton-impact target excitation, and proton-impact target electron loss.

A major part of this thesis is dedicated to the critical assessment of the used publications and the therein used theoretical and experimental methods. A special focus is put on the convergent close-coupling method for electron-impact cross sections and the atomic-orbital close-coupling method for proton-impact cross sections. The former was used by I. Bray to calculate cross sections for all electron-impact transitions of interest especially for this database, the latter was used by J. Schweinzer for exactly the same reasons but for hydrogen ions as projectiles.

Nonetheless, the introduced database is not only a simple collection of published experimental and theoretical data, but it also consists of elaborate fits of the cross section data. A previously used set of fit formulae has been modified and adapted. These formulae and the use of the Levenberg-Marquardt-method for non-linear fits implemented in the open source plotting software `gnuplot 4.0` produced excellent fits for all processes in question.

The derived fit formulae and the resulting fit parameters are meant to be implemented in the simulation software package `Na_simula`. This code has been working so far with a very rudimentary database that basically uses lithium cross sections and if needed sodium threshold energies.

Finally, certain well established scaling relations are presented that will be used to implement collisions of sodium atoms with impurity ions in the simulation code.

Kurzfassung

In den letzten Jahren gab es in der Kernfusionsforschung große, vielversprechende Fortschritte, die den Weg für einen Kernfusionsreaktor weiter bereiten. Die genaue Kenntnis der Plasmarandschicht ist unabdingbar für weitere erfolgreiche Forschung und Entwicklung. Zum Messen der Elektronendichte in dieser Schicht kann unter anderem die "aktive Neutralteilchenstrahl Methode" verwendet werden. Hierbei wird ein Strahl aus neutralen Atomen in das Plasma eingeschossen, die Intensität bestimmter Emissionslinien spektroskopisch bestimmt und schliesslich die Elektronendichte rekursiv berechnet. In der Vergangenheit wurden vielversprechende Experimente und Simulationen auf diesem Gebiet gemacht und damit die experimentelle Durchführbarkeit der Methode sehr zufriedenstellend nachgewiesen. Sowohl neutrale Lithium- als auch Heliumstrahlen wurden ausführlich untersucht. Diese Diplomarbeit beschäftigt sich nun mit einer weiteren Entwicklung dieser Messmethode: die Verwendung von neutralen Natriumatomen als Strahlatome.

Es wurde eine umfassende Datenbank mit Wirkungsquerschnitten erstellt. Die interessanten und berücksichtigten Prozesse sind Elektron-induzierte Anregung und Ionisation sowie Proton-induzierte Anregung und der Proton-induzierte Verlust eines Elektrons.

Ein grosser Teil dieser Diplomarbeit ist der kritschen Aufarbeitung der verwendeten Publikationen gewidment, vor allem im Hinblick auf die darin angewandten experimentellen und theoretischen Methoden. Besonders ausführlich werden die *convergent close-coupling* Methode und die *atomic-orbital close-coupling* Methode beschrieben. Erstere wurde von I. Bray zur Berechnung für Elektronen-Wirkungsquerschnitte für alle interessanten Übergange verwendet, letztere von J. Schweinzer aus eben diesem Grund aber für Protonen-Wirkungsquerschnitte. Beide Berechnungen wurde speziell für diese Datenbank gemacht.

Die vorgestellte Datenbank ist aber nicht nur eine einfache Sammlung von veröffentlichten Daten experimenteller oder theoretischer Natur. Sie beinhaltet auch ausgefeilte Fits der Wirkungsquerschnitte. Es wurde einige schon früher verwendete Regressionsformeln angepasst und verwendet. Mit Hilfe dieser Formel entstanden durch die Levenberg-Marquardt-Methode, die in die Open Source Software `gnuplot 4.0` implementiert ist, hervorragende Fits für alle in Frage kommenden Übergänge.

Die entwicklten Fit Formeln und die daraus resultierenden Fit Parameter sind dafür gedacht in das Simulationssoftware-Paket `Na_simula` eingebaut zu werden. Bis dato arbeitete dieser Code mit einer sehr rudimentären Datenbank, die faktisch Lithium-Wirkungsquerschnitte verwendete und nur wenn notwendig die entsprechenden Natrium Schwellenergien benützt.

Abschliessend werden einige gut etablierte Skalierungsvorschriften angegeben. Diese werden dazu verwendet Stösse mit Verunreinigungsionen in den Simulationscode mit einzubauen.

Contents

Chapter 1

Introduction

To meet the demand for energy is one of the greatest challenges for humankind in the beginning of the third millennium. The fast growing consumption of energy, be it electrical energy or any other type, opposes the limited energy repositories on our planet. Without the development of economical and sustainable energy sources humankind will face a complete disaster, exploiting its resources and ruining its environment. Judging from today's developments, sustainable energy sources such as water, wind, solar, biomass, or geothermal power will not be able to cover the energy needs any time in the near future. Also their negative impacts on the environment cannot be neglected. In the course of the last fifty years, scientists all around the globe have investigated the feasibility of nuclear fusion , the energy source of our sun, not only as a sustainable energy source but also with the power to produce enough affordable energy for all of humankind. If two nuclei fuse, a substantial amount of energy is released, way more than e.g. in nuclear fission, see Fig.1.1.

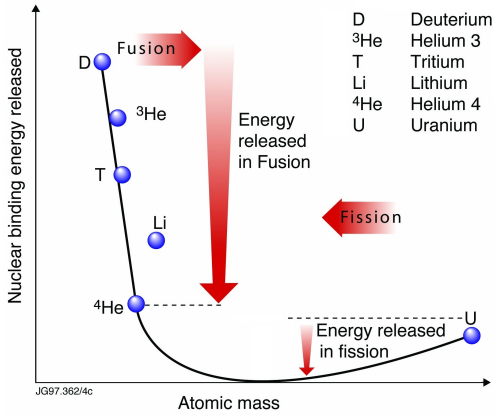

Figure 1.1: Released nuclear energy in nuclear fission and nuclear fusion [1]

Several concepts for nuclear fusion in a laboratory environment have been put forth. Among these, the concept of thermonuclear fusion has been proved to be the most promising. A deuterium or deuterium-tritium gas is heated until a plasma is formed. The gas atoms are ionized and collide inside the hot plasma. If the collision energy of two ions is high enough, the coulomb repulsion is overcome and the strong nuclear force unites the two nuclei, see Fig.1.2.

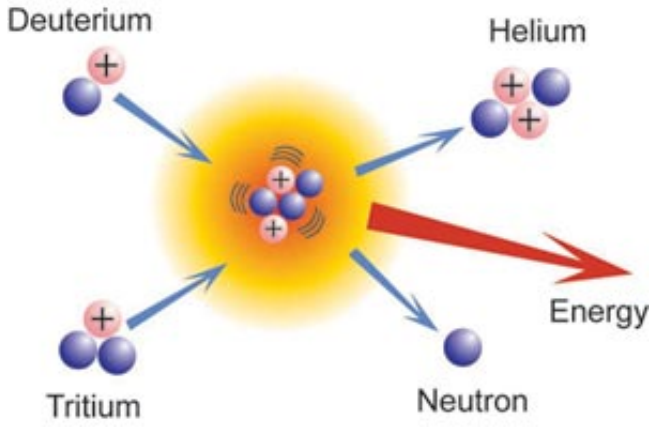

Figure 1.2: Nuclear fusion reaction of deuterium and tritium producing a fast helium nucleus (α particle) and a neutron [1]

For the feasibility of thermonuclear fusion, it is essential that the plasma particles are kept in a well defined volume. For this purpose, toroidal plasma chambers are used that are evacuated to ultra high vacuum. In these vessels, the particles are confined with the help of strong magnetic fields since they influence the paths of electrically charged particles. At the moment, the continued development of two concepts is pursued, the tokamak and the stellerator, see Fig.1.3 and Fig.1.4. The tokamak produces the confining magnetic field with toroidal and poloidal magnetic field coils, the stellerator uses individually formed field coils that keep the particles on track. Already in very early development stages the tokamak configuration produced very promising results. Thus, this experimental setup is further developed than the stellerator.

So far, the conditions in the plasma core have been studied and understood to an extensive and satisfying degree. What remains critical to the feasibility of nuclear fusion with a tokamak is its behavior in the plasma edge region and the plasma-wall interactions. A number of diagnostic methods have been developed for a better understanding of the particle transport, the particle density, and the particle temperature in the plasma edge region. A possible way to measure the electron density in the edge of a fusion plasma is injecting a beam of neutral atoms into the plasma. Since impurities of high atomic numbers Z are under no circumstances desirable in the central regions of a fusion plasma, only light elements such as lithium, helium, or sodium should be used for neutral beam diagnostics.

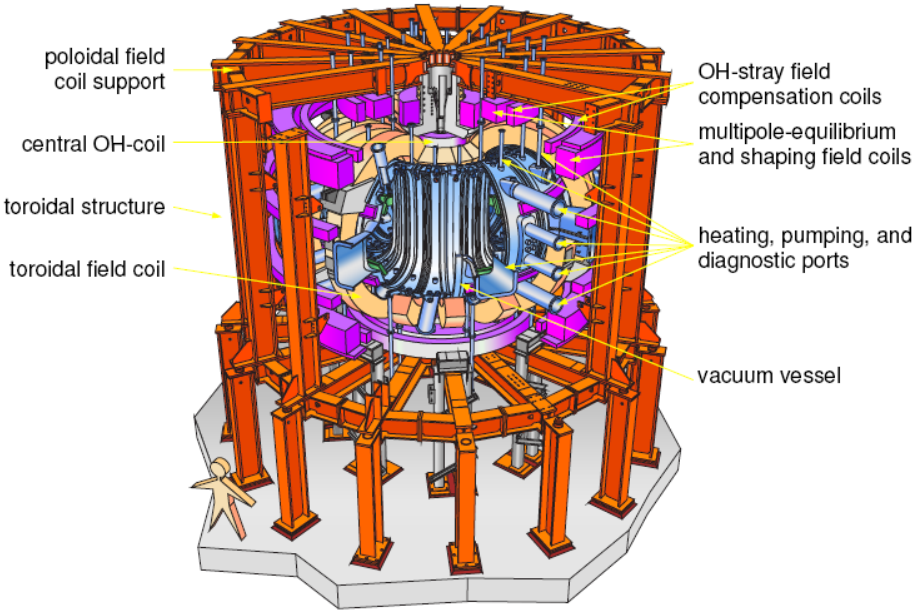

Figure 1.3: The configuration of the ASDEX-Upgrade tokamak at the IPP, Garching [2]

Figure 1.4: The configuration of the W7-X stellerator at the IPP, Greifswald [3]

Interaction of neutral beam atoms with plasma particles leads among other processes to electron loss and excitation of the beam atoms. The excited atoms are eventually de-excited by emitting photons. The resulting line spectrum can be detected and analyzed by spectrometers with regard to the emitted intensities and wavelengths. The electron loss leads to beam attenuation and has to be modeled in order to be able to retrieve information on the electron density from the line emission signals.

In this spirit there have been large efforts at the Institut für Allgemeine Physik (IAP) in Vienna and the Institut für Plasmaphysik (IPP) in Garching to establish neutral beam diagnostics with both a lithium beam [2]–[12] and a helium beam [13]–[18].

This diploma thesis now deals with the theoretical basis for the use of fast neutral sodium beams as a new tool for plasma edge diagnostics. Sodium is an alkali metal. Thus, it has an electronic structure rather similar to hydrogen with a single electron in the M shell. The energy levels of Na are shown schematically in Fig.1.5. The database will include cross sections for transitions including levels up to the 5s excited state with the excited 4f state being the energetically highest level. All states are shown in Tab.1 ranked according to their ionization energy.

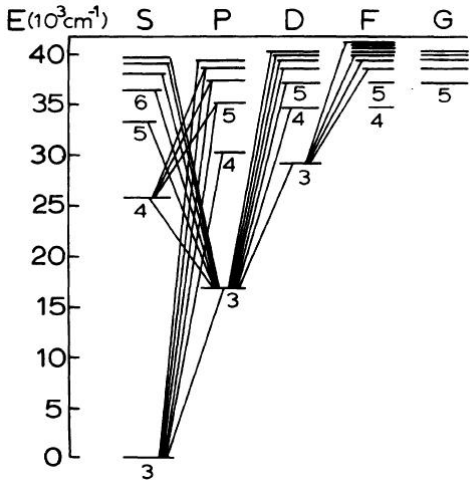

Figure 1.5: Energy levels of sodium, [19]

Sodium beam plasma diagnostics offers several advantages to the case of lithium beams (see Fig.1.6), such as

1. A higher neutralization efficiency of Na ions in Na vapor than for Li ions.

2. An increased quantum efficiency signal of photomultipliers at 590 nm (NaI) as compared to 670 nm (LiI). This further improves the photon signal-to-noise ratio.

3. The shorter lifetime of excited sodium states should lead to a smaller "decay-time distortion" of

Sodium state	Ionization energy $[eV]$
3s	5.13891
3p	3.03954
4s	1.94699
3p	1.52249
4p	1.38643
5s	1.0218
4d	0.854444
4f	0.850363

Table 1.1: Sodium states included in the database ranked according to their ionization energy

the NaI emission profiles, which will make the reconstruction of the density profiles easier.

4. The charge exchange spectroscopy diagnostics of impurity density and temperatures should benefit from increased capture cross sections from Na into excited impurity ion states.

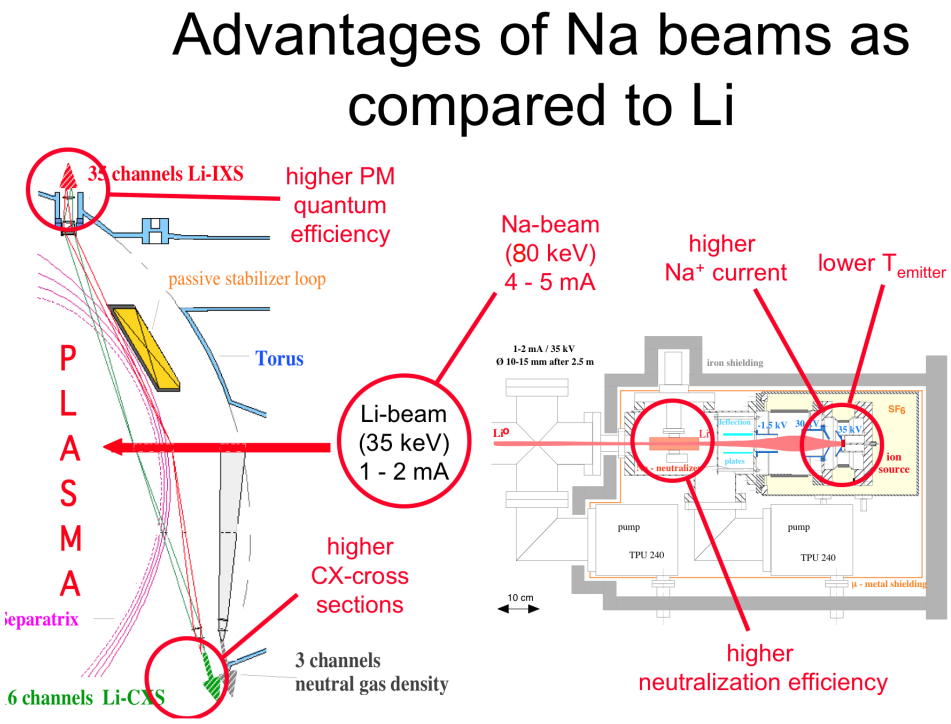

Figure 1.6: Advantages of the new Na-beam with respect to the present Li-beam diagnostics shown for an implementation in the present setup at AUG.

Considerable efforts have been made at IAP and IPP not only to experimentally establish this method, but also to make proper simulations of the interaction of a Na beam with a fusion plasma. D. Bridi (IAP) and E. Wolfrum (IPP) configured the LIA and LIC spectrometers, originally used for lithium, to wavelength around 590 - 595 nm so that both thermal and Doppler-shifted NaI peaks could

be detected. Furthermore, the Hungarian KFKI-Research Institute for Particle and Nuclear Physics has already developed a special emitter dedicated for Na-beam diagnostics. First tests of this emitter show that at the same beam energy a comparable ion beam intensity compared to Li is possible with this kind of Na-emitter. Moreover, this sodium emitter operates at a lower temperature than the lithium emitter simplifying the handling.

The simulations require among others cross section formulae for electron-impact excitation and ionization and proton-impact excitation and target electron loss. For the simulations the code `Na_simula` was developed and used. It is based on the code `simula` that simulates lithium beam intensities [4]. The code requires analytical cross section formulae with corresponding parameters. It then calculates the values of the required cross sections only in the region of interest. It thus provides a much faster computation than if a complete cross section database has to be evaluated for each cross section. Before rewriting the simulation code to fully comply with the needs of sodium, preliminary simulations were carried out using `simula` which had been slightly adapted for the use with sodium. Despite the unfavorable conditions a strong resemblance of the lithium and sodium results could be observed, see Fig.1.7. Surprisingly, it was also found that plasma penetration of the 40 keV Na-atom beam is almost as efficient as 40 keV Li beam penetration, despite the lower ionization potential of Na atoms. The purpose of this work was to improve the analytical formulae used for sodium and the respective parameters and thus achieve better simulation results.

Chapter 2 is devoted to the cross section database. To improve the database, an extensive literature research has been carried out, see section 2.1. The used data were collected in text files, plotted, and fitted. The fit formulae are described in sections 4.1 to 4.4 and the resulting fit parameters are listed in section 5.2. `gnuplot 4.0`, [21] was used for fitting which uses the Levenberg-Marquardt-Method for non-linear fits described in section 4.5. The data were weighted according to their credibility. The data of I. Bray and J. Schweinzer, that were computed especially for this work, see section 2.2 and 2.3,were considered to deserve the highest credibility. Chaper 4 is devided into sections 4.1–4.4 dealing with the fit formulae, followed by section 4.5 describing the Levenberg-Marquardt-algorithm and section 4.6 describing a set of C++ programs developed in the course of this diploma work to simplify certain tasks.

In springtime 2007, this database will be implemented into the simulation code package `Na_simula` by Dorian Bridi. It is strongly expected that the improved database will enhance the quality of the simulations. These simulations will be compared with experimental data collected at ASDEX-Upgrade at the IPP Garching during the springtime research campaign 2007 by Dorian Bridi, Elisabeth Wolfrum and others.

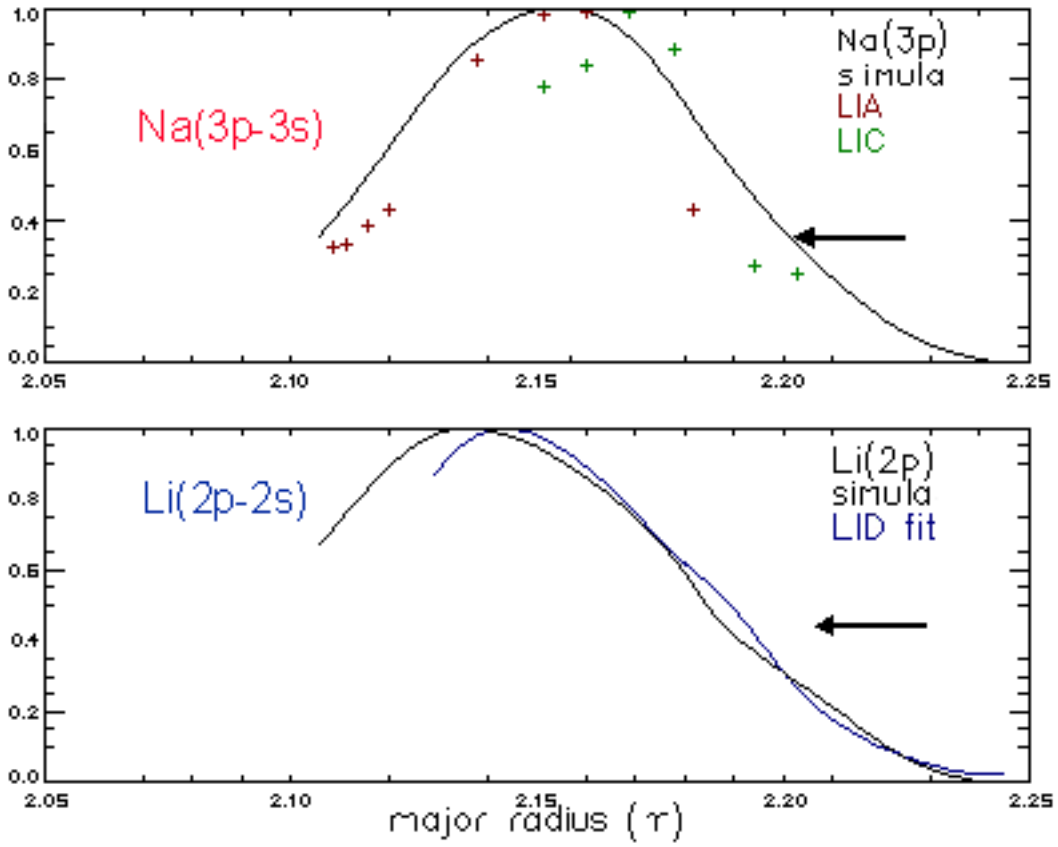

Figure 1.7: top: Normalized Na I emission intensity as experimentally detected at AUG by the spectrometers LIA and LIC against the simulation profile calculated by `simula`.
bottom: corresponding Li I emission profile [20]

Chapter 2

Data Acquisition, Theoretical and Experimental Methods

The scattering of particles by central fields is one of the basic processes in atomic physics and quantum mechanics. In a typical scattering experiment, in atomic and subatomic dimensions, a stream of usually charged particles emerges from a source in multiple direction. After being collimated, the beam is directed onto a thin foil or gas target. The beam particles are scattered in different directions by the target particles. It is now useful to define the *impact parameter* b as the shortest distance at which the projectile could pass the target particle, also called scattering center, if there was no interaction between the projectile and the target. The geometry of such a transition is shown in Fig.2.1. [22] [23]

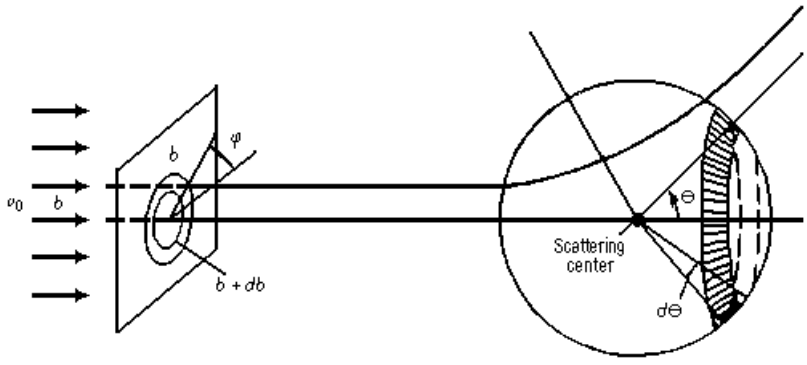

Figure 2.1: Scattering of incident particles by a force field [22]

In the experiment, the fraction of incident particles scattered through various solid angles Ω is observed. It is customary to express the results in terms of a *cross section* σ defined as follows

$$n \cdot d\sigma = \frac{dN}{N} \tag{2.1}$$

where N is the incident number of particles, n is the number of scattering centers in the foil per unit area, and dN is the number of particles scattered through a solid angle between Ω and $\Omega + d\Omega$. In this case, $d\sigma$ is called *differential cross section*. Integrating over all solid angles gives the *total cross section* σ. [22] [23]

$$\sigma = \int_0^{2\pi} \int_0^{\pi} \sigma(\theta, \varphi) \sin\theta d\theta d\varphi \tag{2.2}$$

In this thesis, only total cross sections are of interest.

In the following chapters, the target is always a sodium atom in its various states and the projectiles are always either electrons or protons. The scattering of electrons and protons by sodium vapors has been subject of numerous experimental and theoretical investigations. The simple electronic structure of the sodium atom, with its weakly bound 3s electron outside a neon-like core, makes sodium particularly amenable to theoretical investigations. Assuming the core to be inert, the cross sections are expected to resemble those of hydrogen. However, this is not the case, as the sodium 3p excited state is only 2.1 eV above the 3s ground state, giving sodium an enormous dipole polarisability. Consequently, the strong coupling between the 3s and 3p levels has large effect on the characteristics of both elastic and inelastic scattering. While experiments on sodium are naturally not as simple as those performed on the inert gases, the low temperatures required to make a dimer-free sodium beam makes experiments with sodium comparatively easy. [24]

2.1 Data Acquisition

A comprehensive data evaluation is only granted if a reasonable amount of data is available for comparison. Therefore, the importance of the actual search for usable, reliable data cannot be emphasized enough. In this diploma work, a substantial amount of time was devoted to this matter. There are several methods that help and simplify the research. I want to comment shortly on these methods.

Once, a potentially useful paper has been found, it references several other papers. Mostly there are more useful papers among these references. This is called the *avalanche method*, because the number of papers multiplies quickly. Of course there is a natural limit to the number of papers that can be found in this way.

Sometimes the web pages of the journals, e.g. Physical Reviews of the American Physical Society, offer the possibility to list all papers that cited a certain paper. This option is exceptionally useful when you found a quite old publication that could possibly have been cited by many others because it is considered to be one of the first basic publications on this topic.

Several database listing publications from different journals are available on the internet. Especially useful is the Atomic and Molecular Bibliographical Database (AMBDAS) [25] of the International Atomic Energy Agency (IAEA). It not only offers the possibility to define the collision parameters precisely in terms of the elements and the charge state but also the collision type, such as e.g. photo excitation, can be selected.

Another useful search engine is google's scholar search engine, [26]. It searches through the meta texts of journals available on the internet. It therefore reaches a great amount of journals. This is especially useful when looking for rare papers that are either published before the introduction of digitized journals or are published in a less known journal. Sometimes even translations of the titles and journals of non-english publications, especially russian, can be found using scholar.google.com.

2.2 Convergent Close-Coupling & Pseudostate Method for Electron-Impact Cross Sections

Developed by I. Bray, A.T. Stelbovics, and their co-workers, [27] [28] the theory of convergent close-coupling is among the most elaborate techniques for the computation of electron impact cross sections like excitation and ionization. The theory is based on the partial wave theory for electron - hydrogen atom collisions by I.C. Percival and M.J. Seaton [29]. The results agree excellently with reliable experimental data. Furthermore they give reasonable results in energy ranges where there are no experimental data available for comparison. The close-coupling equations provide a complete description of the scattering process without applying an approximation, but only if the correct boundary conditions are applied to the channels with three free particles in the asymptotic region.

Starting from the full, time-dependent Schrödinger equation, the target states are expanded in an orthogonal L^2 Laguerre basis. Then, the close-coupling equations, a set of coupled first-order differential equations of the expansion coefficients, are derived via various transformations of the Schrödinger equation. The channels are coupled via the applied potential. Convergence is established by simply increasing the basis size.

In a system, where an electron scatters with a hydrogen-like atom, the Hamiltonian can be written as [27]

$$H = K_1 + V_1 + K_2 + V_2 + V_3 \tag{2.3}$$

with
- K_1 projectile-electron kinetic energy operator
- K_2 target-electron kinetic energy operator
- V_1 projectile electron - proton potential
- V_2 target electron - proton potential
- V_3 projectile electron - target electron potential

To solve the full Schrödinger equation

$$(E - H)|\Psi^S\rangle = 0 \tag{2.4}$$

the wavefunction is expanded over a complete set of both discrete and continuous target states $\Phi_i(\mathbf{r})$ under the consideration of the wavefunction's symmetry. This sum over the discrete and integral over the continuous target states is often referred to as **pseudostate method**. [27]

$$\Psi^S(\vec{r_1}, \vec{r_2}) = \sum_i \int \Phi_i(\vec{r_2}) f_i^S(\vec{r_1}) = (-1)^S \sum_i \int \Phi_i(\vec{r_1}) f_i^S(\vec{r_2}) \tag{2.5}$$

The target states $\Phi_i(\mathbf{r_i})$ are exact eigenstates of the target Hamiltonian in terms of the target electron Schrödinger equation

$$(K_2 + V_2)|\Phi_i\rangle = \varepsilon_i|\Phi_i\rangle. \tag{2.6}$$

The functions $f_i^S(\mathbf{r})$ must satisfy the symmetry condition

$$\langle\Phi_j|f_k^S\rangle = (-1)^S\langle\Phi_k|f_j^S\rangle. \tag{2.7}$$

The necessary condition that the functions $f_i^S(\vec{r})$ are unique can be achieved. Now, the close-coupling equations can be derived. To avoid summation over channel indices, projections over the complete set of target states are used and labeled in an obvious way. Two identity operators I_1 and I_2 are defined [27]

$$I_1 = \sum_i \int |\Phi_i\rangle\langle\Phi_i|, \qquad I_2 = \sum_i \int |\Phi_i\rangle\langle\Phi_i| \tag{2.8}$$

Now the multichannel expansion (2.5) can be rewritten as

$$|\Psi^S\rangle = I_2|\Psi^S\rangle \tag{2.9}$$

and hence

$$P_r|\Psi^S\rangle = I_1P_rI_2|\Psi^S\rangle \tag{2.10}$$

where P_r is a projection operator. Writing $I_2|\Psi^S\rangle$ instead of $|\Psi^S\rangle$ explicitly indicates that the multichannel expansion for the complete wave function is used. Using the transformed form of the symmetry condition (2.7) [27]

$$I_2|\Psi^S\rangle = (-1)^SI_1P_rI_2|\Psi^S\rangle \tag{2.11}$$

the full Schrödinger equation (2.4) transforms into

$$0 = (E - H)I_2|\Psi^S\rangle = (E - H)\frac{1}{2}\left[1 + (-1)^SP_r\right] \;\; I_2|Psi^S\rangle \tag{2.12}$$

The introduced operator $\frac{1}{2}\cdot\left[1 + (-1)^SP_r\right]$ commutes with the Hamiltonian and it symmetrizes $|\Psi^S\rangle$ numerically. If $|\Psi^S\rangle$ already had the required symmetry this operator would be redundant [27]. Using I_2 as a projection operator leads to

$$I_2(E - K_1 - K_2 - V_2)I_2|\Psi^S\rangle = I_2V^SI_2|\Psi^S\rangle \tag{2.13}$$

where $V^S = V_1 + V_3 + (-1)^S(H - E)P_r$. Employing an arbitrary constant C that incorporates condition (2.11) for $C \neq 0$ the potential V^S transforms into

$$V^S(C) = V_1 + V_3 - ECI_1 + (-1)^S \left[H - E(1 - C)\right] P_r \tag{2.14}$$

Rather than solving explicitly for the functions $f_i^S(\vec{r})$ the Lippmann-Schwinger equation for the T matrix is formed. [27]

$$T^S = \langle \vec{k}\phi | I_2 V^S(C) I_2 | \Psi^{S(+)} \rangle \tag{2.15}$$

where $|\vec{k}\phi\rangle$ are the asymptotic states satisfying

$$I_2(E - K_1 - K_2 - V_2) I_2 |\vec{k}\phi\rangle = 0 \tag{2.16}$$

and where the notation (+) indicates that the boundary conditions of the outgoing spherical wave are applied [27]. Combining all the information and forming the T matrix for the transition of the target in the initial state ϕ_{i0} to the final state ϕ_i on impact of projectile $\vec{k_0}$, the Lippmann-Schwinger equation can be written in the following way

$$\langle \vec{k}\phi_i | T^S | \phi_{i0}\vec{k_0} \rangle = \langle \vec{k}\phi_i | V^S(C) | \phi_{i0}\vec{k_0} \rangle + \sum_i \int d^3k' \frac{\rangle \vec{k}\phi_i | V^S(C) | \phi_{i'}\vec{k'} \rangle \langle \vec{k'}\phi_{i'} | T^S | \phi_{i0}\vec{k_0} \rangle}{E - \varepsilon_{i'} - k'^2 + i_0} \tag{2.17}$$

where any nonzero C implements the symmetry condition (2.11) and leads to a unique answer independent of C. So even though the V-matrix elements have an arbitrary constant the solution of the integral equation is independent of this constant. [28] [27]

2.3 Atomic-Orbital Close-Coupling Calculations of Proton-Impact Cross Sections

The atomic-orbital close-coupling method was used by J. Schweinzer for calculations of proton-impact cross sections. It can be considered the most reliable source of cross section data for all the considered processes: proton-impact target excitation, target ionization, and single electron charge transfer. In the following section, I shall give a short summary of the close-coupling method using atomic orbital basis states. A complete description is given in [30] and [31].

The close-coupling equations provide a semi-classical description of the scattering process. The equation of motion of the active electron in the effective potential of the projectile core $V_p(\vec{r_p})$ and the target core $V_t(\vec{r_t})$ can be written as time-dependent Schrödinger equation

$$i\frac{\partial}{\partial t}\Psi(\vec{r},t) = H_e(t)\Psi(\vec{r},t) \tag{2.18}$$

$$H_e(t) = -\frac{1}{2}\nabla_r^2 + V_p(\vec{r_p}(\vec{r},t)) + V_t(\vec{r_t}(\vec{r},t)) \tag{2.19}$$

where the time derivative has to be calculated in an inertial system. The vector $\vec{r}$ refers to the chosen inertial system whereas the vectors $\vec{r_p}$ and $\vec{r_t}$ refer to the system of the projectile or respectively the target. The potentials have to describe the interaction of the active electron with the nucleus and as well, if existing, with the projectile core. Especially at small distances this results in a deviation from the form of the Coulomb potential.

To solve the Schrödinger equation (2.18), a set of basis states $\chi_k(\vec{r},t)$ is to be defined. These states do not necessarily need to be orthonormal. Thus, the complete wave function $\Psi(\vec{r},t)$ can be expanded according to

$$\Psi(\vec{r},t) = \sum_k a_k(t)\chi_k(\vec{r},t) \tag{2.20}$$

Choosing atomic eigenstates $\chi_k(\vec{r},t)$, the time-dependent electronic wave function decomposes into a set of atomic orbitals. The time-dependence now consists only of a phase factor

$$\chi_k(\vec{r},t) = \varphi_k(\vec{r})\exp(-i\int^t E_k dt') \tag{2.21}$$

where E_k is the time-independent energy eigenvalue of the atomic state. With the help of this expansion and within the subspace spanned by the atomic basis states, the Schrödinger equation (2.18) transforms to

$$\left[i\frac{\partial}{\partial t} - H_e\right]\sum_k a_k(t)\varphi_k(\vec{r})e^{-iE_kt} = 0 \tag{2.22}$$

Using the following properties of the atomic basis states φ_k

$$(-\frac{1}{2}\nabla_r^2 + V_p)\varphi_k = E_k\varphi_k \qquad \varphi_k \ldots \text{projectile state} \tag{2.23}$$

$$(-\frac{1}{2}\nabla_r^2 + V_t)\varphi_i = e_i\varphi_i \qquad \varphi_i \ldots \text{target state} \tag{2.24}$$

$$\tag{2.25}$$

the new form of the Schrödinger equation (2.22) can be written as

$$\sum_k \left(E_k a_k(t) + i\frac{d}{dt}a_k(t) - E_k a_k(t) - a_k(t)V\right)\varphi_k(\vec{r})e^{-iE_kt} = 0 \tag{2.26}$$

where V can either be V_p or V_t. Multiplying (2.26) from the left hand side with a basis state χ_i gives

$$\sum_k \left(\langle\varphi_i|\varphi_k\rangle i\frac{da_k(t)}{dt} - \langle\varphi_i|V|\varphi_k\rangle a_k(t)\right)e^{-i(E_k-E_i)t} = 0 \tag{2.27}$$

An "overlap"-matrix S_{ik} and a potential matrix M_{ik} can be defined by

$$S_{ik} = \langle\chi_i|\chi_k\rangle \quad \text{and} \quad M_{ik} = \langle\chi_i|V|\chi_k\rangle \tag{2.28}$$

The overlap matrix **S** consists of two submatrices, the $n\times n$ and $m\times m$ one-center overlap matrices of respectively the target or the projectile states. The term "one-center" implies that only states defined on the same center of impact are used in the calculation of the respective matrix element. Taking this into account, (2.27) can be written in a concise manner as

$$i\ \mathbf{S}\ \frac{d}{dt}\mathbf{a} = \mathbf{M}\ \mathbf{a} \tag{2.29}$$

Thus, a coupled, linear set of first-order differential equations is obtained for the expansion coefficients $a_k(t)$. These equations are called the *coupled-channel equations*. The coupling of the different atomic states is a result of the effective potentials of the projectile and the target. The atomic basis states are in principle atomic wavefunctions acquired by various methods.

$$\varphi(\vec{r}) = R_{nl}(r)Y_{lm}(\Omega) \tag{2.30}$$

Since the spherical harmonics $Y_{lm}(\Omega)$ are known, the problem reduces to the determination of the radial parts $R_{nl}(r)$. Hydrogen-like wavefunctions can also describe highly excited states of the active

electron in projectile with core electrons. The electron configuration of the outermost shell of alkali atoms can be reduced to one-electron systems by the selection of the correct pseudopotentials.

The influence of the core electrons on the wavefunctions is twofold. The core electrons shield the field of the nucleus on the one hand and on the other hand, due to Pauli's exclusion principle, is the wavefunction of the valence electron forced to be orthogonal to the core orbitals.

A different method used for obtaining the correct wavefunctions is the Hartree-Fock method. This method is based upon the central field approximation of the Hamiltonian and the variation principle. [30] [31]

The system of coupled first-order differential equations is solved under the consideration of the following initial conditions

$$|a_i(t \to -\infty)|^2 = 1 \qquad \text{for the initial state} \tag{2.31}$$

$$|a_k(t \to -\infty|^2 = 0 \qquad \forall k \neq i \tag{2.32}$$

The partial cross section for a transition $i \to k$ can be defined as follows

$$\sigma_{ik} = 2\pi \int |a_k(t \to \infty)|^2 b db \tag{2.33}$$

Resulting in the following definition of the total cross section

$$\sigma_{tot} = 2\pi \int (1 - |a_i(t \to \infty)|^2) b db = \sum_k \sigma_{ik} \tag{2.34}$$

The close-coupling method can be divided in three steps: first the selection and calculation of the basis states, followed by the determination of the matrix elements, and in the end the time-integration of the coupled-channel equations. [30]

2.4 Additional Theoretical Methods Used in the Selected Publications to Calculate Data

The simple electronic structure of the sodium atom, with its weakly bound 3s electron outside a neon-like core, makes sodium particularly amenable to theoretical investigations. Thus a great number of papers were dedicated to this topic using many different theoretical approaches. At lower velocities $v_p \leq v_e$ where v_e is the orbital velocity of the target electron, molecular treatments of the problem are more suitable whereas at high velocities $v_p \gg v_e$, theoretical methods such as Plane Wave Born Approximation (PWBA) are better capable of reproducing the experimentally observed results. [24] [32]

2.4.1 Molecular-Orbital Calculations

In the treatment of slow ion-atom collisions, it is reasonable to assume the formation of a quasi-molecule with a very short lifetime during the collision process. The kinetic energy of the relative movement can be treated as a perturbation of the system. This led to the theory of *perturbed stationary states (PSS)* by Massey & Smith (1933) [33]. Thus, this method is used to calculate proton-impact cross sections. Starting from

$$H_e \Phi_k(\vec{r}, R) = \varepsilon_k(R) \Phi_k(\vec{r}, R) \tag{2.35}$$

where R is the internuclear distance which is time-dependent. Thus the $\Phi_k(\vec{r}, R)$ are also time-dependent. Expanding the wavefunction in terms of the eigenstates of the quasi-molecule

$$\Psi(\vec{r}, t) = \sum_k a_k(t) \Phi_k(\vec{r}, R) \exp\left(-i \int^t \varepsilon_k(r) dt'\right) \tag{2.36}$$

leads to the time-dependent Schrödinger equation

$$\left(i\frac{\partial}{\partial t} - H_e\right) \sum_k a_k(t) \Phi_k \exp\left(-i \int^t \varepsilon_k(r) dt'\right) = 0 \tag{2.37}$$

$$\sum_k \exp\left(-i \int^t \varepsilon_k(R) dt'\right) \left[i\frac{da_k(t)}{dt} + a_k(t)\left\{i\frac{\partial}{\partial t} + \varepsilon_k(R) - \varepsilon_k(R)\right\}\right] \Phi_k(\vec{r}, R) = 0 \tag{2.38}$$

$$\tag{2.39}$$

Multiplying from the left hand side by the basis states and using the orthogonality of the basis states gives

$$\sum_k \left[\frac{da_k(t)}{dt}\delta_{ik} + a_k(t)\langle\Phi_i|\frac{\partial}{\partial t}|\Phi_k\rangle\right] \exp\left(-i \int^t \varepsilon_k(r) - \varepsilon_i(R) dt'\right) = 0 \tag{2.40}$$

This finally leads to a system of coupled first-order differential equations of the complex expansion coefficients $a_i(t)$:

$$\langle\Phi_i|\frac{\partial}{\partial t}|\Phi_i\rangle = \frac{1}{2}\frac{\partial}{\partial t}\langle\Phi_i|\Phi_i\rangle = 0 \tag{2.41}$$

$$\frac{da_i(t)}{dt} = -\sum_{k\neq i} a_k(t)\langle\Phi_i|\frac{\partial}{\partial t}|\Phi_k\rangle \exp\left(-i\int^t(\varepsilon_k-\varepsilon_i)dt'\right) \tag{2.42}$$

$$\tag{2.43}$$

Here, the states are coupled via the operator $\frac{\partial}{\partial t}$. The system of coupled first-order differential equations is solved under the consideration of the following initial conditions

$$|a_i(t\to-\infty)|^2 = 1 \qquad \text{for the initial state} \tag{2.44}$$

$$|a_k(t\to-\infty|^2 = 0 \qquad \forall k\neq i \tag{2.45}$$

The partial cross section for a transition $i\to k$ can be defined as follows

$$\sigma_{ik} = 2\pi\int|a_k(t\to\infty)|^2 bdb \tag{2.46}$$

Resulting in the following definition of the total cross section

$$\sigma_{tot} = 2\pi\int(1-|a_i(t\to\infty)|^2)bdb = \sum_k \sigma_{ik} \tag{2.47}$$

The close-coupling method can be divided in three steps: first the selection and calculation of the basis states, followed by the determination of the matrix elements, and in the end the time-integration of the coupled-channel equations. [30]

2.4.2 Coupled-Sturmian-Pseudostate Approach

The coupled-Sturmian-pseudostate approach is another possibility to calculate proton-impact cross sections. A set of Sturmian basis functions is centered on each nucleus, i.e., on the proton (charge $Z_A = 1$) and the sodium nucleus (charge $Z_B = 11$). The Sturmian function is simply a polynomial multiplied by a fixed exponential $\exp[-\zeta_\alpha r_\alpha/(l_\alpha + 1)]$ for a given angular momentum L_α, where r_α is the distance from the nucleus α (A or B) to the electron, multiplied by a spherical harmonic. The polynomials form a complete set. ζ_α are the two Sturmian charges and they are arbitrary. [34]

Furthermore a potential is needed. The correct asymptotic form of this potential has to be

$$\begin{aligned} r_B \to 0: &\qquad -\tfrac{Z_B}{r_b} \\ r_B \to \infty: &\qquad -\tfrac{1}{r_B} \end{aligned} \tag{2.48}$$

There are two specific types of analytic Hartree-Fock potentials that show promising properties. On the one hand the Green-Sellin-Zachor Potential (GSZ) in eq.2.49 [35] and on the other hand the potential given by Shingal et al. in [36] in eq.2.50.

$$V(r_B) = \frac{-[(Z_B - 1)(Kd\{e^{r_B/d} - 1\} + 1)^{-1} + 1]}{r_B} \tag{2.49}$$

with $K = 2.85$ and $d = 0.584$ for sodium. [35]

$$v(r_B) = -\frac{1}{r_B} - \frac{e^{-3.56 r_B}}{r_B}(10 + 17.1 r_B) \tag{2.50}$$

The one-electron Hamiltonian of sodium $-\frac{1}{2}\nabla^2 + V(r_B)$ is diagonalized in the Sturmian basis centered on the nucleus B, and the one-electron Hamiltonian of the hydrogen atom, $-\frac{1}{2}\nabla^2 + V(r_A)$, is diagonalized in the Sturmian basis centered on the nucleus B. [34]

Differently sized Sturmian basis sets can be applied to the problem. When using the GSZ potential, 73- and 77-term bases are necessary for the higher s, p and d functions to produce negative energies for the $n = 4$ and $n = 5$ states of Na. By varying the value of the Sturmian charge ζ_B arbitrarily, in order to get an energy spectrum as close as possible to the observed experimental values or to the Hartree-Fock limit, the GSZ eigenvalues are obtained. The thus obtained binding energies are normalized to the experimental values to significantly improve the cross section when compared to experimental values. [34]

The two-center direct matrix elements of the analytic Hartree-Fock potentials, (2.49) and (2.50), and the two-center charge exchange matrix elements of both potentials are evaluated numerically in prolate spheroidal coordinated.

The convergence of the final cross sections are tested with respect to the range of $z = v \cdot t$ and the internuclear separation R beyond which charge-exchange matrix elements are neglected. [34]

2.4.3 Classical Overbarrier Model

The classical over-barrier model (COBM) [37] is applicable to proton-impact collisions resulting in charge-transfer from the target to the projectile. A standard scattering experiment between a target nucleus and a projectile nucleus with only one active electron is evaluated. For both the target and the projectile hydrogenlike approximations are considered. All particles are considered to be classical objects. Only electron transfer can be described using this model.

The COBM for electron capture by slow highly charged projectiles has been proven to be fairly successful in predicting the total charge transfer cross section. In this model capture is assumed to take place at a crossing of the diabatic potential curves at large internuclear distances R provided the charge transfer simultaneously becomes classically allowed: that is, the electron can overcome the barrier between the potential wells generated by the ionic charges of the target and the projectile. The success of this simple model stems in part from the fact that the resonant charge transfer populates preferentially states with large quantum numbers n and l, yielding large and essentially "geometric" cross sections for capture into the principal shell n. In the limit of large quantum numbers and with a large number of open reaction channels, the shell cross section (summed over many substates) becomes independent of the quantum dynamics of individual state amplitudes. The COBM is static in the sense that the projectile velocity does not enter as a system parameter. [37]

The transition within this classical picture takes place at an internuclear separation $R \leq R_m$ with

$$R_m = \frac{2\sqrt{q}+1}{I_t} \tag{2.51}$$

where q is the charge of the projectile and I_t the ionization potential of the target atom [30] [31]. Electron transfer is assumed to take place near the crossing of diabatic potential curves, given by

$$I_t - \frac{q}{R} = -\frac{q^2}{2n^2} - \frac{1}{R} \tag{2.52}$$

From this the crossing radius of the over-barrier transition can be derived.

$$R_c \lesssim \frac{(2q^{1/2}+1)}{2|I_t|}\left[1 + \frac{(2(1+q^{1/2})^2 \cdot |I_t| \cdot L^2}{(2q^{1/2}+1)^2 \cdot q}\right] \tag{2.53}$$

where L is the angular momentum in the projectile frame [37]. Now the total electron transfer cross section can be approximated by

$$\sigma_{tot} \approx A \cdot \pi \cdot R_c^2 \tag{2.54}$$

where $A = 0.5$ is a factor of proportionality applicable for projectiles with a low charge q.

2.4.4 Classical Trajectory Monte Carlo Simulations

Classical trajectory Monte Carlo simulations (CTMC) [38] are especially used if the basic model of the interactions cannot or only very insufficiently be described by an analytical or closed algorithm. It is based on the assumption that certain subsystems, such as e.g. incident particles, can be described individually. Each interaction happens with a certain probability and is selected by a random number generator. To achieve reasonable results on the behavior of the whole system a great number of single sequences (histories) each with many interactions and a variety of possibilities have to be evaluated in term of the wanted parameters. CTMC simulations are time-consuming and thus require carefully written algorithms. [38]

The application of the CTMC method in atomic scattering problems is most suitable in the intermediate to high projectile velocity range ($\frac{v_p}{v_e} \sim 0.5 - 4$) to study electron capture and ionization processes in ion-atom collisions. The method is easy to apply for a wide range of incident ions and targets yielding both the electron capture and ionization cross sections simultaneously. [32]

The CTMC procedure is basically a treatment of the three-body problem, i.e. the projectile ion, the active electron and the target core in a three dimensional frame work. Hamilton's equation of motion with an appropriate Hamiltonian is established for all the three partners which are integrated numerically to determine their trajectories. A model interaction potential is used to describe the interaction between the active electron and the target ionic core [32]. For the electron-alkali ionic core interaction, the following model interaction potential is used

$$V(r) = \frac{-[(Z-z)e^{-Ar} + Bre^{-Cr} + z]}{r} \tag{2.55}$$

Where Z is the atomic charge, z is the net charge seen by the electron far from the nucleus and A, B, and C are constants. The core-core and projectile-electron interactions are taken to be as pure Coulomb potential. This model has the correct asymptotic behavior at large and small values of 'r'. [32]

Hamilton's equations of motion are solved numerically with this model interaction potential for several thousand classical trajectories which are finally tested for the occurrence of capture or ionization processes. Respective probabilities and hence the cross sections are calculated. The initial conditions of the projectile are specified by its relative velocity v_p, the impact parameter b, and the position

with respect to the center of the mass of the target core and electron. The position of the target electron with respect to the target core an its momentum distribution is obtained by solving the Kepler's equation. The total cross section for both ionization or charge transfer is determined using the formula [32]

$$\sigma_{ION/CT} = \frac{N_{ION/CT}}{N_T} \cdot \pi b_{max}^2 \tag{2.56}$$

where N_T is the total number of trajectories calculated with impact parameter b lying in the range $0 \leq b \leq b_max$ and $N_{ION/CT}$ is the number of trajectories that satisfy the criteria for the specified reaction (ION: ionization, CT: charge transfer) to take place. [32]

2.4.5 Distorted-Wave-Type Approximation

The distorted wave approximation [39] can be used to calculate electron-impact cross sections. The atomic wavefunctions describing the 3s, 3p, and 3d levels of sodium are obtained by solving the one-electron Schrödinger equation

$$\frac{d^2 P_{nl}}{d^2 r} - \left(V_{mod}(r) - E_{nl} + \frac{l \cdot (l+1)}{r^2} \right) P_{nl}(r) = 0 \tag{2.57}$$

where the model potential $V_{mod}(r)$ is the potential experienced by the optical (nl) electron and E_{nl} is its eigenvalue. This potential includes corrections due to core-polarization effects plus linear terms to simulate nonlocal change effects. The linear parameters are calculated by a least-squares fit to the lowest 20 observed experimental values for the atomic levels. [40] The excitation cross section of incident energy T_i and charge Z_P is then given by

$$\sigma if = 8\pi a_0^2 \frac{M}{m} \frac{R}{T_i} \int_{K_{min}}^{K_{max}} \frac{d(Ka_0)}{(Ka_0)^3} |T_{if}|^2 \cdot |Z_{eff}(k)|^2 \tag{2.58}$$

where $K_{min} = k_i - k_f$ and $K_{max} = k_i + k_f$. [40] For a bare structureless projectile, its effective charge $Z_{eff}(K)$ is constant and equal to Z_P. When the projectile which carries electrons, has nuclear charge Z, and the electrons' role is taken into account explicitly, the $Z_{eff}(K)$ is momentum-transfer dependent involving elastic and inelastic form factors of the projectile. [40] Specifically, when the projectile remains in its ground state after collision, the absolute value of $Z_{eff}(K)$ comes to

$$|Z_{eff}(K)| = |Z - \sum_i \frac{1}{\left[1 + (\frac{Ka_0}{2Z})^2\right]^2} \tag{2.59}$$

where $i = 1, \ldots, n$ runs through the number of electrons present on the projectile. [40] When the projectile leaves the collision area excited or ionized, the excitation cross section formula is increased

by the addition of new terms, which e.g., for the one-electron case and using a closure relation, can be approximated by

$$\Delta\sigma_{if} = 8\pi a_0^2 \frac{M}{m}\frac{R}{T_i} \cdot \int_{\langle K\rangle}^{K_{max}} \frac{d(Ka_0)}{(Ka_0)^3} |T_{if}|^2 \left(1 - \frac{1}{\left[1 + (\frac{Ka_0}{2Z})^2\right]^4}\right) \tag{2.60}$$

where $\langle K\rangle$ is taken equal to the value of K_{min} appropriate to the lowest excited state of the projectile and T_{if} are the transition probabilities between states $|i\rangle$ and $|f\rangle$. [40] They are calculated using the Vainshtein-Presnyakov-Sobel'man approximation, see section 2.4.8, which accounts for the distortion, during the collision, of the projectile's wavefunction. [40]

2.4.6 Plane Wave Born Approximation

The Born approximation is the treatment of perturbed states with perturbation theory. It is one of the oldest and simplest techniques for calculating electron excitation and ionization of atoms and ions [41]. Starting from the Lippmann-Schwinger equation

$$\begin{aligned} \Psi^{\pm}(\vec{k},\vec{r}) &= \Phi(\vec{k},\vec{r}) + \int d^3r' G_0^{\pm}(\vec{k};\vec{r},\vec{r'}) \cdot U(\vec{r'}) \cdot \Psi^{\pm}(\vec{k},\vec{r'}) \\ |\Psi_{\vec{k}}^{\pm}\rangle &= |\vec{k}\rangle + G_0^{\pm} \cdot U \cdot |\Psi_{\vec{k}}^{\pm}\rangle \end{aligned} \tag{2.61}$$

where $\Phi(\vec{k},\vec{r})$ is the solution of the homogeneous Schrödinger equation, $G_0^{\pm}(\vec{k};\vec{r},\vec{r'})$ is the Green function of the Helmholtz equation, $U(\vec{r'}) = \frac{2m}{\hbar^2} \cdot V(\vec{r})$ where $V(\vec{r})$ can be for example an atomic field with $V(\vec{r}) = -\frac{Ze^2}{r} + e^2 \cdot \int \frac{\rho(r')d^3r'}{|\vec{r}-\vec{r'}|}$, and the plus sign is indicating an outbound wave (respectively the minus sign an incident wave). [42]

Rewriting (2.61) leads to

$$|\Psi_{\vec{k}}^{\pm}\rangle = \frac{1}{1 - G_0^{\pm}(k) \cdot U} \cdot |\vec{k}\rangle \tag{2.62}$$

Comparing this form of the Lippmann-Schwinger equation with the geometric progression $\frac{1}{1-x} = \sum_{n=0}^{\infty} x^n$ leads to

$$|\Psi_{\vec{k}}^{\pm}\rangle = \left(\sum_{n=0}^{\infty} \left(G_0^{\pm}(k) \cdot U\right)^n\right) |\vec{k}\rangle \tag{2.63}$$

Inserting this equation in the formula of the exact perturbation amplitude $f(\Theta,\varphi) = -2\pi^2 \cdot \langle\vec{k'}|U|\Psi_{\vec{k}}^{\pm}\rangle$ results in the perturbation amplitude in Born approximation. [42]

$$f(\Theta,\varphi) = -2\pi^2 \cdot \sum_{n=0}^{\infty} \langle\vec{k'}|U \cdot \left(G_0^{\pm}(k) \cdot U\right)^n |\vec{k}\rangle \tag{2.64}$$

Under the assumption that only elastic scattering is taken into account, multiple scattering can be neglected, only a two-body problem is considered, and the spin is ignored, the cross section in Born approximation is calculated via

$$\sigma = \int d\Omega |f(\Theta, \varphi)|^2 \tag{2.65}$$

There is an excellent agreement of PWBA cross sections and more elaborate theories such as convergent close-coupling, see section 2.3, at intermediate and high energies. For these energies, the application of more powerful methods is complicated due to the large number of channels that need to be included. [41]

2.4.7 Variation of the Plain Wave Born Approximation Using the Relaxed-Orbital Hartree-Fock and Sudden Perturbation Methods

The obvious shortcomings of the PWBA in the low energy region close to the threshold gave rise to new methods trying to improve the accuracy. The relaxed-orbital (RO) Hartree-Fock method can be applied within the PWBA for impact electrons close to the ionization threshold. In the case of high energy electrons the sudden perturbation (SP) method can be applied from within PWBA. [41]

The RO approximation [41] represents the situation when the emitted electron is slow. After the interaction of the projectile electron with the whole cloud of atomic electrons, the vacancy in an inner shell arises. Due to the relaxation of spectator electrons, one of them becomes superfluous and has to leave the atom. Therefore, the escaping electron feels the screening field created by the remaining electrons . The radial orbitals of these remaining electrons should be calculated for the ion with a vacancy in an inner shell. The radial orbitals of continuum electrons are obtained by solving the Hartree-Fock equations for the average of configuration of the ion-electron system [41]. The PWBA cross section can be written

$$\sigma(i \to f, \varepsilon_0) = \frac{8\pi a_0^2}{\varepsilon_0} \int_0^{\frac{\varepsilon_0 - 1}{2}} d\varepsilon \int_{q_{min}}^{q_{max}} \frac{dq}{q^3} \sum_{\lambda=0}^{\infty} \sum_{\kappa, L'S'} |\langle f \varepsilon \lambda L'S' || j_\kappa(\vec{qr}) || i \rangle|^2 \tag{2.66}$$

where i is the initial and f the final state, ε is the energy of the escaping electron, ε' is the energy of the projectile before the ionization of an atom, $j_\kappa(\vec{qr}) = j_\kappa(qr) Y_{\kappa,\mu}(\hat{q}) Y_{\kappa,\mu}(\hat{r})$ with $j_\kappa(qr)$ being the spherical Bessel function (the hat on q and r indicates the spherical angles θ and ϕ of $\vec{q}$ and $\vec{r}$, respectively), $L'S'$ are the total orbital and spin angular quantum numbers of the electron-ion system, a_0 stands for the Bohr radius, q denotes the absolute value of the transferred momentum as in

$$\begin{aligned} \vec{q} &= \vec{k_0} - \vec{k_0'} \\ q_{max} &= \sqrt{2\varepsilon_0} + \sqrt{2(\varepsilon_0 - I - \varepsilon)} \\ q_{min} &= \sqrt{2\varepsilon_0} - \sqrt{2(\varepsilon_0 - I - \varepsilon)} \end{aligned} \tag{2.67}$$

where I is the ionization energy of an atom. [41]

In SP approximation, the ionization cross section from the initial state i to the final state f is equal to the product of two terms

$$\sigma(i \to f) = \sigma^{ion}(i \to f')P(f' \to f) \tag{2.68}$$

here $\sigma^{ion}(i \to f')$ is the single ionization cross section to the intermediate state f' of the ion described by the atomic radial orbitals of discrete electrons when all spectator electrons remain in their initial states. The second term is called relaxation (shake) probability

$$P(f' \to f) = |\langle f'|f\rangle|^2 \tag{2.69}$$

This probability is usually independent of the projectile causing ionization and represents post collision interaction. [41]

2.4.8 The Vainshtein-Presnyakov-Sobel'man Approximation (VPSA)

The basic concept and novelty of the VPS approximation [43] is to take the distortion due to the interaction between the projectile and the active atomic electron into account. The interaction for electron-impact is repulsive and for proton-impact attractive. In addition, the approximate wavefunctions used are required to satisfy the correct boundary conditions. [43]

Considering a structureless projectile of mass M_P, charge Z_P, and momentum $\vec{k_i}$ impacting on a target atom with mass (nuclear plus nonactive electrons) M_T. Fig.2.4.8 depicts the relevant geometry with the quantities defined as follows:

$$\vec{R} = \vec{r} - \vec{x}, \quad \vec{\sigma} = b\vec{r} - \vec{x}, \quad \vec{\rho} = \vec{r} - a\vec{x} \tag{2.70}$$

$$a = \frac{M_P}{M_P + 1}, \quad b = \frac{M_T}{M_T + 1} \tag{2.71}$$

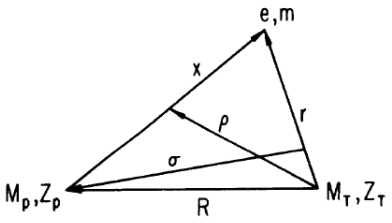

Figure 2.2: Geometry of the collision by a structureless projectile of mass M_P and net charge Z_P and a (hydrogen) atom. M_T, Z_T are the mass and (net) charge of the target core (nucleus), and e is the atomic electron undergoing a transition [43]

In the center-of-mass system the Hamiltonian of the system is

$$H = H_0 + V_{pT} + V_{pe} + VeT \tag{2.72}$$

where V_{pT}, V_{pe}, and V_{pT} give the respective interaction potentials for the systems projectile-target core, projectile-active target electron and target electron-target core. [43] H_0 is the kinetic energy operator and takes its simplest form in

$$H_0 = -\frac{1}{2a}\nabla^2_{\vec{x}} - \frac{1}{2\mu'}\nabla^2_{\vec{p}} \tag{2.73}$$

with $\mu' = \frac{M_T(M_P+1)}{M_P+M_T+1}$. Since asymptotically at large separations before the collision, the wavefunction reduces to

$$(H_0 + V_{eT} - E)\psi_i = 0 \tag{2.74}$$

where E is the total energy of the system and ψ_i takes the form

$$\psi_i = \exp(i\vec{k_i}\cdot\vec{\sigma})\Phi_i(\vec{r}) \tag{2.75}$$

where $\Phi_i(\vec{r})$ is the target eigenfunction and $\vec{k_i}$ is the projectile's relative momentum. Now the matrix element of the transition matrix can be written as

$$T_{if} = \langle\psi_f^-|V_i|\psi_i\rangle = \langle\psi_f^-|V_{pe} + V_{pT}|\psi_i\rangle \tag{2.76}$$

where ψ_i^- is the system's final-state wavefunction and is defined according to incoming spherical wave boundary conditions. V_{pe} and V_{pT} refer to the initial state. [43]

The Schrödinger equation for the projectile-target system after the collision resulting into the excitation of the target is

$$(H_0 + V_{pT} - \frac{Z_P}{x} + V_{eT} - E)\psi_f^- = 0 \tag{2.77}$$

where V_{eT} is the atomic potential in the final state and $V_{pe} = -Z_P/x$. If now

$$\psi_f^- = \Phi_f(\vec{r})g(\vec{x}, \vec{\rho}) \tag{2.78}$$

it follows that [43]

$$\Phi_f(\vec{r})(H_0 + V_{pT} - Z_P/x - E - \varepsilon_f)g = \frac{1}{b}\nabla_{\vec{r}}\Phi_f\nabla_{\vec{r}}g \tag{2.79}$$

2.5 Experimental Methods Used in the Selected Publications to Acquire Cross Section Data

In the following sections, a short description is given of some typical experimental geometries and methods which have been used to determine collisional cross sections involving Na atoms.

2.5.1 Crossed-Beam Method

Crossed-Beam Apparatus for Proton-Impact Collisions

Fig.2.3 shows schematically the main components of the experimental setup of a crossed beam apparatus designed by Aumayr et al. [44] for the measurement of proton-impact collisions. H^+ ions from a Duoplasmatron source are accelerated to the required impact energy, focused by a magnetic quadrupole doublet and charge-to-mass separated by means of an analyzing magnet. The narrow and nearly parallel H^+ ion beam is formed by a series of apertures, crossed with a sodium atom beam and subsequently collected in a shielded Faraday cup.

The target atom beam is produced by effusion of Na vapour in a cell that is implemented in an oven. To produce a well collimated, sufficiently intense and stable Na beam, the exit lid of the oven needs to be kept at a slightly higher temperature than the oven itself.

After crossing the ion beam the Na beam is collected on a trap, see Fig.2.3, which also provides additional pumping. The line radiation from the ion-atom interaction zone could be detected in either direction with vacuum grating spectrometers. For detection of visible line radiation, interference filter–photomultiplier combinations can be used.

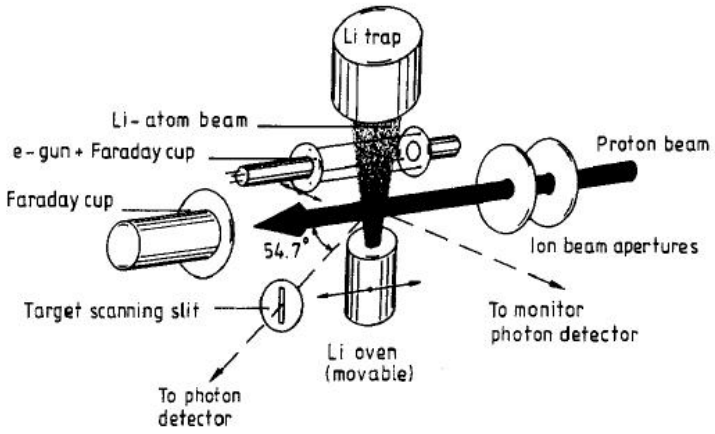

Figure 2.3: Schematic experimental setup of a crossed beam apparatus after F. Aumayr [44]; This setup uses Li which can easily be substituted by Na

Crossed-Electron-Beam-Metal-Atom-Beam Scattering Apparatus

In the apparatus used by Srivastava and Vušković [45], a monoenergetic beam of electrons of desired incident energy is produced by heating a tungsten filament and passing the thermoionically emitted electrons through a set of cylindrical electron lenses and a hemispherical energy analyzer. The beam of sodium is generated by resistive heating of a stainless steel crucible. In order to avoid effects of magnetic fields a coaxial heating wire is wrapped around the crucible. It is heated to the point where the Na density in the atomic beam is high enough to observe sufficient electron scattering. The steady state value of the current does not change during the entire experiment. The scattered electrons pass through a hemispherical energy analyzer which determines their energy loss. These electrons are detected by a spiraltron and are counted by a conventional pulse amplification and multichannel scaling technique. Possible sources of errors are the presence of molecular Na_2 in the target beam and multiple scattering. At the vapor pressure and temperatures encountered during the measurements the presence of Na_2 could be ruled out. Multiple scattering can occur if the mean free path of the electron is smaller than or comparable to the target size. This was taken into account in the design of the apparatus. [45]

2.5.2 Apparatus Using a Sodium Vapor Target

In Fig.2.4a a typical apparatus using a gas vapor target for optical excitation measurements is depicted [46]. A positive hydrogen ion beam is extracted from an ion source, e.g. a duoplasmatron ion source. The ions are accelerated and focused by a gap lens and two einzel lenses. The beam momentum is analyzed using a 10^0 bending magnet and the beam is collimated before it enters the Na vapor target shown in Fig.2.4b. The Na vapor target is in a stainless steel box. Directly beneath the center of the target is a reservoir of liquid Na connected to the box by a tube. Both the liquid Na reservoir and the target are heated electrically. The Na density in the target is governed by the temperature of the target. The target is kept around 150°C hotter than the reservoir to prevent Na from condensing on the target walls and windows. The ion beam enters the target through a stainless steel tube. The pressure in the chamber containing the target and the reservoir is typically around 6.6 mPa.

Inside the Na vapor target is an electron gun and a suppressed Faraday cup. Both are coaxial with the ion beam. The electron gun filament can be rotated in and out of the beam axis. Thus either an electron or and ion beam can pass through the Na vapor interaction region and enter the Faraday cup. Since the interaction geometry of the electron beam is identical to that of the ion beam, it is possible to measure directly the ratio of the apparent cross section of Na(3p) production by incident H^+ ions

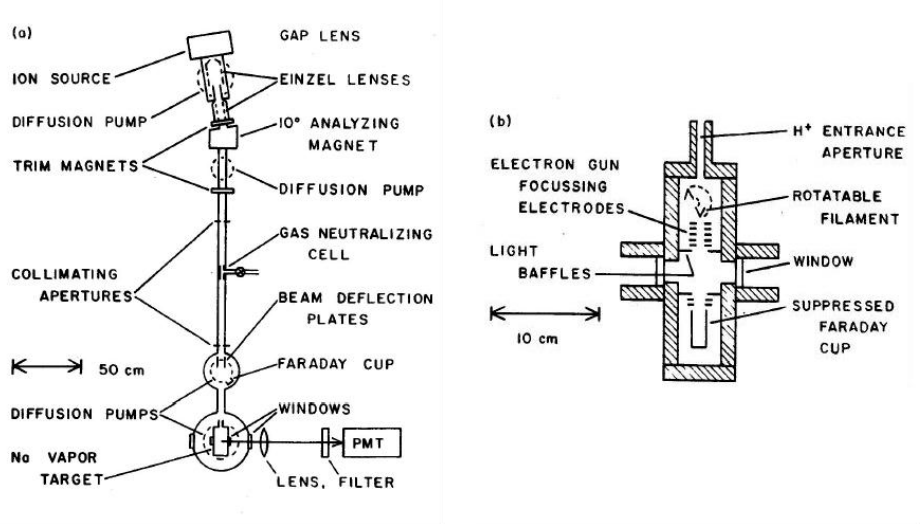

Figure 2.4: Schematic diagram of an apparatus using a gas vapor target: (a) overview, (b) detail of the Na vapor target including the electron gun. [46]

to the apparent cross section for Na(3p) production by incident electrons from the corresponding intensity ratio of the 3p → 3s emission. The apparent cross section is the sum of the cross section for direct excitation of Na(3p) plus the contributions of radiative cascades, see also section 2.5.4. The resonance radiation from the collision region inside the vapor target exits the target cell through a sapphire window on the side. The light passes through a narrow band interference filter and is focused onto the cathode of a photomultiplier tube. [46]

2.5.3 Optical Excitation Function Measurements

In optical excitation function experiments dealing with excitation of ground-state atoms, the essential experimental criterion is to focus the electron beam at all energies through a fixed region of uniform atom beam density and optical detection sensitivity. In such experiments, variations of electron beam position or size with energy can therefore be tolerated to an extent determined by the design of atom beam and detection optics. For electron collisions with excited atoms, the electron beam must pass through a region of spatially homogeneous density of excited atoms. This is particularly important at low energies where electrons are prone to deflection by small residual electric and magnetic fields. Considerable care has therefore been taken to ensure such a spatially homogeneous excited atom region and that the entire electron beam traverses this region. [47]

2.5.4 The Influence of Cascade Effects of Electrons on Experimental Cross Sections

Cascading arises when the incident electrons or protons have sufficient energy to excite the sodium atoms to levels above the 3p state. These atoms can decay to the 3p state and from there to the 3s state. Thus, cascade effects will contribute to the measured intensity of the 3p–3s resonance radiation. An estimate of the cascade contribution can be made by comparing the measured cross sections of lower transitions, such as e.g. 3s → 3p, with those of higher transitions. This is done by measuring the intensities on an absolute scale and normalizing them by means of a standard light source. Summing these cross sections up give a good estimate of the total cascade contribution. Cascading contributions as large as 16% of the total 3p-3s fluorescence have been oberserved. [48] [49]

Chapter 3

Listing of Used Papers

In this section, the referenced papers used in the database are shortly described in terms of the method, the credibility, the weight in the fit, and errors. A listing of the used figures and tables is given for each reference stating the authors and the source of the data as well as data that were referenced by the authors. A rough division is made between electron-impact and proton-impact cross sections. The papers are listed in alphabetical order by the first author's last name. The data are in general considered to deserve a high level of credibility if they follow the general trend of the cross sections very well, i.e. they are confirmed by other independent experiments and/or theories. Data predating 1980 were generally considered to be not as accurate as more recent ones.

Table of Contents of Chapter 3

3.1 Data for Electron-Impact Cross Sections

E.A. Enemark, A. Gallagher (1972): Electron Excitation of the Sodium D Lines; [48]

E.A. Enemark and A. Gallagher report measurements of electron excitation cross sections in the energy range from threshold to 1000 eV of the resonant sodium D lines. Cascade contributions were corrected. The excitation functions have been normalized to the Born theory in the high energy

limit. The resulting normalized cross sections are in excellent agreement with earlier close-coupling calculations in the energy range from the threshold to 5 eV by Karule and Peterkop (1965) [50]. The used crossed-beam apparatus is described in detail in the paper in terms of the electron gun, the sodium oven, the detection system, and the instrumental polarization.

The uncertainties are standard deviations of the mean averaged data. These uncertainties also include possible errors due to sodium-beam density fluctuations. [48]

Despite their early date of publication the values of Enemark and Gallagher proved to be of high agreement with much more recent theoretical approaches. Thus, they were weighted highly in the fit.

Source	Process	Used Data	Published in	Weight in Fit
Tab. 2	Excitation Na(3s) → Na(3p)	Q_D, normalized direct cross section (πa_0^2)	Enemark, Gallagher (1972) [48]	High

Table 3.2: Used data from Enemark, Gallagher (1972) [48]

P.S. Ganas (1985): Excitation of sodium atoms by electron impact; [51]

In this article, Ganas presents PWBA cross sections, see section 2.4.6, calculated with the help of generalized oscillator strengths (GOS) following the suggestion of Bethe (1930) [52] and optical oscillator strengths (OOS). For the excitation from Na(3s) to Na(3p) the calculated curve is compared with experimental values. Due to the known shortcomings of PWBA calculations, the general agreement of the cross sections was very poor, it is not reasonable to include them in the database. Only the reference to Zapesochnyi et al. (1976), see Tab.3.3, was used from this publication.

Source	Process	Used Data	Published in	Weight in Fit
Fig.2	Excitation Na(3s) → Na(3p)	Open circles	Zapesochnyi et al. (1976) [53]	Very low

Table 3.3: Used data from Ganas (1985) [51]

A.R. Johnston, P.D. Burrow (1995): Electron-impact ionization of Na; [54]

Motivated by unsatisfying results concerning the agreement of CCC calculations with experiment data, Johnston and Burrow made new measurements of total ionization cross sections. They used a crossed-beam apparatus that had been previously used. Although their results follow the general trend very well, the discrepancy becomes larger at energies where ionization from the lower 2p subshell might possibly occur. Thus they could only be moderately weighted.

Source	Process	Used Data	Published in	Weight in Fit
Tab.1	Ionization from Na(3s)	Column titled "Cross Section ($Å^2$)"	Johnston, Burrow (1995) [54]	Moderate

Table 3.4: Used data from Johnston, Burrow (1995) [54]

Y.-K. Kim (2001): Scaling of plane wave Born cross sections for electron-impact excitation of neutral atoms; [55]

Introducing two simple scaling methods for first-order, plane-wave Born cross sections, see section 2.4.6, for electron-impact excitations, Kim claims that the accuracy of the cross sections can be improved up to a level comparable to other far more sophisticated and complicated theories, such as e.g. convergent close coupling, see section 2.3. Unfortunately the accuracy of the cross sections of low projectile energy could not be improved to a satisfying degree. So, up to an impact energy of 100 eV, the cross sections were only poorly weighted. Above this limit, a moderate weight it is reasonable.

Source	Process	Used Data	Published in	Weight in Fit
Fig.6	Excitation Na(3s) → Na(3p)	Tab.2 column labeled "Na"	Kim (2001) [55]	Below 100 eV: very low Above 100 eV: moderate

Table 3.5: Used data from Kim (2001) [55]

E.J. McGuire (1971): Inelastic Scattering of Electrons and Protons by the Elements He to Na; [56]

In this very early publication, McGuire promotes PWBA cross section, see section 2.4.6, using a method suggested by Bethe [52] [57]. This method implements generalized oscillator strengths (GOS) in the Born approximation. Despite the improvement that this method supplies, the general agreement outside the high energy region is still poor. Thus only data values corresponding to high impact energies could be trusted to a satisfying degree. All others were only poorly weighted in the fit.

Source	Process	Used Data	Published in	Weight in Fit
Fig. 13	Ionization from Na(3s)	Dashed line marked Na and $\sigma_i(3s)$	McGuire (1971) [56]	Low energy: low High energy: moderate

Table 3.6: Used data from McGuire (1971) [56]

E.J. McGuire (1997): Systematics of *ns* subshell electron ionization cross sections; [58]

With a focus to electron-impact ionization cross sections, E.J. McGuire compares PWBA, see section 2.4.6, with other more recent and more elaborate theories, in particular CCC, see section 2.3. The hypothesis that PWBA calculations are accurate to 10 % at high energies for both neutral atoms and ions could be backed up. McGuire's PWBA calculations show indeed an extraordinary agreement with the recent CCC calculations of I. Bray [27] in the high energy tail. Close to the maximum this agreement decreases to a certain degree. Thus, the data were not weighted very strongly in this region, but nevertheless great trust was put in the high energy tail of McGuire's calculations.

Source	Process	Used Data	Published in	Weight in Fit
Fig. 9	Ionization from Na(3s)	Solid line marked $\sigma_i(3s)$	McGuire (1997) [58]	Low energy: low High energy: high

Table 3.7: Used data from McGuire (1997) [58]

J. Mitroy, I.E. McCarthy, A.T. Stelbovics (1987): Electron scattering from sodium at intermediate energies; [24]

Mitroy et al. present two- and four-channel close-coupling calculations using Hartree-Fock wavefunctions, see also section 2.3. The calculations are restricted to the energy range 10 eV $\leq$ E $\leq$ 217 eV. Elastic and inelastic differential cross sections are presented as well as compared with experiments. Mitroy, McCarthy, and Stelbovics mention a certain discrepancy of their theoretical results with previous experimental studies. When looking at the general trend of the electron-impact target excitation cross sections from the ground state to the first excited state, it can be observed that both the calculated data of Mitroy et al. (1987) [24] as well as the compared experimental results from Buckman, Teubner (1979) [59] show a rather large variance. Both data sets are weighted poorly in the fit.

Source	Process	Used Data	Published in	Weight in Fit
Tab.4	Excitation Na(3s) $\rightarrow$ Na(3p)	CC4–C1	Mitroy et al. (1987) [24]	Low
Tab.4	Excitation Na(3s) $\rightarrow$ Na(3p)	BT	Buckman, Teubner (1979) [59]	Low

Table 3.8: Used data from Mitroy, McCarthy, Stelbovics (1979) [24]

D.L. Moores, D.W. Norcross (1972): The scattering of electrons by sodium atoms; [60]

Moores and Norcross present close-coupling cross sections, see section 2.3, in particular for electron-impact target excitation. Since their results were already published in 1972, the development of the

close-coupling method had not yet reached today's elaborate level. Data for several transitions were included in the database. These data were weighted according to Tab.3.9. Used references for electron-impact excitation cross section from the ground state to the first excited state from Fig.4 [60] are also listed in Tab.3.9.

Source	Process	Used Data	Published in	Weight in Fit
Tab.6	Excitation Na(3s) → Na(3p) four state	Q($3s \rightarrow 3p$)	Moores, Norcross (1972) [60]	Low
Tab.6	Excitation Na(3s) → Na(3d) four state	Q($3s \rightarrow 3d$)	Moores, Norcross (1972) [60]	Low
Tab.6	Excitation Na(3s) → Na(4s) two state	Q($3s \rightarrow 3p$)	Moores, Norcross (1972) [60]	Low
Fig.4	Excitation Na(3s) → Na(3p)	Data points marked with K	Karule, Peterkop (1965) [50]	Low
Fig.4	Excitation Na(3s) → Na(3p)	Narrowly dashed line	G. Gould (1970) [61]	Low

Table 3.9: Used data from Moores, Norcross (1972) [60]

K. Omidvar, H.L. Kyle, E.C. Sullivan (1972): Ionization of Multielectron Atoms by Fast Charged Particles; [62]

The authors used plane waves to describe the incident and scattered particles and screened hydrogenic and Coulomb functions to describe the atomic electrons before and after ejections. Their results were in fact so poor that they were not included in the database. Only the reference to Bates et al. in Fig.10 was included.

Source	Process	Used Data	Published in	Weight in Fit
Fig. 10	Ionization from Na(3s)	Dashed line marked BBP(3s)	Bates et al. (1965) [63]	Low

Table 3.10: Used data from Omidvar, Kyle, Sullivan (1972) [62]

J.O. Phelps, C.C. Lin (1981): Electron-impact excitation of the sodium atom; [19]

James O. Phelps and Chun C. Lin carried out a very extensive experimental study of electron-impact excitation of sodium. Direct excitation cross sections of 14 states (4s, 5s, 6s, 7s, 3p, 4p, 5p, 6p, 3d, 4d, 5d, 6d, 6f, and 7f) have been determined via measured optical-excitation cross sections, see section 2.5.3. A comparison with theoretical data from Born approximations, see section 2.4.6 and multi-state close-coupling calculations, see section 2.3 was made. Despite their early publication date, the cross sections proved to be of great agreement with newer mostly theoretical data. Thus, while calculating the recommended cross sections, high confidence is put in these experimental data.

In the experimental setup, sodium was evaporated from a sidearm into an evacuated heated collision chamber. A monoenergetic beam of electrons passes through the collision chamber and thus excites

the vapor, see section 2.5.2. The subsequent radiative decay is measured at an angle of 90° to the incident electron beam.

In Tab.1 in [19], not only the measured optical excitation functions are listed, but also the uncertainties. These uncertainties range from 10 to 25 % and correspond to a confidence level of 70%.

Source	Process	Used Data	Published in	Weight in Fit
Tab.3	Excitation from 3s → 4s	Corresponding row	Phelps, Lin (1981) [19]	High
Tab.3	Excitation from 3s → 5s	Corresponding row	Phelps, Lin (1981) [19]	High
Tab.3	Excitation from 3s → 3p	Corresponding row	Phelps, Lin (1981) [19]	High
Tab.3	Excitation from 3s → 4p	Corresponding row	Phelps, Lin (1981) [19]	High
Tab.3	Excitation from 3s → 3d	Corresponding row	Phelps, Lin (1981) [19]	High
Tab.3	Excitation from 3s → 4d	Corresponding row	Phelps, Lin (1981) [19]	High

Table 3.11: Used data from Phelps, Lin (1981), [19]

N. Rakštikas and A. Kupliauskienė (2001): The Influence of Valence Electron State on the 2p Ionization of Atomic Sodium by Electrons; [41]

Despite the title, Rakštikas and Kupliauskienė also present Cross Sections for 3s ionization of atomic sodium. They used the PWBA, see section 2.4.6, but applied variations to this method using the relaxed-orbital (RO) Hartree-Fock and sudden perturbation (SP) methods, see section 2.4.7. In the case of photoionization of atoms, more accurate cross sections for the photon energies close to the ionization threshold can be obtained by using the RO approximation. On the other hand, the SP approximation is more suitable for high photon energies.

The approach chosen by the authors proved to be of excellent agreement with both other theories and experimental data. Thus, it was weighted strongly in the fit.

Source	Process	Used Data	Published in	Weight in Fit
Fig.2	Ionization from Na(3s)	Solid line	Rakštikas, Kupliauskienė (2001) [41]	High

Table 3.12: Used data from Rakštikas, Kupliauskienė (2001) [41]

S.K. Srivastava, L. Vušković (1980): Elastic and inelastic scattering of electrons by Na; [45]

Srivastava and Vušković report experimental cross sections that were measured using a crossed-electron-beam-metal-atom-beam scattering technique, see section 2.5.1. The measurements mainly consisted of differential cross sections, but an integral cross section was also listed in the tables with the results. The results were moderately weighted in the fit.

Source	Process	Used Data	Published in	Weight in Fit
Tab.2	Excitation 3s → 3p	Row with integral cross section	Srivastava, Vušković (1980) [45]	Moderate
Tab.2	Excitation 3s → 4s	Row with integral cross section	Srivastava, Vušković (1980) [45]	Moderate

Table 3.13: Used data from Srivastava, Vušković (1980), [45]

B. Stumpf, A. Gallagher (1985): Electron excitation of Na(3S) and Na(3P) atoms to the Na(3D) state; [47]

B. Stumpf and A. Gallagher measured two specific transitions in electron-impact excitation: 3s → 3d and 3p → 3d. They underline the importance of electron collisions with excited states for plasmas, especially for highly excited gases such as fusion plasmas. First, the excited 3p states are produced by a laser beam intersecting with a neutral sodium beam at 90°. The apparatus is a crossed beam machine, see section 2.5.1. The electron and laser beams enter the collision chamber from opposing sides. The sodium beam enters at 90° from the side. The background which is due to oven-light scattered-off surface, electron excitation of background gas, and the photomultiplier dark current was much smaller than the above surface fluorescence signals. The background was measured and subtracted. Resulting from some construction needs of the apparatus, the data accumulation time especially in the low energy region was typically around 24 h, which resulted in a unexpectedly high statistical error.

Apart from the experimental cross sections, Born-approximation cross sections, see section 2.4.6 were computed. Due to the known discrepancy of Born-approximation cross sections with measured data in the low energy range they were weighted very poorly at energies lower than 20 eV. The high energy tail, though, was considered to be of much higher accuracy.

Source	Process	Used Data	Published in	Weight in Fit
Tab. 2	Excitation 3s → 3d	Q(3S → 3D)	Stumpf, Gallagher (1985) [47]	Low energy: low High energy: high
Tab. 3	Excitation 3s → 3d	$Q_T(3S \rightarrow 3D, 90^\circ)$	Stumpf, Gallagher 1985 [47]	Low energy: low high energy: High
Tab. 3	Excitation 3p → 3d	$Q_T(3P_1 \rightarrow 3D, 90^\circ)$	Stumpf, Gallagher 1985 [47]	Low energy: low High energy: high

Table 3.14: Used data from Stumpf, Gallagher (1985), [47]

W.S. Tan, Z. Shi, C.H. Ying, L. Vušković (1996): Electron-impact ionization of laser-excited sodium atom; [64]

In a rapid communication to Physics Review A in November 1996, Tan et al. reported electron-impact target ionization cross sections of laser-excited target states. The cross sections range from the

threshold to 30 eV. They were measured simultaneously for both ground-state and the 3p-excited-state atoms as a function of electron-impact energy. The excited-state data were calibrated with respect to the ground-state data that were normalized to measurements from Johnston and Burrow [54]. The cross section were measured simultaneously in the same energy range by measuring the ion current with laser off and laser on as a function of energy and other experimental parameters. The results of Tan et al. proved to be of excellent agreement with other data and were therefore weighted strongly in the fit.

Source	Process	Used Data	Published in	Weight in Fit
Tab.1	Ionization from Na(3s)	σ_g	Tan et al. (1996) [64]	High
Tab.1	Ionization from Na(3p)	σ_e	Tan et al. (1996) [64]	High
Tab.1	Ionization from Na(3s)	Column No.4	Zapesochnyi, Aleksakhin (1968) [65]	Low

Table 3.15: Used data from Tan, Shi, Ying, Vuškoivć (1996), [64]

S. Verma, R. Srivastava (1996): Electron impact excitation of the 3^2D states of lithium, sodium and potassium atoms; [39]

Verma and Srivastava present a comparison of several theoretical methods. The method, included in the database, is a distorted wave approximation, see section 2.4.5, where the distortion potential of the excited state is static and exchange potentials are taken in both the initial and the final state. This model is referred to as the *FF model*.

Source	Process	Used Data	Published in	Weight in Fit
Fig.1a (ii)	Excitation Na(3s) → Na(3d)	Full line	Verma, Srivastava (1996) [39]	Low

Table 3.16: Used data from Verma, Srivastava (1996), [39]

3.2 Data for Proton-Impact Cross Sections

R.J. Allan (1986): Charge transfer in H^+–Na^0 collisions: molecular orbital calculations; [66]

Applying a molecular-orbital basis to the close-coupling method, see section 2.4.1, like Allan did in this publication, gives excellent results comparable to those calculated with an atomic-orbital basis. Allan restricts his investigations to the energy range 200 eV $\leq$ E $\leq$ 8 keV and argues that in this energy range the *perturbed stationary state method (PSS)* with linear paths is reasonable. The term PSS is just another name for the close-coupling method using molecular-orbital functions. [30]

Source	Process	Used Data	Published in	Weight in Fit
Tab.4	Charge transfer from Na(3s)	14-state H (all)	Allan (1986) [66]	Very high
Fig.4	Charge transfer from Na(3s)	Open triangles	McCullough (1978) [67]	Extremely low

Table 3.17: Used data from Allan (1986) [66]

F. Aumayr, G. Lakits, H. Winter (1987): Charge transfer and target excitation in H^+-Na(3s) collisions (2–20 keV); [68]

F. Aumayr et al. present absolute cross sections for single-electron capture and Na(3s←3p) emission for H^+ - Na(3s) collisions at impact energies of $2 - 20$ keV. The data agree with quantum mechanical calculations, thus removing discrepancies among experimental and theoretical results. The extensive comparison with other experimental and theoretical data was extraordinarily helpful for the collection of cross section data in terms of section 2.1. The presented data, both for single electron charge transfer and target excitation 3s $\rightarrow$ 3p, agree extremely well with much more recent data. They were given the highest weight in the fit.

Source	Process	Used Data	Published in	Weight in Fit
Tab.1	Charge transfer from Na(3s)	σ_{10}	Aumayr et al. (1987) [68]	Very high
Tab.1	Excitation 3s $\rightarrow$ 3p	$\sigma_{Na(3p)}$	Aumayr et al. (1987) [68]	Very high

Table 3.18: Used data from Aumayr, Lakits, Winter (1987), [68]

G.V. Avakov, L.D. Blokhintsev, A.S. Kadyrov, A.M. Mukhamedzhanov (1992): Electron capture in proton collisions with alkali atoms as a three-body problem; [69]

Avakov et al. present calculations of electron transfer reactions. Applying only pure Coulomb interaction in the impact parameter representation (IPFA), the electron transfer reactions were treated as a

three-body problem. This approach offers the possibility to describe cross sections over a wide range of energies [69]. This method proved to be quite accurate when compared to the general trend and the CCC calculations. It was given moderate weight in the fit.

Source	Process	Used Data	Published in	Weight in Fit
Fig.2	Charge transfer from Na(3s)	Full curve	Avakov et al. (1992) [69]	Moderate
Fig.2	Charge transfer from Na(3s)	Full inverted triangles	Il'in et al. (1966) [70]	Very low

Table 3.19: Used data from Avakov, Blokhintsev, Kadyrov, Mukhamedzhanov (1991), [69]

K. Basu Choudhury, D.P. Sural (1992): Electron capture in ground and excited states in proton-alkali-metal-atom collisions; [71]

Basu Coudhury and Sural present calculations of electron transfer cross sections of Na-, Ka-, Rb-, and Cs-targets. It is mentioned in the description of Tab.2 [71] that the results of sodium are taken from an earlier work of the authors. Unfortunately this earlier work could not be consulted. It remains unclear if the described method using the wave formulation of the impulse approximation was used. They mention the applicability of high energy neutral particle beams for plasma heating and fueling in fusion experiments.

Source	Process	Used Data	Published in	Weight in Fit
Tab.2	Charge transfer from Na(3s)	Sodium (present)	Basu Choudhury, Sural (1983) [72]	Very low
Tab.2	Charge transfer from Na(3s)	Sodium (eikonal)	Daniele et al. (1979) [73]	Very low
Tab.2	Charge transfer from Na(3s)	Sodium (FBA)	Daniele et al. (1979) [73]	Very low

Table 3.20: Used data from Basu Choudhury, Sural (1992), [71]

R.D. Dubois (1986): Charge transfer leading to multiple ionization of neon, sodium, and magnesium; [74]

DuBois reports experimental cross sections measured with a crossed-beam apparatus, see section 2.5.1. A collimated, momentum-analyzed ion beam passed through a diffuse atomic beam. The collision products were electrostatically charge-state analyzed. A definition of the used variables is given on page 2743 in [74]. The influence of the inner-shell contribution to the capture cross sections is indicated by a change in the slope of impact velocities near the velocity of the sodium L-shell electrons.

The charge transfer cross sections were weighted high below an impact energy of 30 keV. Above the limit they are weighted lower by a factor 10^4 because in this energy region the influence of cascade

effects cannot be neglected, see section 2.5.4. The ionization cross sections were given a moderate weight that does not differ over the whole range of values.

Source	Process	Used Data	Published in	Weight in Fit
Fig. 2, H^+ + Na	Ionization	σ_1^{11}	DuBois (1986) [74]	Moderate
Fig. 2, H^+ + Na	Charge Transfer	σ_1^{10}	DuBois (1986) [74]	Below 30 keV: high Above 30 keV: low

Table 3.21: Used data from DuBois (1986), [74]

R.D. DuBois, L.H. Toburen (1985): Electron capture by protons and helium ions from lithium, sodium, and magnesium; [75]

DuBois and Toburen present among others single-electron capture cross sections. The absolute cross sections were measured using the growth-curve method. The absolute cross sections determined are believed to be accurate to approximately ±15% with most of the uncertainty due to the absolute target densities measured. [75]

The presented data were weighted very high for energies below 30 keV. Above this limit, they were weighted lower by a factor of 10^3. In this energy range the contributions from the inner shells cannot be neglected anymore and cause the cross sections to show larger values than for pure electron capture from the ground state alone. Referenced data from Fig.6

Source	Process	Used Data	Published in	Weight in Fit
Tab. 2	Charge transfer from Na(3s)	Column with H^+ as impact particle	DuBois, Toburen (1985) [75]	Below 30 keV: very high Above 30 keV: low
Fig.6	Charge transfer from Na(3s)	Open triangles	Barnett et al. (1977) [76]	Low

Table 3.22: Used data from DuBois, Toburen (1985), [75]

F. Ebel, E. Salzborn (1987): Charge transfer of $0.2-5.0$ keV protons and hydrogen atoms in sodium-, potassium- and rubidium-vapour targets; [77]

Ebel and Salzborn measured single- and double-electron capture by protons from several alkali gas targets (Na, K, Rb). They mention the importance of the energy analysis of the neutral hydrogen atoms as a possible diagnostic for fusion plasma research. For the measurements an apparatus using a gas vapor target was used, see section 2.5.2. The purity of the used sodium was 99.95%. The validity of the single-collision condition was carefully checked by the linear dependence of the product particle intensity on the target thickness. The results were moderately weighted in the fits. Tab. 1 in [77] not

only present the measured values but also the absolute errors. Ebel and Salzborn reference a number of other papers, see Tab.3.23. They are all single-electron charge transfer cross sections.

Source	Process	Used Data	Published in	Weight in Fit
Tab.1	Charge transfer from Na(3s)	Sodium σ_{+0}	Ebel, Salzborn (1987) [77]	Moderate
Fig.4	Charge transfer from Na(3s)	Full line	Kubach, Sidis (1981) [78]	Low
Fig.4	Charge transfer from Na(3s)	Full and dotted line	Kimura et al. (1982) [79]	Very low
Fig.4	Charge transfer from Na(3s)	Fully and doubly dotted line	Ermolaev (1984) [80]	High

Table 3.23: Used data from Ebel, Salzborn (1987), [77]

W. Fritsch (1984): Atomic-basis study of electron transfer in H^+ + Na and H^+ + K collisions; [81]

Fritsch uses in this articles basically the same method as J. Schweinzer did in the AO-CC calculations for proton-impact cross sections, see section 2.3. It is therefore not supprising that the results agree excellently not only with Schweinzer's cross sections but also with the general trend of the other collected data. Fritsch's cross sections are very highly weighted in the fit.

Source	Process	Used Data	Published in	Weight in Fit
Tab.1	Charge transfer from Na(3s)	σ_{tot}	Fritsch (1984) [81]	Very high

Table 3.24: Used data from Fritsch (1984), [81]

W. Grüebler, P.A. Schmelzbach, V. König, P. Marmier (1970): Charge Exchange Collisions between Hydrogen Ions and Alkali Vapour in the Energy Range of 1 to 20 keV; [82]

In this very early publication Grüebler et al. used an apparatus with a sodium vapor target, see section 2.5.2. A systematic study of one- and tow-electron charge exchange processes was carried out with low energy positive hydrogen ions. The dependence on the incident energy was studied.The results are evaluated in terms of their applicability to the construction and design of polarized ion sources. The results were poorly weighted in the fit.

Source	Process	Used Data	Published in	Weight in Fit
Fig.6	Charge transfer from Na(3s)	σ_{10} with closed dots	Grüebler et al. (1970) [82]	Low

Table 3.25: Used data from Grüebler, Schmelzbach, König, Marmier (1970), [82]

A.M. Howald, L.W. Anderson, C.C. Lin (1982): Excitation of the Na(3p) Level by H^+, H_2^+, or H_3^+ Ions; [46]

The reported measurements are in the energy range $1-25$ keV and were carried out using a gas-vapor apparatus, see section 2.5.2. The cross section are "apparent cross sections", the sum of the cross section for production of Na(3p) level atoms by direct excitation and the cross section for production of Na(3p) level atoms by radiative cascade from higher levels. These cascades only occur at energies above the excitation energy of the Na(3d) level, see 2.5.4. Due to this effect, the cross section cannot considered to be of high accuracy especially in the high energy region. Thus, they were given a low weight in the fit.

Source	Process	Used Data	Published in	Weight in Fit
Fig.2	Excitation Na(3s) → Na(3p)	Open triangles for H^+ impact	Howald et al. (1982) [46]	Low

Table 3.26: Used data from Howald, Anderson, Lin (1982), [46]

A. Jain, T.G. Winter (1995): Electron transfer, target excitation, and ionization in H^++Na(3s) and H^++Na(3p) collisions in the coupled-Sturmian-pseudostate approach; [34]

A. Jain and T.G. Winter present calculated cross sections of various transitions from both ground state sodium and first excited state sodium. They used the coupled-Sturmian-pseudostate approach, see section 2.4.2, to calculate cross sections for charge exchange, target excitation, and ionization. Additionally an extensive investigation of the possible sources of error was performed. It resulted in an estimated accuracy of the target excitation and charge exchange cross sections within 10%, except for ionization cross section, which are within a 25% accuracy. [34]

The charge transfer cross section from ground state sodium proved to be of excellent agreement with other data. It was thus weighted with the highest value used. Both the target excitation and ionization cross sections generally follow the trend well. They were thus considered to deserve to be highly weighted.

W. Jitschin, S. Osimitsch, D.W. Mueller, H. Reihl, R.J. Allan, O. Schöller, H.O. Lutz (1986): Excitation of the Na 3p state by proton impact; [86]

Jitschin et al. present experimental cross sections as well as new calculations. The theoretical curves were computed using the PWB approximation, see section 2.4.6, and were of such poor agreement that they had to be ignored. Using a crossed-beam apparatus, see section 2.5.1, the experimental data do not follow the genereal trend of the curve too well. Nevertheless, they were included in the

Source	Process	Used Data	Published in	Weight in Fit
Tab.2	Charge transfer from Na(3s)	σ_{cap}^{tot}	Jain, Winter (1995) [34]	High
Tab.2	Excitation Na(3s) → Na(3p)	$\sigma_{exc}^{3s\rightarrow 3p}$	Jain, Winter (1995) [34]	High
Tab.2	Excitation Na(3s) → Na(3d)	$\sigma_{exc}^{3s\rightarrow 3d}$	Jain, Winter (1995) [34]	High
Fig.12	Ionization from Na(3s)	Solid line	Jain, Winter (1995) [34]	Moderate
Fig.1	Charge transfer from Na(3s)	Crosses	Anderson et al. (1979) [83]	High
Fig.10	Excitation Na(3s) → Na(3d)	Closed triangles	Allen et al. (1988) [84]	Moderate
Fig.12	Ionization from Na(3s)	Dotted line	Fritsch (1987) [85]	Moderate

Table 3.27: Used data from Jain, Winter (1995), [34]

database but only poorly weighted.

Source	Process	Used Data	Published in	Weight in Fit
Fig.1	Excitation Na(3s) → Na(3p)	Full squares	Jitschin et al. (1986) [86]	Low

Table 3.28: Used data from Jitschin et al. (1986), [86]

C.J. Lundy, R.E. Olson (1996): A classical analysis of proton collisions with ground-state and excited, aligned sodium targets; [87]

Lundy and Olson present CTMC calculations, see section 2.4.4. The theoretical results reproduce the general trend exhibited by the experimental measurements and other theoretical computations with the largest window of discrepancy occurring in the region of the maximum cross section. Thus they can be highly weighted in the fit.

Source	Process	Used Data	Published in	Weight in Fit
Fig.1	Charge transfer from Na(3s)	Full curve	Lundy, Olson (1996) [87]	High
Fig.6	Ionization from Na(3s)	Dashed curve	Lundy, Olson (1996) [87]	Moderate

Table 3.29: Used data from Lundy, Olson (1996), [87]

T. Nagata (1980): Charge Changing Collisions of Atomic Beams in Alkali-Metal Vapors. IV. Total Cross Sections for Single-Electron Capture by H^+ Ion and H(1s) Atom; [88]

In this early publication, Nagata describes measurements of the type

$$H^+ + M \longrightarrow H^0 + M^+ \qquad (\sigma_{+0}). \tag{3.1}$$

Nagata does not differ between the final H^0 states, but comments that "almost all of the H^0 atoms will be in the 1s or the 2s state within very short time after the collision ($\lesssim 10^{-18}$ sec)" [88]. Nagata

uses a crossed beam apparatus, see section 2.5.1. The main error sources in this measurement are the estimations of the target atom density in the cell, the effective collisions length, the correction factors of the efficiency of the product counters, and the scattering effects. The overall error in the measurement of the charge transfer cross sections for sodium are ±48% at 5.0 keV and ±60% at 0.5 keV. Due to these large errors the cross sections cannot be considered to be very accurate. They were therefore given a low weight in the fit.

Source	Process	Used Data	Published in	Weight in Fit
Fig.3A	Charge transfer from Na(3s)	Closed triangles	Nagata (1980) [88]	Low

Table 3.30: Used data from Nagata (1980), [88]

B.G. O'Hare, R.W. McCullough, H.B. Gilbody (1975): Ionization of sodium and potassium vapour by $20-100$ keV H^+ and He^+ ions; [89]

O'Hare, McCullough, and Gilbody use a crossed-beam method, see section 2.5.1, to study the ionization of sodium and potassium by incident protons in the energy range of $20-100$ keV. Measurements of the gross yield of electrons arising from the crossed-beam intersection region are used to determine absolute cross section σ_e for electron production. Secondary ions formed through both ionizing and charge-changing collisions are being analyzed using a mass spectrometer, and cross sections for the formation of both singly and doubly charged ionized ions are determined separately. The extent to which charge transfer contributes to secondary ion formation is also assessed from measurements, in a subsidiary experiment, of cross sections σ_{10} for one-electron capture by primary ions. The analysis of the sodium data is much simpler than for potassium because of the relatively minor role of processes involving Na^{2+} formation. For both charge transfer and ionization the cross sections do not follow the general trend of the curves too well. Thus, they were given little weight in the fits.

Source	Process	Used Data	Published in	Weight in Fit
Fig.3	Ionization from Na(3s)	σ_e	O'Hare et al. (1975) [89]	Moderate
Fig.3	Charge transfer from Na(3s)	σ_{10}	O'Hare et al. (1975) [89]	Low

Table 3.31: Used data from O'Hare, McCullough, Gilbody (1975), [89]

A.N. Perumal, D.N. Tripathi (1997): Charge Transfer and Ionization in Proton-Alkali Atoms Collisions with and without Electric Field; [32]

Perumal and Tripathi report classical trajectory Monte Carlo simulations, see section 2.4.4, of collisions of protons with alkali metal atoms in their ground state. The ionization cross section was given medium

to low weight in the fit, mainly because of the poor agreement in the low energy region.

Source	Process	Used Data	Published in	Weight in Fit
Fig.1b	Charge transfer from Na(3s)	Solid line (CTMC)	Perumal, Tripathi (1997) [32]	Moderate
Fig.2b	Ionization from Na(3s)	Solid line (CTMC)	Perumal, Tripathi (1997) [32]	Moderate
Fig.2b	Ionization from Na(3s)	Closed triangles	Garcia et al. (1968) [90]	Moderate
Fig.2b	Ionization from Na(3s)	Open circles	Bates et al. (1970) [91]	Moderate

Table 3.32: Used data from Perumal, Tripathi (1997), [32]

F. Sattin (2001): Further study of the over-barrier model to compute charge-exchange processes; [92]

Based on an improved version of the classical over-barrier model, see section 2.4.3, Sattin reports new cross section calculations. The lack of agreement with other calculations and experiments might be due to the not yet fully optimized and understood varied model. Sattin mentions in the end of his article, that there are certain topics requiring further discussion and investigation. The data could only be taken into account to a very small degree when fitting the cross sections.

Source	Process	Used Data	Published in	Weight in Fit
Fig.2	Charge transfer from Na(3s)	Solid line	Sattin (2001) [92]	Very low
Fig.2	Charge transfer from Na(3s)	Open circles	Thomsen et al. (1996) [93]	High

Table 3.33: Used data from Sattin (2001), [92]

R. Shingal, B.H. Bransden, A.M. Ermolaev, D.R. Flower, C.W. Newby, C.J. Noble (1986): Charge transfer in H^+–Na^0 collisions: atomic orbital calculations; [36]

In this article, Shingal et al. present charge transfer cross sections calculated with the atomic-orbital close-coupling method also used by J. Schweinzer, see section 2.3. The AO-CC method was originally chosen by Schweinzer, because it resulted in cross sections that agree excellently especially with experimental data. This opinion is based on calculations like the one presented in this article. The presented cross sections reflect the general trend of the charge transfer cross sections enormously well. Thus, they were very highly weighted in the fit.

Source	Process	Used Data	Published in	Weight in Fit
Fig.2	Charge transfer from Na(3s)	Full line	Shingal et al. (1986) [36]	Very high

Table 3.34: Used data from Shingal, Bransden, Ermolaev, Flower, Newby, Noble (1986), [36]

R. Shingal, B.H. Bransden (1987): Charge transfer, target excitation and ionisation in H^+ + Na(3s) collisions; [94]

This article is a follow-up of the earlier publication by Shingal,Bransden et al. (1986) [36]. The investigations were enlarged and not only charge transfer was treated but also proton-impact excitation and ionization. Tab. 3.35 gives a complete listing of all of the used data.

Source	Process	Used Data	Published in	Weight in Fit
Tab.1	Charge transfer from Na(3s)	σ^c_{tot}	Shingal, Bransden (1987) [94]	Very high
Tab.2	Excitation Na(3s) → Na(3p)	$\sigma_{Na(3p)}$	Shingal, Bransden (1987) [94]	Low
Tab.2	Excitation Na(3s) → Na(3d)	$\sigma_{Na(3d)}$	Shingal, Bransden (1987) [94]	High
Fig.7	Ionization from Na(3s)	Dashed line	Shingal, Bransden (1987) [94]	High
Fig.4	Excitation Na(3s) → Na(3p)	Dashed line	W. Fritsch (1987) [85]	Low
Fig.5	Excitation Na(3s) → Na(3d)	Inverted open triangles	Anderson et al. (1985) [95]	Moderate

Table 3.35: Used data from Shingal, Bransden (1987) [94]

C.E. Theodosiou (1988): Theoretical verification of the differences between excitation of $Na\ 3p$ and $Na\ 3d$ by H^+ and H^- impact; [40]

Theodosiou reports cross section calculations using the distorted-wave-type approximation described in section 2.4.5. The calculated data are compared to earlier experimental data. The actual shape of the experimental curve is reproduced. Nevertheless, the calculated curve is substantially lower than the experimental one. Theodosiou argues that it has to be taken into account that experimental data always contain cascade contributions. It remains unexplained why the difference between theory and experiment is largest in the low energy region below 10 keV where the cascade contributions should only contribute to a small amount. From this it is obvious that not too much confidence can be put in this data. Thus, they are very low weighted in the fit.

Source	Process	Used Data	Published in	Weight in Fit
Fig.3	Excitation 3s → 3d	Solid line marked H^+	Theodosiou (1988) [40]	Low

Table 3.36: Used data from Theodosiou (1988), [40]

A.N. Tripathi, K.C. Mathur, S.K. Joshi (1969): Impact ionization of Na, K, Rb and Cs by electron and proton impacts; [96]

In this very early paper Tripathi, Mathur, and Joshi present a number of ionization cross sections. Not much is said about the applied theory. It is only stated that a classical impulse approximation using

quantum momentum distribution functions is used, a method developed by Gryzinski in 1959 [97]. This method basically states that inelastic scattering, ionization, excitation, and other interactions between charged particles and atoms are due to the Coulomb interaction with atomic electrons. They depend in a first approximation on their binding energy and momentum distribution. All cross sections can easily be calculated by means of differential cross sections $\sigma(\Delta E)$ and $\sigma(\Delta E, \vartheta)$ derived in the binary encounter approximation.

The agreement of the electron cross sections was so poor that the data were not included in the database. Nevertheless the presented proton-impact ionization cross sections reflected the curve's general trend quite well. So they were weighted moderately in the fit.

Source	Process	Used Data	Published in	Weight in Fit
Fig.2A	Ionization from Na(3s)	Solid line	Tripathi et al. (1969) [96]	Moderate

Table 3.37: Used data from Tripathi, Mathur, Joshi (1969), [96]

Chapter 4

Fit Formulae, Method for Non-Linear Fits, and Tools

As mentioned above, the collected data need to be fitted so that a recommended cross section can be derived for the later use in simulations. Thus, it is essential to obtain analytical fit functions and corresponding fit parameters for each considered process. In the earlier works of D. Wutte et al. [98] and J. Schweinzer et al. [99], a set of fit formulae was provided for the following transitions in the lithium atom:

- Electron-impact target excitation
- Electron-impact target ionization
- Proton-impact target excitation
- Proton-impact target electron loss

With small but necessary changes these formulae were adapted for the corresponding cross sections and a sodium target.

4.1 Electron-Impact Target Excitation

The fit formula from [99], see eq. (4.1), was chosen and adapted for sodium.

$$\textbf{Li}: \quad \sigma_{e^-}^{EXC}(E/eV)[cm^2] = \frac{5.984 \cdot 10^{-16}}{E}\left[\frac{E-\Delta E}{E}\right]^{A_6} \cdot \left[\sum_{j=1}^{4}\frac{A_j}{(E/\Delta E)^{j-1}} + A_5 \ln\left(\frac{E}{\Delta E}\right)\right] \quad (4.1)$$

with

$A_1 - A_6$: Fit parameters

E: Energy in eV

ΔE: Threshold energy of the considered excitation

First, an additional parameter A_7 was introduced instead of the numerical value 5.984 for a more flexible adjustment. Furthermore, it also became necessary to limit the fitting range in the low-energy region. The high energy tail of the cross sections is of much higher importance for the later use of the recommended cross sections than the low energy region, because of the high kinetic energies of the particles in a fusion plasma. In most cases the lower energy limit is the lowest value of the available data. Due to irregular behaviors in the low energy region, in some cases, this energy limit had to be chosen between 0.1 and 5 eV higher than the lowest available data point. The limitation of the fit formula was achieved by multiplying with a Θ-function.

$$\Theta(x) = \begin{cases} 0 & \text{if } x < 0 \\ 1 & \text{if } x > 0 \end{cases} \tag{4.2}$$

In gnuplot syntax this is:

```
theta(x) = (x => 0) ?  1:1/0
```
(4.3)

Where 1/0 gives an undefined value. This is not the "classical" Θ-function, (4.2), but adapted so that the low energy region is really cut off and not only set to zero. The final form of the chosen fit formula is:

$$\sigma_{e^-}^{EXC}(e/eV)[cm^2] = \frac{A_7 \cdot 10^{-16}}{E}\left[\frac{E-\Delta E}{E}\right]^{A_6} \cdot \left[\sum_{j=1}^{4} \frac{A_j}{(E/\Delta E)^{j-1}} + A_5 \cdot \ln\left(\frac{E}{\Delta E}\right)\right] \cdot \Theta(E - E_{low}) \tag{4.4}$$

with

$A_1 - A_7$: Fit parameters

E: Energy in eV

ΔE: Threshold energy of the considered excitation

E_{low}: Energy limit in the low energy region

4.2 Electron-Impact Target Ionization

A similar approach was chosen to adapt the Li fit formula for the use with Na cross sections. The fit formula for Li(2s) electron-impact ionization from [98] was chosen to be changed for our purposes.

$$\textbf{Li}: \qquad \sigma_{e^-}^{ION,Li(2s)}(E/eV)[cm^2] = \frac{10^{-13}}{I_{2s}\cdot E}\left[A\ln\left(\frac{E}{I_{2s}}\right)+\sum_{j=1}^{3}B_j\left(1-\frac{I_{2s}}{E}\right)^j\right] \tag{4.5}$$

with

A, $B_1 - B_3$:	Fit parameters
E:	Energy in eV
I_{2s}:	Ionization energy for Li(2s)

Like in electron-impact target excitation, an additional factor, B_5, was introduced for more flexibility. It also became necessary to introduce the above described Θ-function (4.3). This comes to

$$\sigma_{e^-}^{ION}(E/eV)[cm^2] = \frac{A_5\cdot 10^{-13}}{E\cdot I_{nl}}\cdot\left[A_4\cdot\ln\left(\frac{E}{I_{nl}}\right)+\sum_{j=1}^{3}A_j\cdot\left(1-\frac{I_{nl}}{E}\right)^j\right]\cdot\Theta(E-E_{low}) \tag{4.6}$$

with

$A_1 - A_5$:	Fit parameters
E:	Energy in eV
I_{nl}:	Ionization energy for Na(nl); $n = 3-5$
E_{low}:	Energy limit in the low energy region

This formula can be used for all considered states, not only for the 3s ground state, as one could claim according to [98].

In reality, the electron-impact target ionization cross sections are influenced by the electrons in the lower shells. There are considerable contributions in the region above the binding energies of the 2p and the 2s electrons and must thus be added to the recommended cross section. The contributions from the 1s electrons can be neglected. In a series of papers, W. Lotz provided an analytical formula for electron-impact ionization under the consideration of the core electrons (2s, 2p), [100], [101].

$$\sigma = \sum_{i=1}^{N} a_i q_i \frac{\ln(E/P_i)}{E\cdot P_i} 1 - b_i\cdot\exp(-c_i(E/P_i-1)); \qquad E \geq P_i \tag{4.7}$$

with

E:	Energy of the impact electron
P_i:	Binding energy of electrons in the i-th subshell
P_1:	Ionization potential
q_i:	Number of equivalent electrons in the i-th subshell
a_i, b_i, c_i:	Individual constants

P_2	P_3	q_2	q_3	a_2	a_3	b_2	b_3	c_2	c_3
34	67	6	2	3.0	4.0	0.9	0.7	0.2	0.5

Table 4.1: Input values for the Lotz Formula 4.7

N is set equal to 3 for sodium-like ions in order to get a better approximation at the high energy tail. No distinction is made between the L_{II} and the L_{III} shells, it is assumed that all the 2p electrons are equivalent and thus form one subshell. Since only the contributions of the core electrons are required for the core corrected recommended cross sections, i will start not equal to 1 (this is for the 3s electrons) but equal to 2. The necessary parameters were found in [100] in table 1 and in [101] in tables 4 and 5. There are listed in table 4.1. Fig.4.1 presents ground state electron impact ionization. It shows very clearly that the contributions from the core electrons are substantial in the high energy region and cannot be neglected. Therefore these contributions of the core electrons were added to all electron-impact target ionization cross sections. It is expected that the relative change between the recommended cross section with and without the core corrections diminishes with the excitation state, i.e. the higher excited the electron is the smaller is the difference the core correction makes. This trend can be observed when comparing Fig.4.1 for ground state ionization and Fig.4.2 for ionization from the excited 5s state (the highest excited state considered). This confirms the need for the core corrections.

The final form of the used fitting formula for electron-impact target excitation is therefore

$$\begin{aligned}\sigma_{e^-}^{ION}(E/eV)[cm^2] =& \frac{A_5 \cdot 10^{-13}}{E \cdot I_{nl}} \cdot \left[A_4 \cdot \ln\left(\frac{E}{I_{nl}}\right) + \sum_{j=1}^{3} A_j \cdot \left(1 - \frac{I_{nl}}{E}\right)^j \right] \cdot \Theta(E - E_{low}) + \\ &+ \sum_{i=2}^{3} a_i q_i \frac{\ln(E/P_i)}{E \cdot P_i} 1 - b_i \cdot \exp(-c_i(E/P_i - 1)) \cdot \Theta(E - P_2);\end{aligned} \tag{4.8}$$

with

$P_2 = 34\ eV$:	Binding energy of electrons in the 2p subshell
$P_3 = 67\ eV$:	Binding energy of electrons in the 2s subshell
$q_2 = 6$:	Number of equivalent electrons in the 2p subshell
$q_3 = 2$:	Number of equivalent electrons in the 2s subshell
$a_2 = 3.0,\ b_2 = 0.9,\ c_2 = 0.2$:	Individual constants for the 2p electrons
$a_3 = 4.0,\ b_3 = 0.7,\ c_3 = 0.5$:	Individual constants fr the 2s electrons

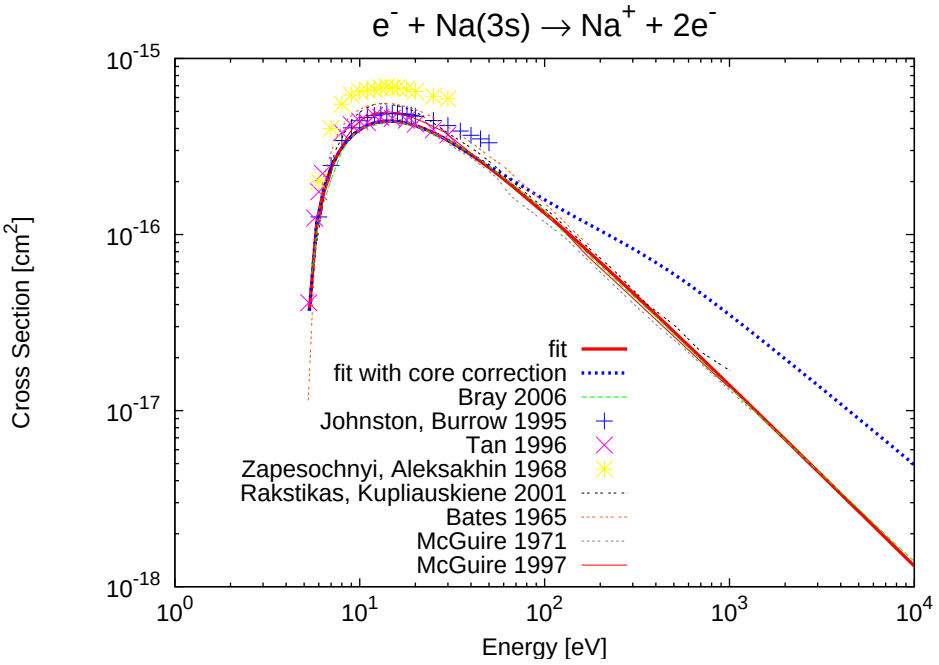

Figure 4.1: Electron-impact target ionization from Na(3s)

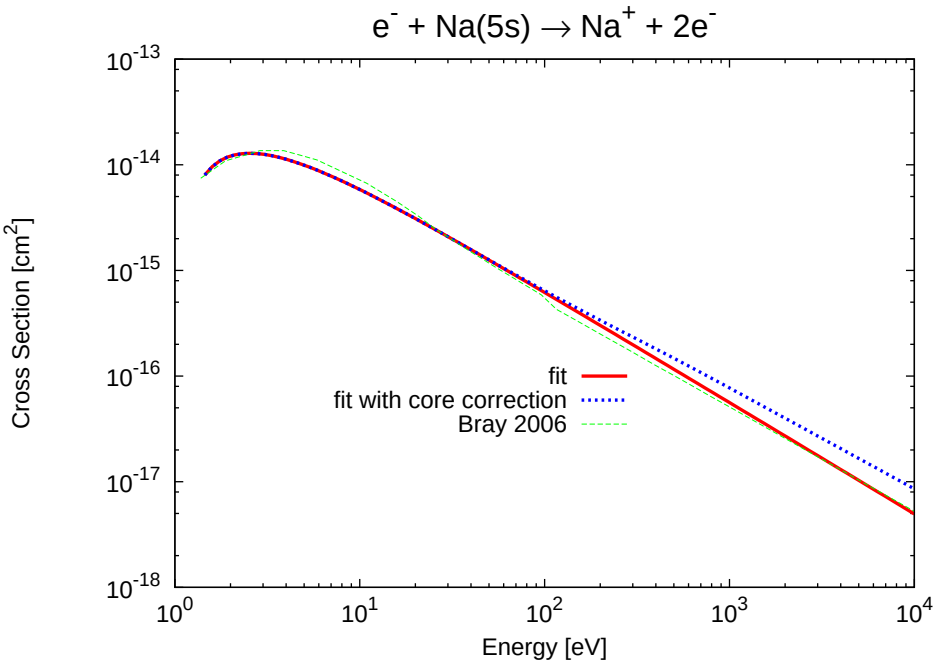

Figure 4.2: Electron-impact target ionization from Na(5s)

4.3 Proton-Impact Target Excitation

The fit formula from [99] could be used without any changes. Nevertheless, for the sake of consistence, the low energy region was treated the same way as in the case of electron impact cross sections.

$$\sigma_{H^+}^{EXC}(E/keV)[cm^2] = A_1 \cdot 10^{-16}\Big\{\frac{e^{-A_2/E}\cdot(A_{12}+\ln(A_{11}+A_3E))}{E}+ \\ + A_4\cdot\frac{e^{-A_5E}}{E^{A_6}} + A_7\cdot\frac{e^{-A_8/E}}{1+A_9\cdot E^{A_{10}}}\Big\}\cdot\Theta(E-E_{low}) \tag{4.9}$$

with

$A_1 - A_{12}$:	Fit parameters
E:	Energy in keV
E_{low}:	Energy limit in the low energy region

4.4 Proton-Impact Target Electron Loss

Proton impact target electron loss consists of two contributions: proton-impact target ionization and proton-impact charge transfer. We are only interested in the probability that a sodium atom loses an electron, the target electron loss cross section. Unfortunately these cross sections have not been published anywhere else. Nevertheless there are plenty of data available for both proton-impact single electron charge transfer and proton-impact target ionization. Only [98] provided a fit formula for proton-impact target ionization. However, no good fits could be achieved with this formula. Luckily, the formula for proton-impact target excitation, see eq.4.9, could be used to fit the ionization cross sections reasonably well. Since the fitting routine needs reasonable start parameters, the final parameters for $H^+ + Na(4s) \rightarrow H^+ + Na(4f)$ were taken as start parameters, because in this case, the fitting curve resembled the ionization data the most.

A similar problem occurred for **proton-impact single electron charge transfer**. Here, there was no analytical fit formula available in [98] or [99]. Anyway, it turned out that also the fit formula for proton-impact target excitation could be used to fit the data for proton-impact charge transfer. The final parameters for $H^+ + Na(3s) \rightarrow H^+ + Na(4d)$ were chosen as start parameters. The used fit formula for both proton-impact ionization and single electron capture is:

$$\sigma_{H^+}^{ION,CT}(E/keV)[cm^2] = A_1 \cdot 10^{-16}\Big\{\frac{e^{-A_2/E}\cdot(A_{12}+\ln(A_{11}+A_3E))}{E}+ \\ + A_4\cdot\frac{e^{-A_5E}}{E^{A_6}} + A_7\cdot\frac{e^{-A_8/E}}{1+A_9\cdot E^{A_{10}}}\Big\}\cdot\Theta(E-E_{low}) \tag{4.10}$$

with

$A_1 - A_{12}$: Fit parameters

E: Energy in keV

E_{low}: Energy limit in the low energy region

According to this formula, the collected data were fitted for ground state ionization and single electron transfer, see Tab.4.2, Fig.4.3, and Fig.4.4. These figures show in both cases that the calculated cross sections of J. Schweinzer, [102], match the recommended cross section extraordinarily well. Therefore it can be argued, that the Schweinzer calculations for higher state target electron loss suffice for the calculation of the recommended cross sections. Fig.4.5underlines this argumentation showing electron loss as sum of ionization and single electron charge transfer and comparing this sum with the AO-CC calculations by Schweinzer.

	$\mathbf{E_{low}}$	$\mathbf{A_1}$	$\mathbf{A_2}$	$\mathbf{A_3}$	$\mathbf{A_4}$	$\mathbf{A_5}$	$\mathbf{A_6}$	$\mathbf{A_7}$	$\mathbf{A_8}$	$\mathbf{A_9}$	$\mathbf{A_{10}}$	$\mathbf{A_{11}}$	$\mathbf{A_{12}}$
ION	1	8.389	8.83	$-7.95\cdot10^{-4}$	-0.179	0.4266	-2.554	1.13	2.095	$1.52\cdot10^{-3}$	1.998	2.02	21.21
CT	0.5	24.21	1.0	0	$1.68\cdot10^{-3}$	5.02	-18.34	3.342	0.798	$8.155\cdot10^{-4}$	3.25	1.0	0

Table 4.2: Fit parameters for proton-impact target ionization (ION) and single-electron charge transfer (CT) from Na(3s)

In the earlier publication [99], Schweinzer et al. offer two fit formulae for electron loss in the case of non-resonant and of almost resonant charge transfer (both together with ionization). It turned out, though, that the formula which takes the non-resonant charge transfer into account could be used for all processes with sodium.

$$\textbf{Li}: \quad \sigma_{H^+}^{ELOSS}(E/keV)[cm^2] = A_1 \cdot 10^{-16} \left\{ \frac{e^{-A_2/E} \cdot \ln(1 + A_3 E)}{E} + A_4 \cdot \frac{e^{-A_5 E}}{E^{A_6} + A_7 E^{A_8}} \right\} \tag{4.11}$$

with

$A_1 - A_8$: Fit parameters

E: Energy in keV

All of the considered transitions could be fitted without the fit parameter A_7, i.e. $A_7 = 0$. Whenever $A_7 = 0$, there is no use for the fit parameter A_8, because $A_7 \cdot E^{A_8}$ will equal zero anyway. Thus, both A_7 and A_8 were removed from the formula. To be consistent with the other cross section formulae, the same Θ-function was introduced to limit the low energy range. This leads to the following formula:

$$\sigma_{H^+}^{ELOSS}(E/keV)[cm^2] = A_1 \cdot 10^{-16} \left\{ \frac{e^{-A_2/E} \cdot \ln(1 + A_3 E)}{E} + A_4 \cdot \frac{e^{-A_5 E}}{E^{A_6}} \right\} \cdot \Theta(E - E_{low}) \qquad (4.12)$$

with

$A_1 - A_6$: Fit parameters

E: Energy in keV

E_{low}: Energy limit in the low energy region

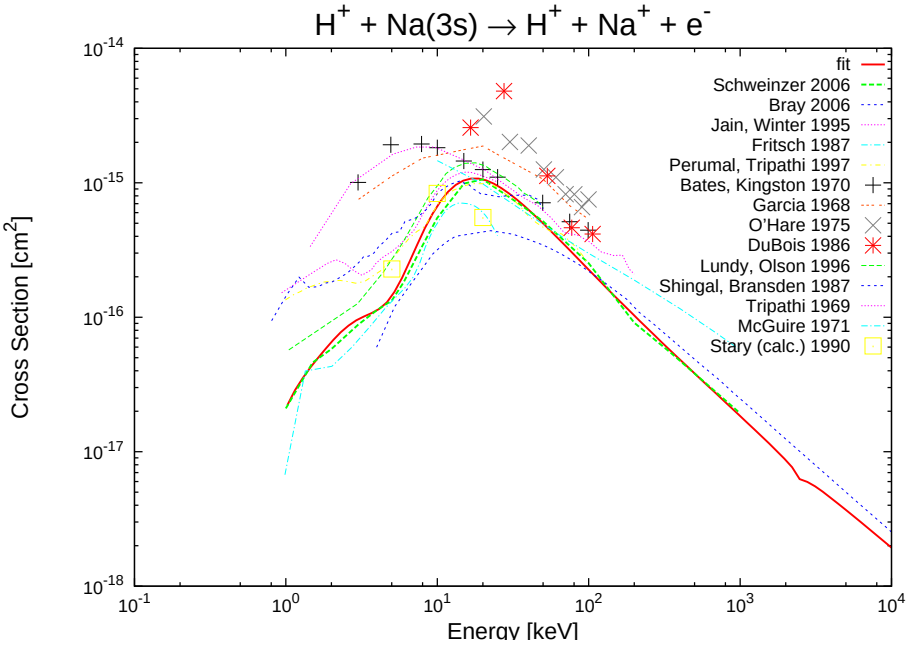

Figure 4.3: Cross sections for proton-impact target ionization from Na(3s)

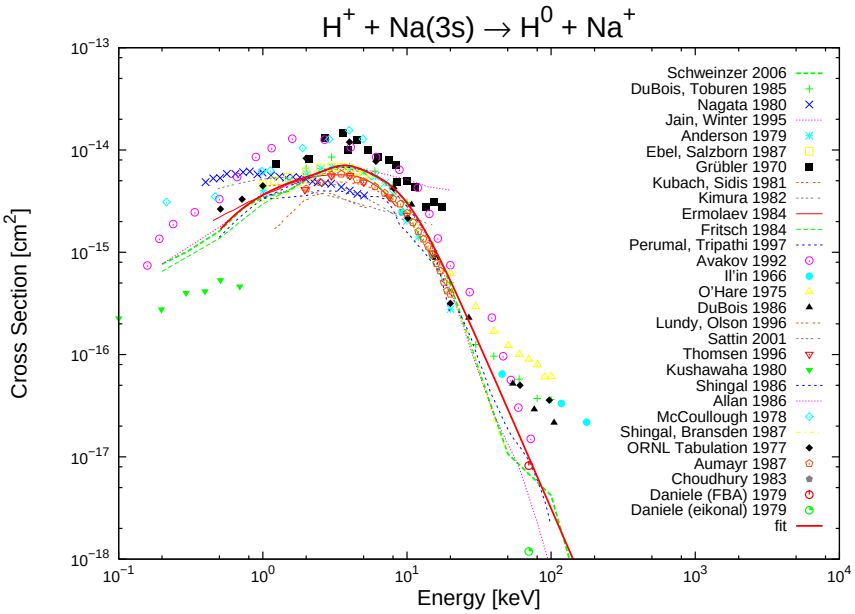

Figure 4.4: Cross sections for proton-impact single-electron charge transfer from Na(3s)

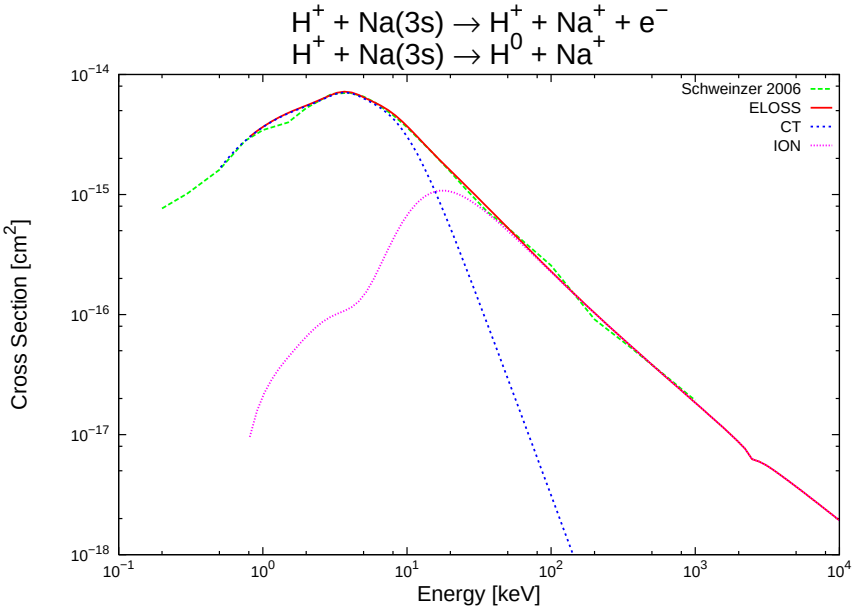

Figure 4.5: Comparison between electron loss (ELOSS) as sum of ionization (ION) and single electron charge transfer (CT) and AO-CC calculations of electron loss by Schweinzer [102]

4.5 Levenberg-Marquardt-Method for Non-Linear Fits

Gnuplot [21] uses a special least square fitting routine for non-linear fits called the *Levenberg-Marquardt Method* [38]. This method is a numerical optimization algorithm that minimizes non-linear functions over the space of the parameters of the function. It varies smoothly between the Gauß-Newton method (also: inverse-Hessian method) and the method of steepest gradient descent. The Levenberg-Marquardt Method is more robust than the Gauß-Newton algorithm, which means that in many cases it finds a solution even if it starts very far off the final minimum. It is nevertheless useful to provide a reasonable set of start parameters especially with regard to the computation time. [38]

In error estimations, the distance is adopted with its square, because negative and positive distances are equally weighted and further off points are considered to be more important. For a general model function $y = y(x; \mathbf{a})$ with $x = (x_1, \dots x_N)$ a possible error function (also: merit function) can be

$$\chi^2(\mathbf{a}) = \sum_{i=1}^{N} \left[\frac{y_i - y(x_i; \mathbf{a})}{\sigma_i} \right] \tag{4.13}$$

The gradient of χ^2 with respect to the parameters $\mathbf{a}$, which will be zero at the minimum of χ^2, has components

$$\frac{\partial \chi^2}{\partial a_k} = -2 \sum_{i=1}^{N} \frac{[y_i - y(x_i; \mathbf{a})]}{\sigma_i^2} \frac{\partial y(x_i; \mathbf{a})}{\partial a_k} \qquad k = 1, 2, \dots, M \tag{4.14}$$

Taking an additional partial derivative gives

$$\frac{\partial^2 \chi^2}{\partial a_k \partial a_l} = 2 \sum_{i=1}^{N} \frac{1}{\sigma_i^2} \left[\frac{\partial y(x_i; \mathbf{a})}{\partial a_k} \frac{\partial y(x_i; \mathbf{a})}{\partial a_l} - [y_i - y(x_i, \mathbf{a})] \frac{\partial^2 y(x_i, \mathbf{a})}{\partial a_l \partial a_k} \right] \tag{4.15}$$

Sufficiently close to the minimum, the χ^2 function is supposedly well approximated by a quadratic form

$$\chi^2(\mathbf{a}) \approx \gamma - \mathbf{d} \cdot \mathbf{a} + \frac{1}{2} \mathbf{a} \cdot \mathbf{D} \cdot \mathbf{a} \tag{4.16}$$

where $\mathbf{d}$ is an M-vector and $\mathbf{D}$ is an M x M matrix [38]. If the approximation is a good one, the current trial parameters $\mathbf{a_{cur}}$ can be changed to the minimized parameters $\mathbf{a_{min}}$. [38]

$$\mathbf{a_{min}} = \mathbf{a_{cur}} + \mathbf{D}^{-1} \cdot \left[-\nabla \chi^2(\mathbf{a_{cur}}) \right] \tag{4.17}$$

The matrix $\mathbf{D}$ is the second derivative of the χ^2 function and thus the Hessian matrix. The exact form of χ^2 is known since it is based on the model function $y(x; \mathbf{a})$ that has been specified in the beginning. Thus, the Hessian matrix is known and its inverse can be determined. This method is called the **Gauß-Newton** or **inverse Hessian method**. [38]

It is conventional to remove the factors of 2 in equation (4.15) by defining

$$\beta_k \equiv -\frac{1}{2}\frac{\partial \chi^2}{\partial a_k} \qquad \alpha_k l \equiv \frac{1}{2}\frac{\partial^2 \chi^2}{\partial a_k \partial a_l} = \frac{1}{2}\mathbf{D} \tag{4.18}$$

Thus equation (4.15) can be rewritten as the set of linear equations

$$\sum_{l=1}^{M} = \alpha_{kl}\delta a_l = \beta_k \tag{4.19}$$

This set is solved for the increments δa_l that, added to the current approximation, gives the next approximation. [38]

If the approximation (4.16) is poor, **the steepest gradient method** [38] has to be used. A set of new parameters $\mathbf{a_{next}}$ is defined as follows

$$\mathbf{a_{next}} = \mathbf{a_{cur}} - \text{constant} \times \nabla \chi^2(\mathbf{a_{cur}}) \tag{4.20}$$

where the constant is small enough not to exhaust the downhill direction. Using equation (4.18), the steepest gradient formula (4.20) translates to

$$\delta a_l = \text{constant} \times \beta_l \tag{4.21}$$

According to the propositions of Levenberg, the steepest gradient descent method is used far from the minimum switching to the Gauß-Newton method as the minimum is approached. For the use of the steepest gradient descent method, at least the order of magnitude of the constant in equation (4.21) needs to be known. Marquardt realized that the components of the Hessian matrix $\mathbf{D}$ give some insight about the order-of-magnitude scale of the problem, even is they are not usable in any precise fashion in the Gauß-Newton algorithm. χ^2 is nondimensional, i.e. is a pure number. On the other hand, β_k has the dimensions of $1/a_k$, which may be dimensional in some cases. The constant of proportionality between β_k and δa_k must therefore have the dimensions of a_k^2. The only obvious quantity with these dimensions is $1/\alpha_{kk}$, the reciprocal of the diagonal element. So that must be the scale of the constant. But the scale might itself be too big. Thus, the constant is divided by the nondimensional fudge factor λ with the possibility of setting $\lambda \gg 1$ to cut down the step. [38]

$$\delta a_k = \frac{1}{\lambda \alpha_{kk}}\beta_k \qquad \text{or} \qquad \lambda \alpha_{kk}\delta a_k = \beta_k \tag{4.22}$$

Equations (4.22) and (4.19)an be combined if a new matrix α' is defined by the following prescription

$$\begin{aligned} \alpha'_{jj} &\equiv \alpha_{jj}(1+\lambda) \\ \alpha'_{jk} &\equiv \alpha_{jk} \qquad (j \neq k) \end{aligned} \tag{4.23}$$

and replace both (4.22) and (4.19) by

$$\sum_{l=1}^{M} \alpha'_{kl} \delta a_l = \beta_k \tag{4.24}$$

When λ is very large, the matrix α' is forced into being diagonally dominant and thus equation (4.24) goes over to (4.19). [38]

Given the initial guess of the fit parameters $\mathbf{a}$, the recommended recipe of Marquardt is as follows [38]:

1. Compute χ^2.
2. Pick a modest value for λ.
3. Solve the linear equations (4.24) for $\delta\mathbf{a}$ and evaluate $\chi^2(\mathbf{a}+\delta\mathbf{a})$.
4. If $\chi^2(\mathbf{a}+\delta\mathbf{a}) \geq \chi^2(\mathbf{a})$, increase λ by a substantial factor, e.g. 10, and go back to step 3.
5. If $\chi^2(\mathbf{a}+\delta\mathbf{a}) < \chi^2(\mathbf{a})$, decrease λ by a substantial factor, e.g. 10, update the trial solution $\mathbf{a} \leftarrow \mathbf{a}+\delta\mathbf{a}$ and go back to step 3.

The necessary stopping criterion is quite simple. If χ^2 decreases several times by a negligible amount, the minimum is reached. [38]

4.6 Tools

4.6.1 `addfit`

`addfit` is a C++ code I developed during this diploma thesis to simplify three tasks.

1. Add new data to the database.
2. Fit this new data with gnuplot.
3. Create a new eps plot.

`addfit` is a very straight forward code. It needs the following inputs from the command line.

- The name of the database file to which new data should be added.
- The name of the file with the new data.
- The cross section values are stored in units of cm^2. In some cases the authors of the used publication used different units. In case of $Å^2$ and Mb the easy-to-do conversion should be done while acquiring the values (e.g. digitizing an image). In case of units of πa_0^2 the conversion cannot be done that easily. Thus, `add2db` offers the additional option to choose if the data need to be converted from units of πa_0^2 to cm^2.
- `addfit` calls the local function `write_gpl` which requires the plot style (lines, points, linespoints) to be entered.

`addfit` uses the possibility to pipe other programs, such as gnuplot or ghostview. Its basic structure is shown in the flow diagram in Fig.4.6. The source code is listed in the appendix in chapter B on page 120.

4.6.2 Conversion of Data Files to IPP Format

The simulation code `Na_simula` was developed at the IPP. It requires only the analytical formulae and the corresponding parameters. This information, though, is read from a text file with a certain input format. The C++-code `iap2ipp` was developed to transform the ∗.param files to the required format. It is described in detail by the flow diagrams in Fig.4.7 and Fig.4.8.

The input file for the use with the IPP code is structured as follows: For every process and every transition there is a corresponding line. Each line starts with an explanatory part, e.g.

$$\underbrace{\texttt{1, 2,}}_{\text{initial, final state}} \qquad \underbrace{\texttt{'eexc Na 3s3p'}}_{\text{name of the fit function}}$$

The initial and final states are numbered as shown in Tab.4.3. For ionization and electron loss processes the final state is not listed, but the initial state twice. E.g. for electron impact ionization from Na(3p) it is written: `2, 2, 'eion Na 3p'`

State	Numbering
3s	1
3p	2
3d	3
4s	4
4p	5
4d	6
4f	7
5s	8

Table 4.3: Numbering of the sodium states in an IPP formatted file

This explanatory part of each line is then followed by the necessary constant parameters (ΔE, I_{nl}, E_{low}). The number of columns is a fixed value. Thus, if there are less parameters for one transition than for another, a corresponding number of empty comma-separated columns.

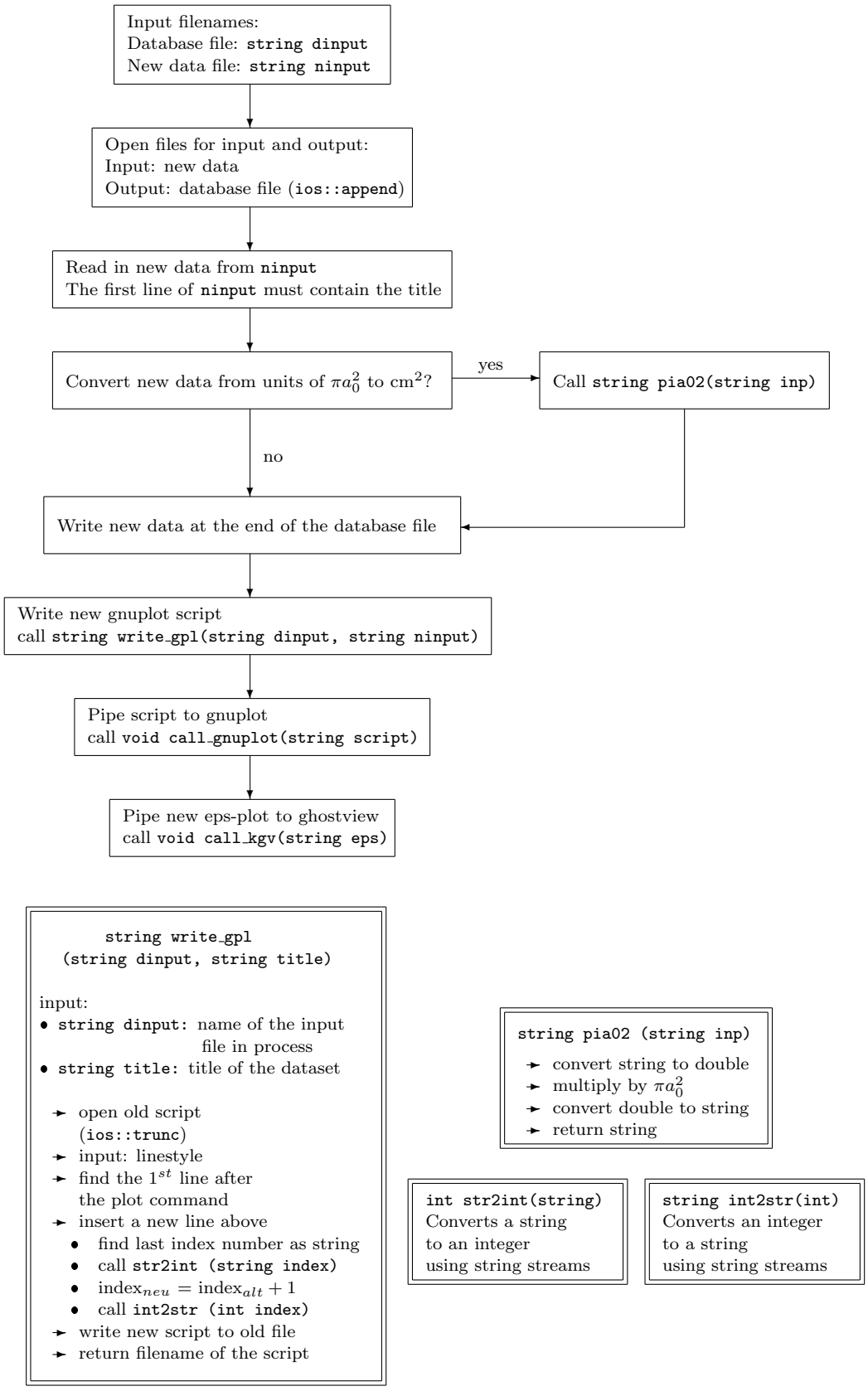

Figure 4.6: Flow diagram of `addfit`

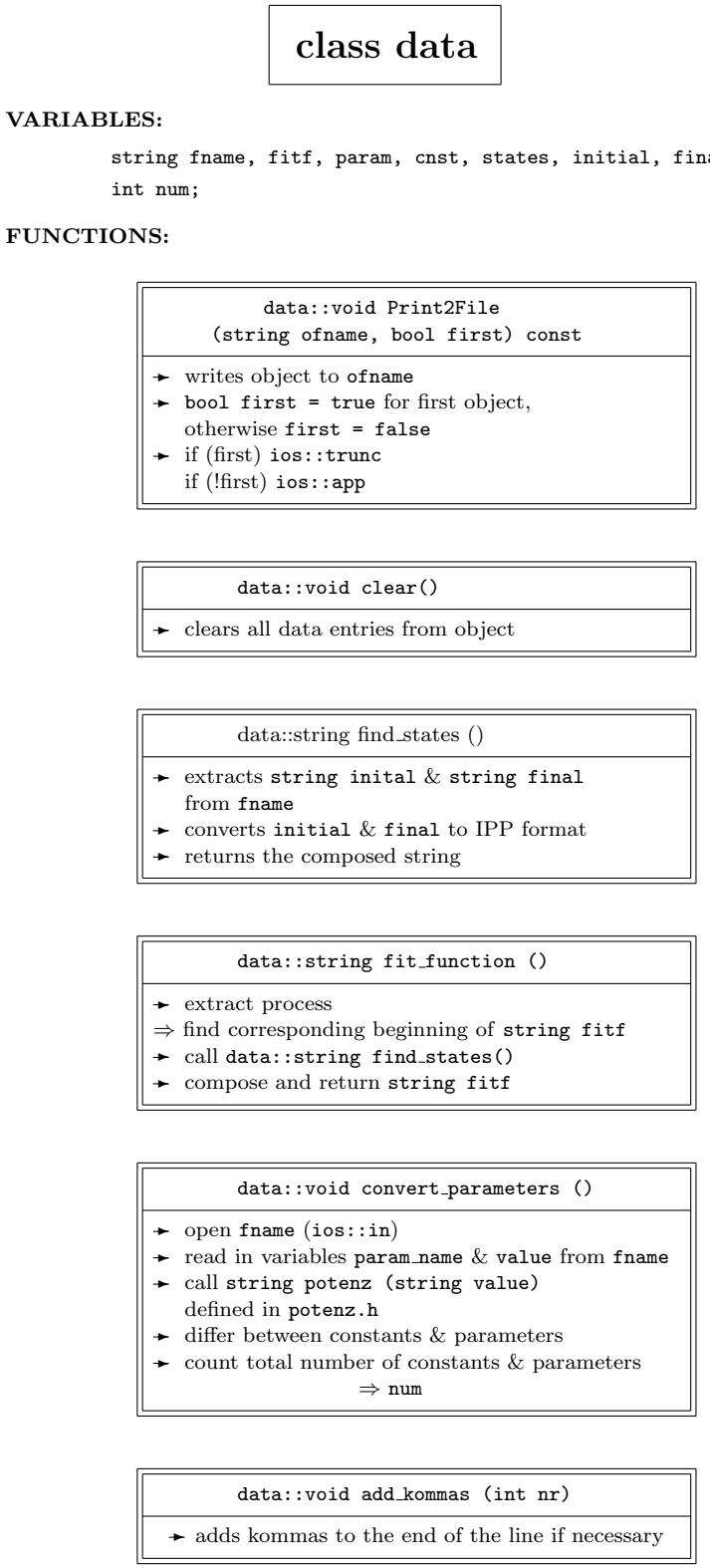

Figure 4.7: Diagramm of `class data` used in `iap2ipp`

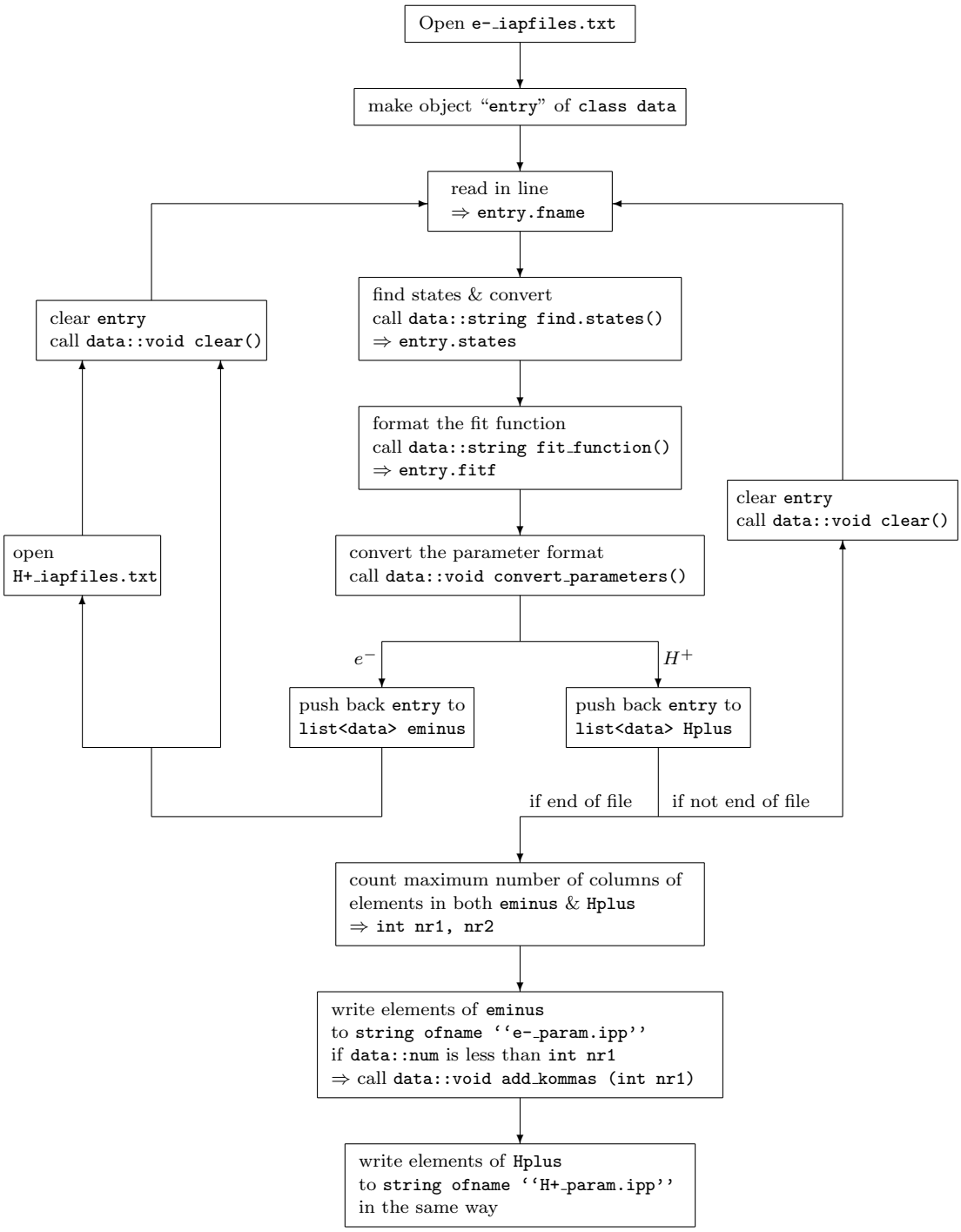

Figure 4.8: Flow diagram of `iap2ipp`

4.6.3 Gnuplot Scripts

To visualize the data, Gnuplot 4.0, [21], was used. For each dataset file, a customized gnuplot script was written. When loaded in gnuplot these scripts output customized eps-plots.

During each call of `addfit` a new gnuplot script is written by the function `write_gpl` where a new plot command for the new data is added, see also Fig.4.6. The title of the new data is the first line of the input file. From the command line, `write_gpl` reads the line style it is supposed to use for the new dataset.

This newly written script is then piped to gnuplot where it is executed. A commented exemplary script can be found in the appendix in chapter D on page 136. Further questions concerning gnuplot are well explained in [103].

When gnuplot plots to enhanced encapsulated poscript files it supports nine different line style. If this number of line styles is exceeded in a plot the tenth line uses the same line style as the first one. Unfortunately, it is not possible to include more line style in gnuplot. Thus, the only possibility left, is to manually change the postscript code. The required steps are descriped in the Appendix section E on page 138.

Chapter 5

Results

5.1 Text Data Files & Parameter Files

For each process, each transition, there is a set of files that belong together. They are each named the same way, according to the described process, and differ only in the file extension, see Tab. 5.1. The file names compose of three parts: the first states the process type, the next the incident particle, and the last the sodium states in question, see Tab. 5.2. Some examples:

- Electron-impact target excitation from Na(4s) to Na(4d): `EXC_e-_4s_4d`
- Electron-impact target ionization from Na(3p): `ION_e-_3p`
- Proton-impact charge transfer from Na(3s): `CT_H+_3s`
- Proton-impact target electron loss from Na(4p): `ELOSS_H+_4p`

File Extension	Content
∗.csv	data file
∗.param	parameter file
∗.gpl	gnuplot script
∗.eps	eps plot

Table 5.1: Explanation of the used file extensions

The data are collected in simple structured ASCII text files that can be read by any text editor on an y operating system. Every data set csv-file starts with a preamble that states the process and the data structure. For example, for electron-impact excitation from the ground state to the first excited state, the preamble looks like

	Possibilities
Process type	EXC: Excitation ION: Ionization CT: Charge transfer
Incident particle	e-: Electron H+: Proton
States in question	Initial state, final state (EXC) Initial state (ION, CT, ELOSS)

Table 5.2: Explanation of the used filename formalism

```
#Cross Sections for electron impact excitation 3s->3p
#x-values = energy [eV]
#y-values = cross section [cm**2]
#
```

This preamble is followed by the data. The data is written in block format. This means, that the data sets are separated by two empty lines. Gnuplot refers to these blocks using indices. Thus, the data sets can be plotted block by block. Every data set block is led in by a comment about the used paper, for example

```
#From:  J.O. Phelps, C.C. Lin:
# Electron-impact excitation of the sodium atom.
# Phys.  Rev.  A, 1981, Vol.  32, No.3, p.1299-1326, Tab.  3, experimental
#
```

Furthermore, for each transition, there is a file containing the values of the necessary parameters for fitting. That is to say, the fit parameters, the threshold energies if needed, and the low energy limit. These parameter files are loaded when the corresponding gnuplot script is loaded.

5.2 Fit Parameters & Recommended Cross Sections

The origin of the fit formulae is described in sections 4.1 to 4.4.

5.2.1 Electron-Impact Target Excitation Cross Sections

Fit formula, see eq. (4.4):

$$\sigma_{e^-}^{EXC}(e/eV)[cm^2] = \frac{A_7 \cdot 10^{-16}}{E}\left[\frac{E-\Delta E}{E}\right]^{A_6} \cdot \left[\sum_{j=1}^{4}\frac{A_j}{(E/\Delta E)^{j-1}} + A_5 \cdot \ln\left(\frac{E}{\Delta E}\right)\right] \cdot \Theta(E - E_{low})$$

nl → n′l′	ΔE	E_{low}	A_1	A_2	A_3	A_4	A_5	A_6	A_7
3s → 3p	2.09937	2.11032	-18.9092	27.9468	11.2965	23.0811	27.2262	1.1869	13.9771
3s → 3d	3.61642	3.69	28.9488	-54.7116	29.6747	-3.73507	-0.2581	-0.8286	2.0066
3s → 4s	3.19192	3.2	4.47925	-10.5276	1.9351	10.8448	0	0.58	6.39143
3s → 4p	3.75248	3.8	2.3	14.3368	-53.4352	51.3017	1.4711	0.9986	3.4
3s → 4d	4.28447	4.5	4.2127	8.0062	-36.4161	31.6055	0.1524	0.51	2.82
3s → 4f	4.28855	4.5	0.0985	3.1461	-7.9142	5.5438	0.01821	0.1865	6.9578
3s → 5s	4.11711	4.4	1.70043	-6.95378	10.1069	-4.94309	0.06017	-1.27482	2.685
3p → 3d	1.51705	1.5444	-193.8	159.454	220.996	-170.076	154.298	0.1226	2.9867
3p → 4s	1.09255	1.1	-11.6517	14.5094	-15.4778	30.7675	11.2656	0.828943	10.0634
3p → 4p	1.65311	1.7	6.32452	-10.3188	11.9379	0	0.311935	0.879263	9.62216
3p → 4d	2.1851	2.3	-2.1686	-36.4101	86.9806	-38.8431	16.307	0.06977	2.2177
3p → 4f	2.18918	2.4	18.5382	-65.7558	79.6491	-32.6882	0.01635	-2.30287	1.9188
3p → 5s	2.01774	2.4	1.2911	-14.0441	29.5538	-16.5211	1.56757	0.02045	3.2114
3d → 4p	0.13606	0.18	-4.5335	-6.44245	134.798	-22.712	12.205	4.1264	54.709
3d → 4d	0.668046	1.4	2.0758	21.5014	-131.69	288.078	0.12386	4.6445	80.4435
3d → 4f	0.672127	1.6	-49.3219	-46.9656	-727.903	$5.37{\cdot}10^{3}$	67.4118	6.0361	15.8765
3d → 5s	0.50069	2	2.9095	-19.4677	40.5386	-24.2794	$8.4{\cdot}10^{-3}$	-10.8462	8.5803
4s → 3d	0.4245	1.3	4.2111	-33.5726	172.199	-83.556	0.0139091	6.08203	135.795
4s → 4p	0.56056	0.81	-893.212	$1.246{\cdot}10^{3}$	0	0	809.432	1.08958	2.74633
4s → 4d	1.09255	1.31	-7.93026	-128.218	498.292	-551.771	-0.0371	1.91423	-11.4158
4s → 4f	1.09663	1.31	310.775	-691.614	553.784	-62.6059	-11.0055	0	0.633695
4s → 5s	0.92519	1.31	8.9011	-54.6408	115.263	-55.0372	0.6503	1.5991	11.8926
4p → 4d	0.531986	0.75	$3.7327{\cdot}10^{5}$	$-3.8638{\cdot}10^{4}$	$-1.345{\cdot}10^{6}$	$8.6627{\cdot}10^{4}$	$-2.5136{\cdot}10^{5}$	3.16917	$-5.3626{\cdot}10^{-3}$
4p → 4f	0.536067	1.3	10.6294	1.2563	-296.219	$1.115{\cdot}10^{3}$	-0.1665	7.1713	85.898
4p → 5s	0.36463	1.2	4.09747	-109.54	797.685	-795.334	1.6164	11.5024	249.496
4d → 4f	$4.08{\cdot}10^{-3}$	0.22	-751.68	$-1.40{\cdot}10^{3}$	431.435	-2.5172	784.257	-5.71266	4.75396
5s → 4d	0.167356	0.38	7.5019	-54.5559	227.922	-92.4478	0.43061	6.3889	195.285
5s → 4f	0.171437	0.38	12.4203	-126.653	615.687	-306.243	-0.041334	4.36124	34.695

Table 5.3: Fit parameters for electron-impact target excitation cross section of Na($nl \rightarrow n'l'$); $n, n' = 3-5$

5.2.2 Electron-Impact Target Ionization Cross Sections

Fit formula, see eq. (4.8):

$$\sigma_{e^-}^{ION}(E/eV)[cm^2] = \frac{A_5 \cdot 10^{-13}}{E \cdot I_{nl}} \cdot \left[A_4 \cdot \ln\left(\frac{E}{I_{nl}}\right) + \sum_{j=1}^{3} A_j \cdot \left(1 - \frac{I_{nl}}{E}\right)^j \right] \cdot \Theta(E - E_{low}) + \\ + \sum_{i=2}^{3} a_i q_i \frac{\ln(E/P_i)}{E \cdot P_i} 1 - b_i \cdot \exp(-c_i(E/P_i - 1)) \cdot \Theta(E - P_2);$$

with

$P_2 = 34\ eV$:	Binding energy of electrons in the 2p subshell
$P_3 = 67\ eV$:	Binding energy of electrons in the 2s subshell
$q_2 = 6$:	Number of equivalent electrons in the 2p subshell
$q_3 = 2$:	Number of equivalent electrons in the 2s subshell
$a_2 = 3.0,\ b_2 = 0.9,\ c_2 = 0.2$:	Individual constants for the 2p electrons
$a_3 = 4.0,\ b_3 = 0.7,\ c_3 = 0.5$:	Individual constants fr the 2s electrons

nl	I_{nl}	E_{low}	A_1	A_2	A_3	A_4	A_5
3s	5.13891	5.2	38.4307	14.1114	58.4617	-2.903	$7.5746 \cdot 10^{-3}$
3p	3.03954	3.4	20.322	8.6464	48.2455	-0.3795	0.0132019
3d	1.52249	1.88	-0.159239	0.064144	-0.328382	0.0116868	-2.7587
4s	1.94699	2.31	0.408646	-0.19513	0.768724	-0.0596801	1.16244
4p	1.38643	1.75	0.749247	-0.48139	1.74819	-0.0552913	0.478343
4d	0.854444	1.88	-0.493	2.0871	-2.8336	0.0265	-0.50585
4f	0.850363	1.21	0.9819	-4.9374	3.0648	0.03269	-0.74012
5s	1.0218	1.38	1.8887	5.3592	-1.2336	-0.23	0.12969

Table 5.4: Fit parameters for electron-impact target ionization cross sections of Na(nl), $n = 3 - 5$

5.2.3 Proton-Impact Target Excitation Cross Sections

Fit formula, see eq. (4.9):

$$\sigma_{H^+}^{EXC}(E/keV)[cm^2] = A_1 \cdot 10^{-16} \Big\{ \frac{e^{-A_2/E} \cdot (A_{12} + \ln(A_{11} + A_3 E))}{E} + \\ + A_4 \cdot \frac{e^{-A_5 E}}{E^{A_6}} + A_7 \cdot \frac{e^{-A_8/E}}{1 + A_9 \cdot E^{A_{10}}} \Big\} \cdot \Theta(E - E_{low})$$

$\mathbf{nl \rightarrow n'l'}$	$\mathbf{E_{low}}$	$\mathbf{A_1}$	$\mathbf{A_2}$	$\mathbf{A_3}$	$\mathbf{A_4}$	$\mathbf{A_5}$	$\mathbf{A_6}$	$\mathbf{A_7}$	$\mathbf{A_8}$	$\mathbf{A_9}$	$\mathbf{A_{10}}$	$\mathbf{A_{11}}$	$\mathbf{A_{12}}$
3s → 3p	0.2	900.204	1.1413	0.0557	0.04877	$4.680{\cdot}10^{-3}$	0.32994	-0.05805	-0.07156	0.10048	1.0941	0.954	0.04912
3s → 3d	0.3	2.41044	14.6178	$1.661{\cdot}10^{8}$	5.21802	3.18791	-5.45716	2.16505	11.354	$3.92{\cdot}10^{-5}$	2.71674	1	10.0434
3s → 4s	0.2	0.5291	11.1454	13.8	2.21	0.9258	-2.8909	-6.0985	4.29572	$2.6{\cdot}10^{-3}$	2.1235	1.4632	93.1684
3s → 4p	0.3	12.287	1.00965	0.19894	-3.3202	4.7024	-6.149	69.9622	30.4996	3.1234	1.48366	1.38235	-0.32704
3s → 4d	1	0.09605	35.1151	0	6.5924	2.4005	-5.09985	21.6803	7.40333	$2.7{\cdot}10^{-3}$	1.91665	1	272.253
3s → 4f	1	0.4652	44.0372	9.4310^{-31}	1.51204	2.38218	-5.305	178.707	27.0857	0.0628	2.30125	$\cdot 10^{-10}$	29.7278
3s → 5s	1	0.64667	58.7286	7.16916	0.13536	0.7344	-3.13535	-30.1094	56.0422	5.33495	0.8346	1.98065	25.9001
3p → 3d	0.3	445.1540	9.8646	0	0.0851	0.8208	-2.1403	-6.61	7.0552	0.2111	1.0887	1	26.1162
3p → 4s	0.76	195.761	8.9968	0.6025	0.02556	0.480576	-1.7062	$1.88{\cdot}10^{-9}$	-2.6613	0.13106	1.5894	-0.45194	-0.28445
3p → 4p	0.3	74.979	2.2993	$3.38{\cdot}10^{-4}$	36.026	9.8582	-3.94005	18.5736	12.4592	4.6141	1.1604	0.6642	0.7065
3p → 4d	0.5	-5.8037	3.0285	1.9	-0.0762	0.2813	-1.6282	-1.8064	12.7822	0.0361	0.95147	-0.94987	-4.32841
3p → 4f	0.5	17.6253	9.36216	0	0.892868	$7.8587{\cdot}10^{-3}$	0.782358	-6.63413	-0.0354364	7.58916	1.01267	1	4.62623
3p → 5s	1.5	5.7944	6.98495	1.13626	107.387	6.9904	-7.1283	8.6305	114.073	0.42788	1.3713	-1.70258	1.675
3d → 4p	1	75.1862	11.4015	9.22876	51.4774	0.0150284	1.04179	-44.2378	-0.461965	0.778454	2.02353	0.13779	43.0644
3d → 4d	0.2	30.3405	6.373	0	0.2148	0.2718	-1.382	2.0156	0.4264	0.8904	2.6894	1	15.5586
3d → 4f	0.2	9.4813	12.1771	0.9871	-1.3157	0.1007	-1.15457	7.31192	0.31236	0.0875	0.66803	6.8210^{-3}	524.367
3d → 5s	0.3	1.9704	2.8269	0	36.1299	8.329	-0.8423	22.1788	0.9813	0.0776	1.8594	1.0	26.1051
4s → 3d	0.2	76.102	0.108	$1.4{\cdot}10^{3}$	4.79189	27.7	-45.7225	74.7606	1.8727	7.4108	1.094	-41.05	-4.97677
4s → 4p	0.7	68.8461	0.14366	15.908	-46.8482	0.12296	0.67477	1.99805	-1.84266	5.73176	-2.3702	-0.1493	43.5228
4s → 4d	0.3	12.2821	7.48675	0	41.5655	2.9866	-2.8764	47.503	67.1931	-0.91548	1.1443	$9.52{\cdot}10^{-31}$	100
4s → 4f	0.2	18.126	7.2308	0	0.3843	1.20817	-4.77267	1.0506	0.2524	$1.{\cdot}10^{-3}$	2.35044	1	13.724
4s → 5s	0.3	338.828	5.01593	$1.0{\cdot}10^{-9}$	0.418	2.41774	-3.2891	-31.6584	5.4	7.31738	0.89388	0	23.7451
4p → 4d	0.2	448.064	20.144	5.0946	2.8524	3.9198	-1.8966	0.7738	3.00791	0.0527	2.32182	0.70697	10.9817
4p → 4f	0.2	98.1211	5.2274	0	0.1986	0.9862	-3.3092	0.5538	0.09157	0.0539	1.0939	1	9.278
4p → 5s	0.2	694.87	0.0244	0.19797	-0.23535	0.37244	-0.25196	0.07725	0.6874	$-1.38{\cdot}10^{-4}$	$-2.86{\cdot}10^{-4}$	0.99867	$5.05{\cdot}10^{-4}$

Table 5.5: Fit parameters for proton-impact target excitation cross sections of Na($nl \rightarrow n'l'$); $n = 3; n' = 3 - 4$

5.2.4 Proton-Impact Target Electron Loss Cross Sections

Fit formula, see eq.(4.12):

$$\sigma_{H^+}^{ELOSS}(E/keV)[cm^2] = A_1 \cdot 10^{-16} \left\{ \frac{e^{-A_2/E} \cdot \ln(1 + A_3 E)}{E} + A_4 \cdot \frac{e^{-A_5 E}}{E^{A_6}} \right\} \cdot \Theta(E - E_{low})$$

nl	E_{low}	A_1	A_2	A_3	A_4	A_5	A_6
3s	0.2	10.4106	2.5784	$\cdot 10^5$	2.663	0.16797	-0.77476
3p	0.2	27.8562	1.5103	$5.72 \cdot 10^4$	1.86786	0.0564	0.1081
3d	0.2	70.6837	1.40569	186.467	7.252	0.33006	-0.02384
4s	0.2	10.283	1.02595	$5.16 \cdot 10^{13}$	42.9201	0.2232	0.0991
4p	0.2	51.9798	0.3421	827.26	18.0557	1.67386	-2.637
4d	0.2	166.075	0.36976	37.9375	3.4934	0.3921	0.40626
4f	0.2	39.6176	0.24942	69.9964	25.9749	0.27383	0.2004
5s	0.2	16	0.2	$5.168 \cdot 10^{13}$	42.9201	0.223185	0.0991

Table 5.6: Fit parameters for proton-impact target electron loss from Na(nl); $n = 3 - 5$

5.3 Enhanced Postscript Plots with Fits

5.3.1 Electron-Impact Target Excitation Cross Sections

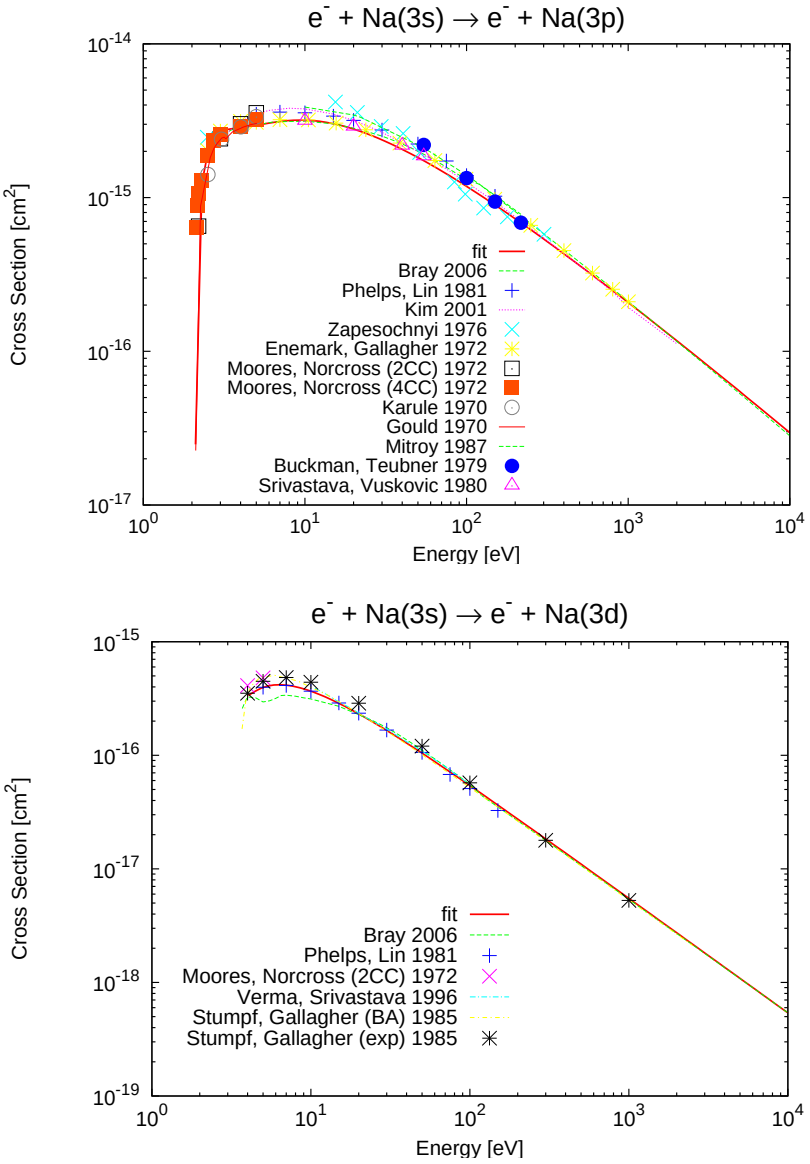

Figure 5.1: Electron-impact target excitation cross sections; 3s → n'l'; $n' = 3 - 4$

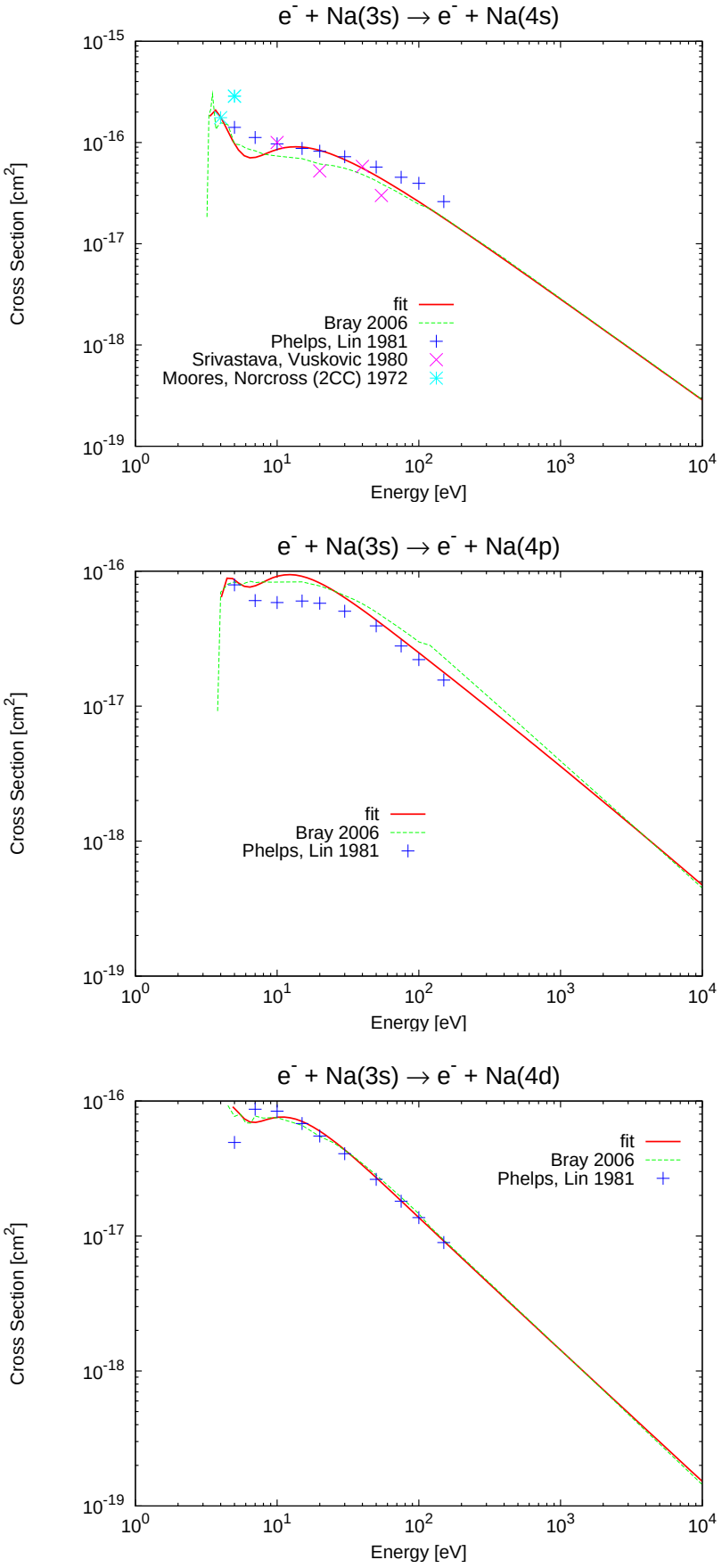

Figure 5.2: Electron-impact target excitation cross sections; 3s → n'l'; $n' = 4$

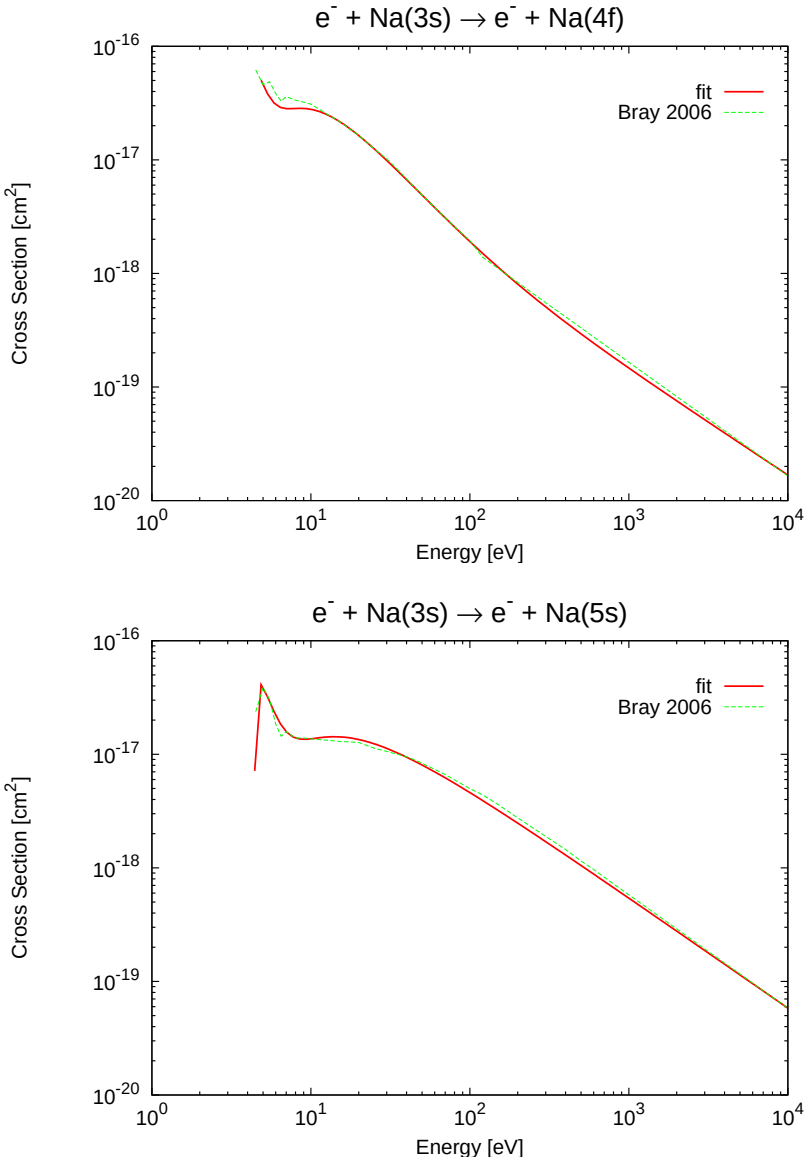

Figure 5.3: Electron-impact target excitation cross section; 3s → n'l'; $n' = 4 - 5$

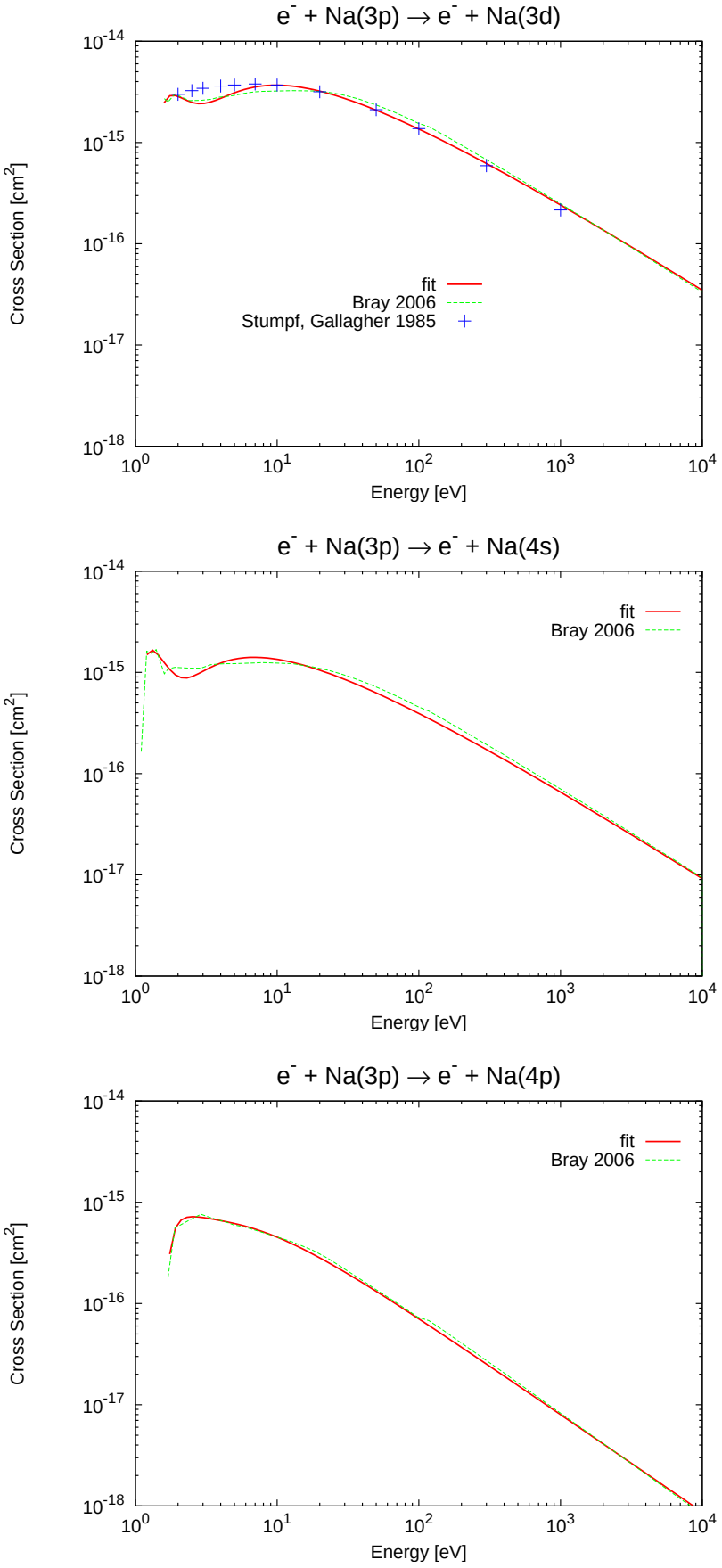

Figure 5.4: Electron-impact target excitation cross sections; 3p → n'l'; $n' = 3 - 4$

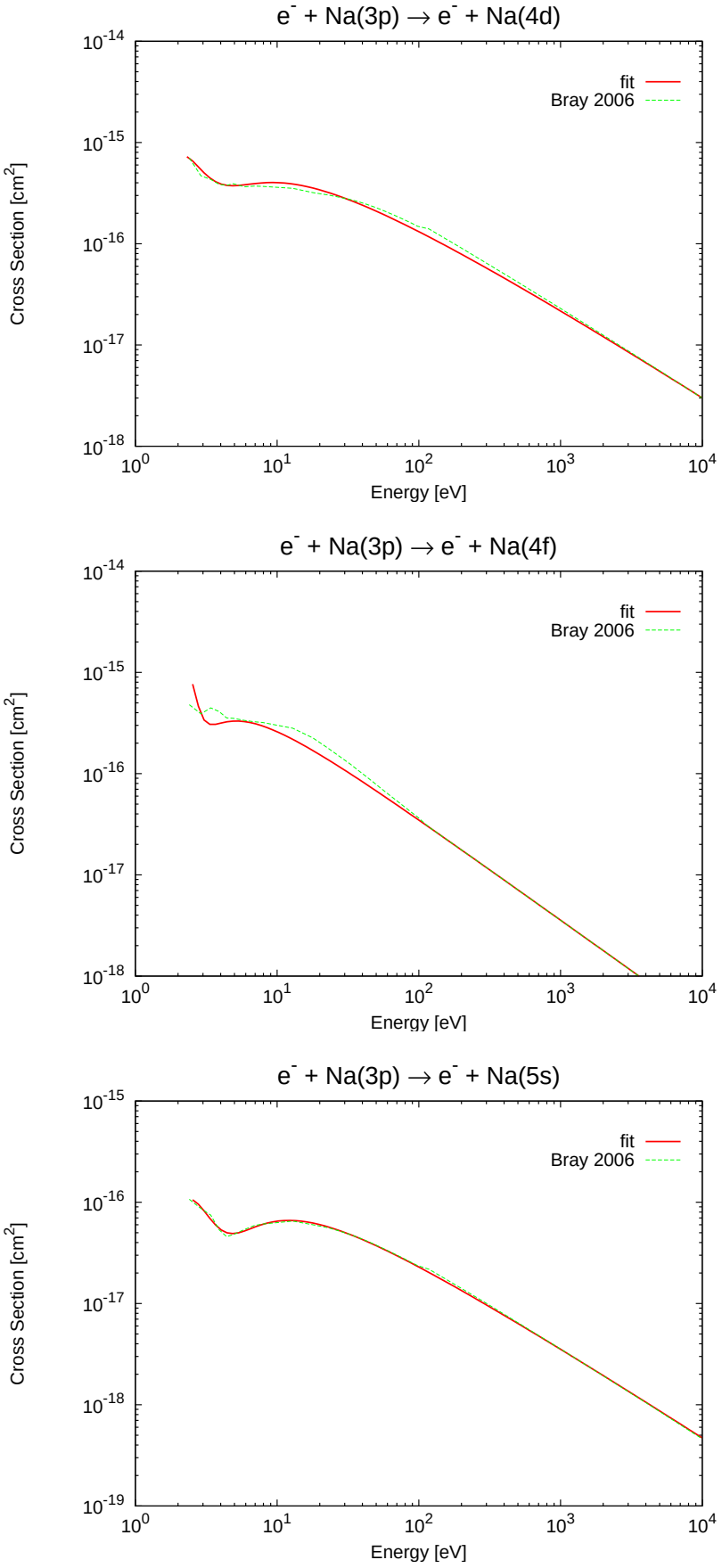

Figure 5.5: Electron-impact target excitation cross sections; 3p → n'l'; $n' = 4 - 5$

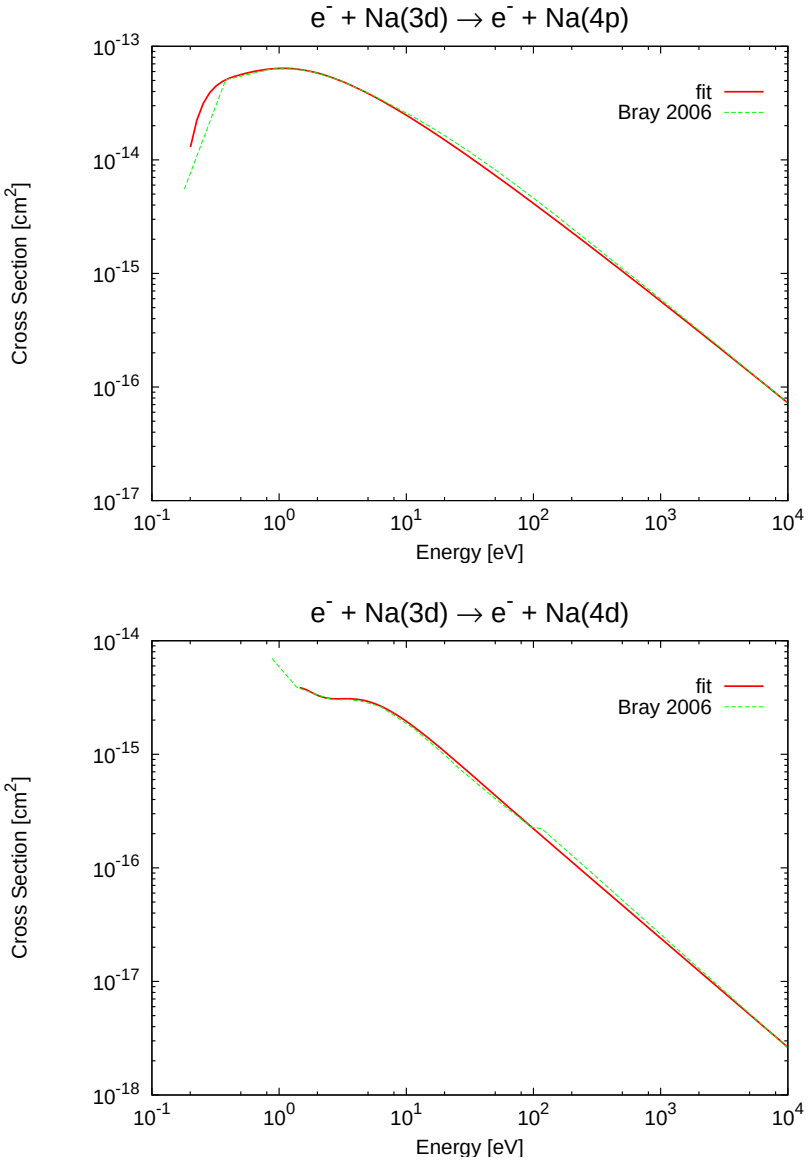

Figure 5.6: Electron-impact target excitation cross sections; 3d → n'l'; $n' = 4 - 5$

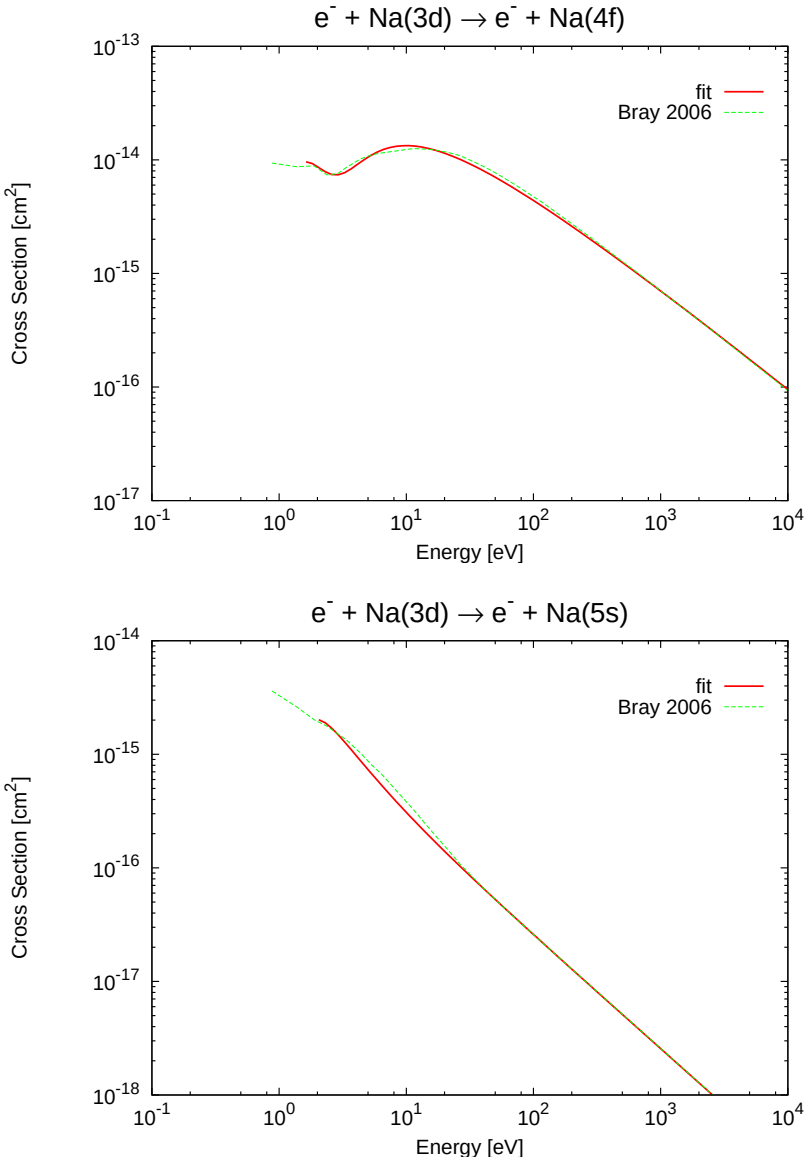

Figure 5.7: Electron-impact target excitation cross sections; 3d → n'l'; $n' = 4 - 5$

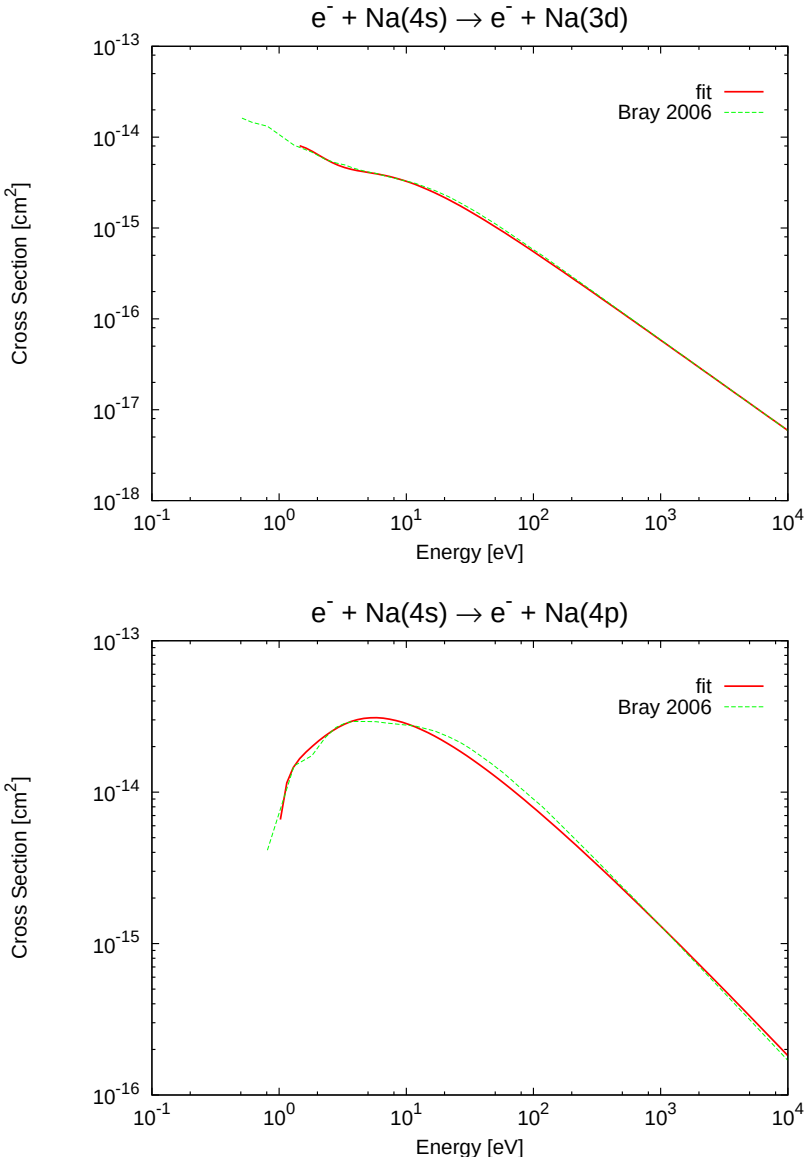

Figure 5.8: Electron-impact target excitation cross sections; 4s → n'l'; $n' = 4 - 5$

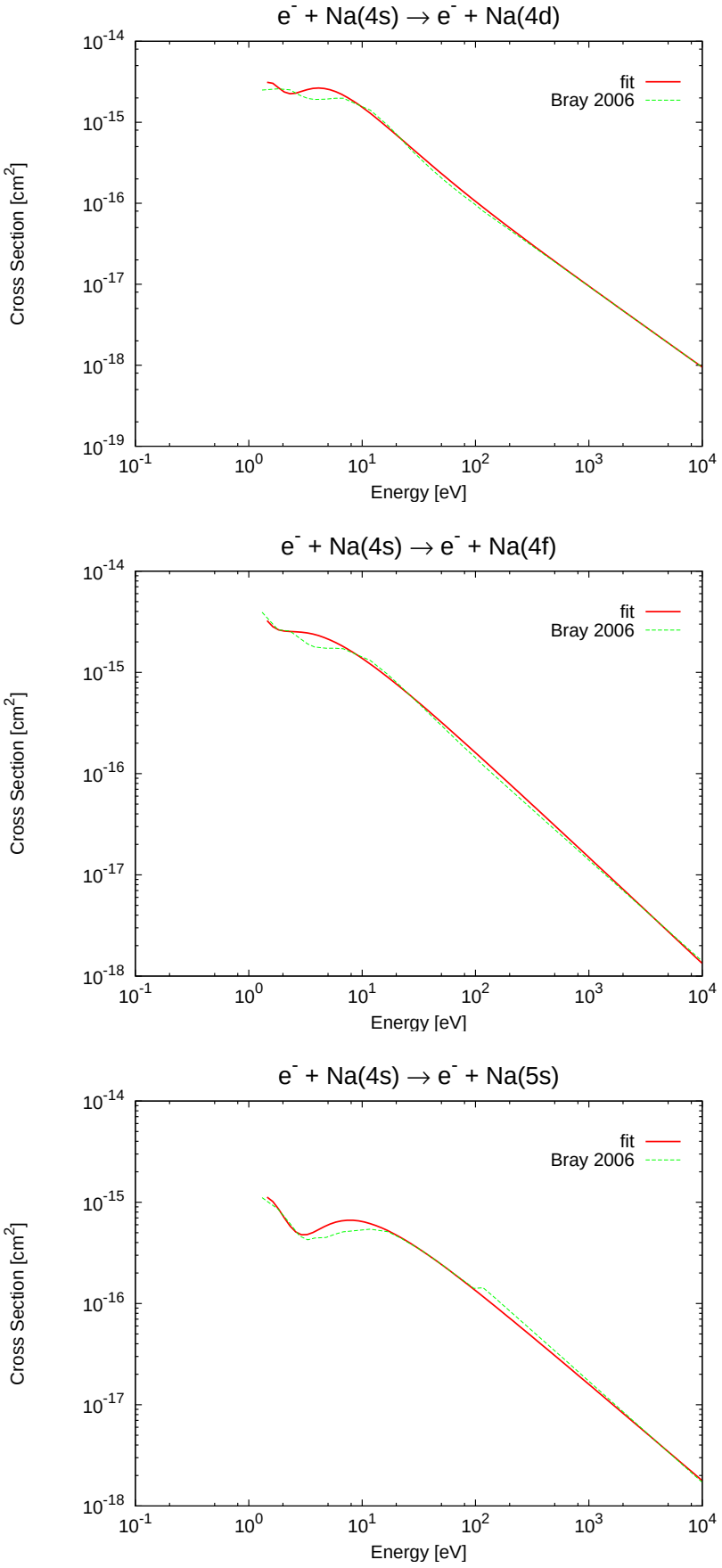

Figure 5.9: Electron-impact target excitation cross sections; 4s → n'l'; $n' = 4 - 5$

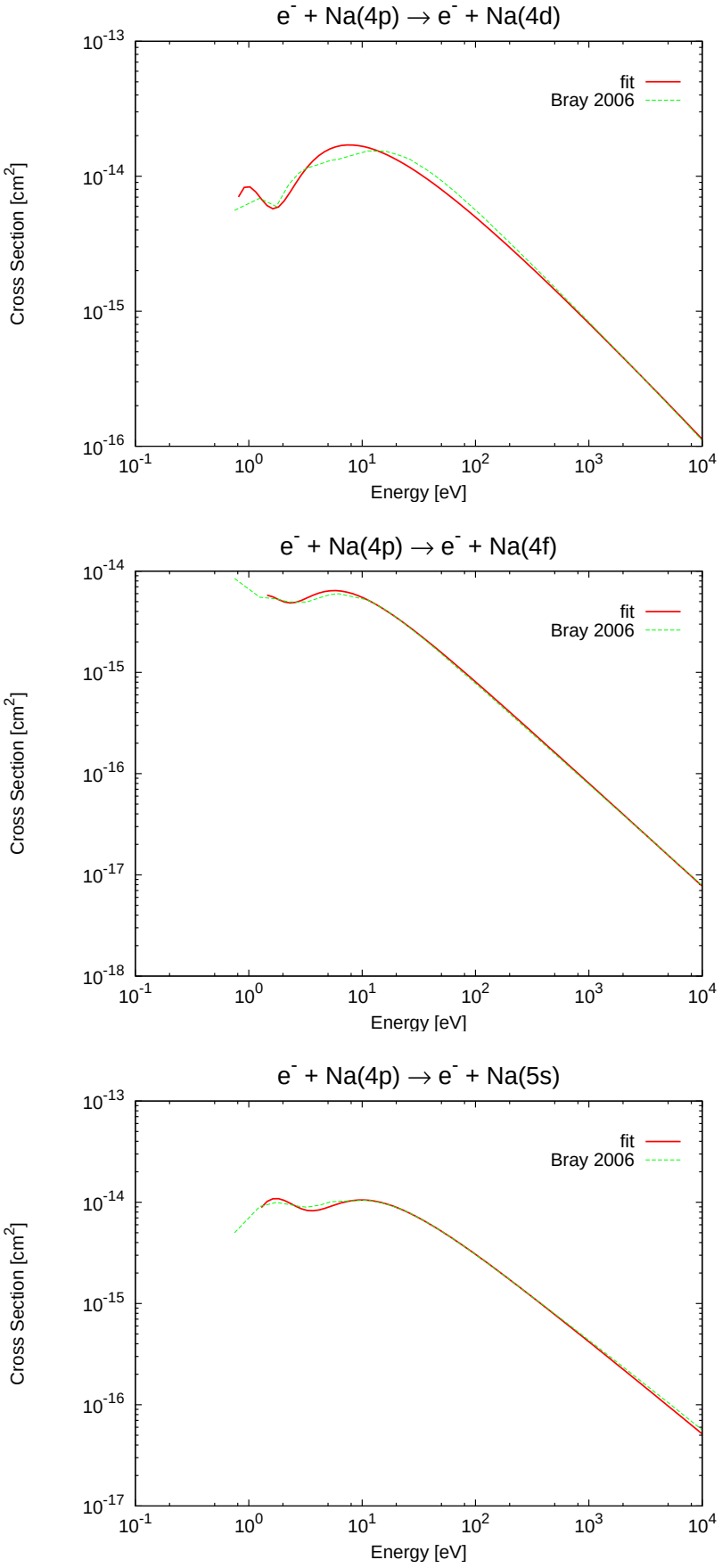

Figure 5.10: Electron-impact target excitation cross sections for 4p → n'l', $n' = 4 - 5$

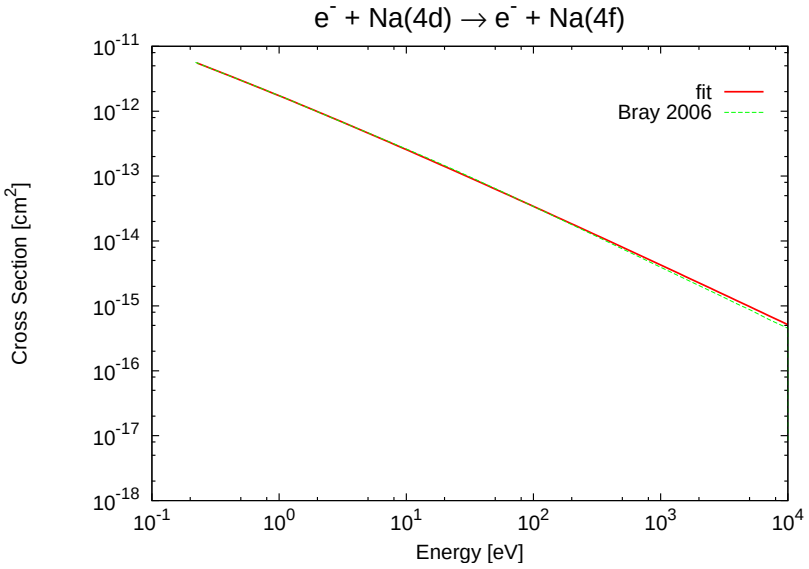

Figure 5.11: Electron-impact target excitation cross sections for 4d → 4f

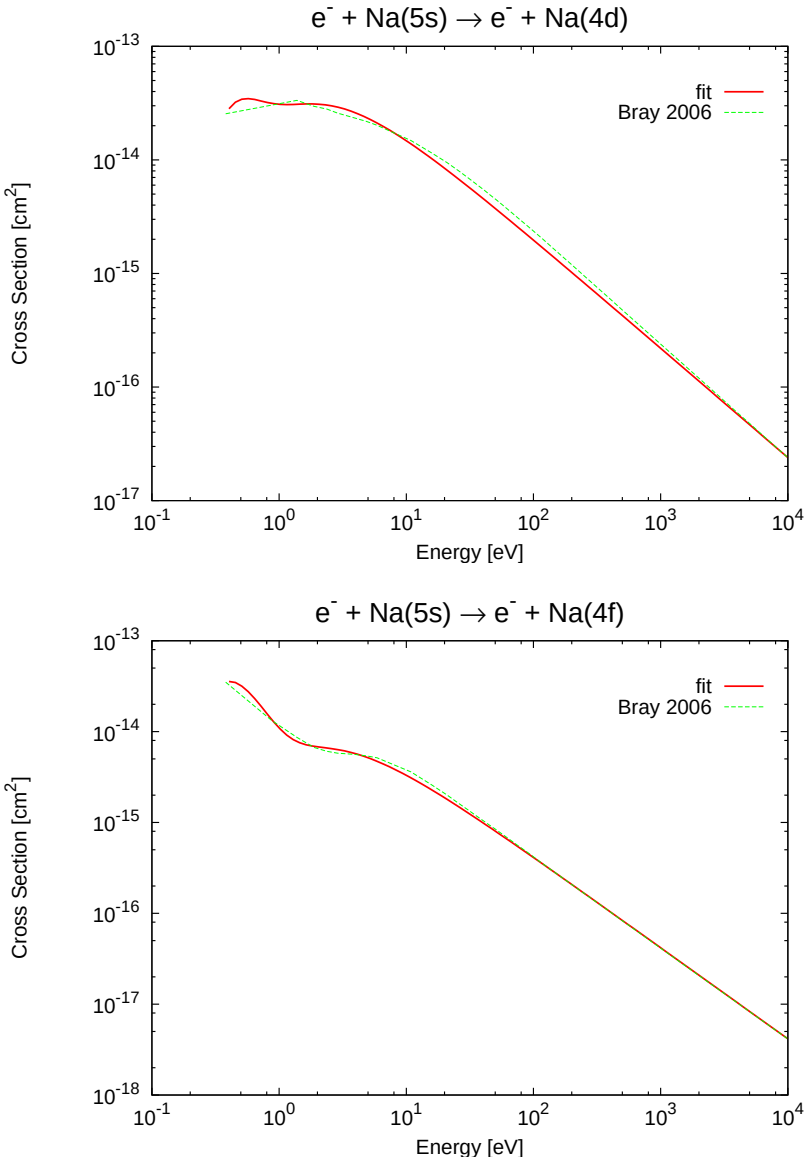

Figure 5.12: Electron-impact target excitation cross sections for 5s → n'l', $n' = 4$

5.3.2 Electron-Impact Target Ionization Cross Sections

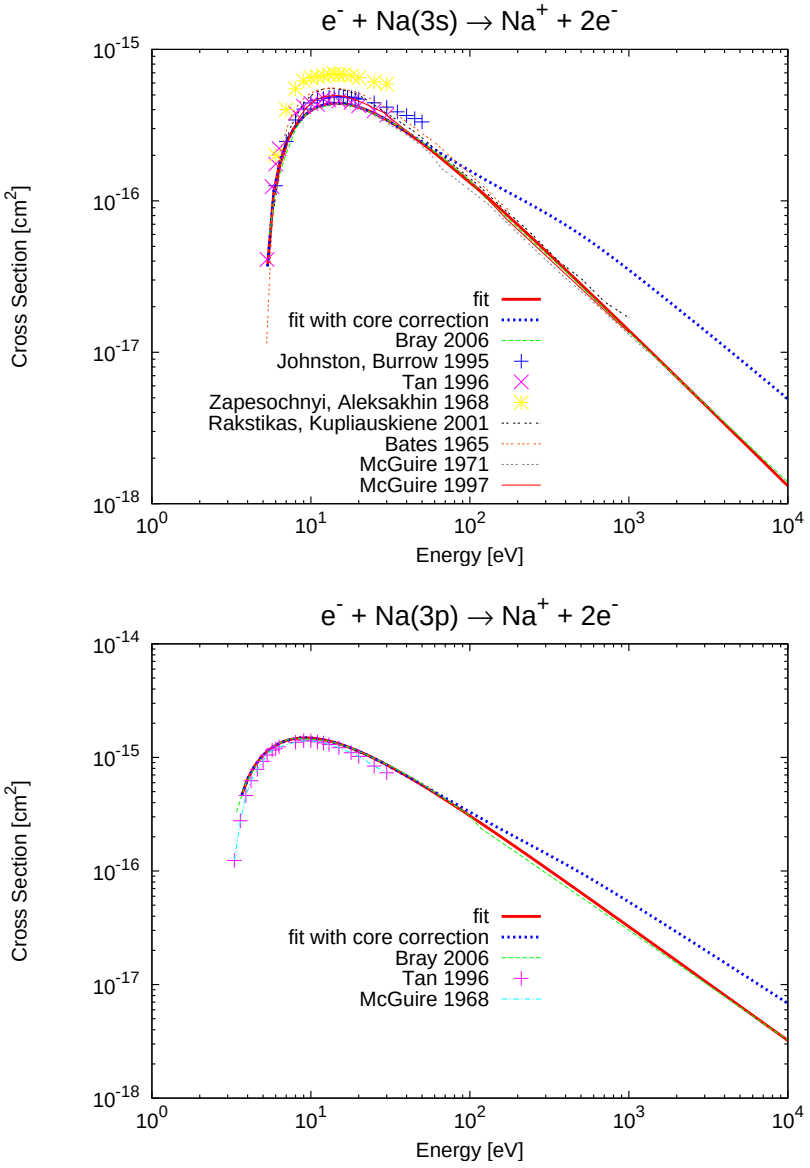

Figure 5.13: Electron-impact target ionization cross sections from Na(nl), $n = 3$

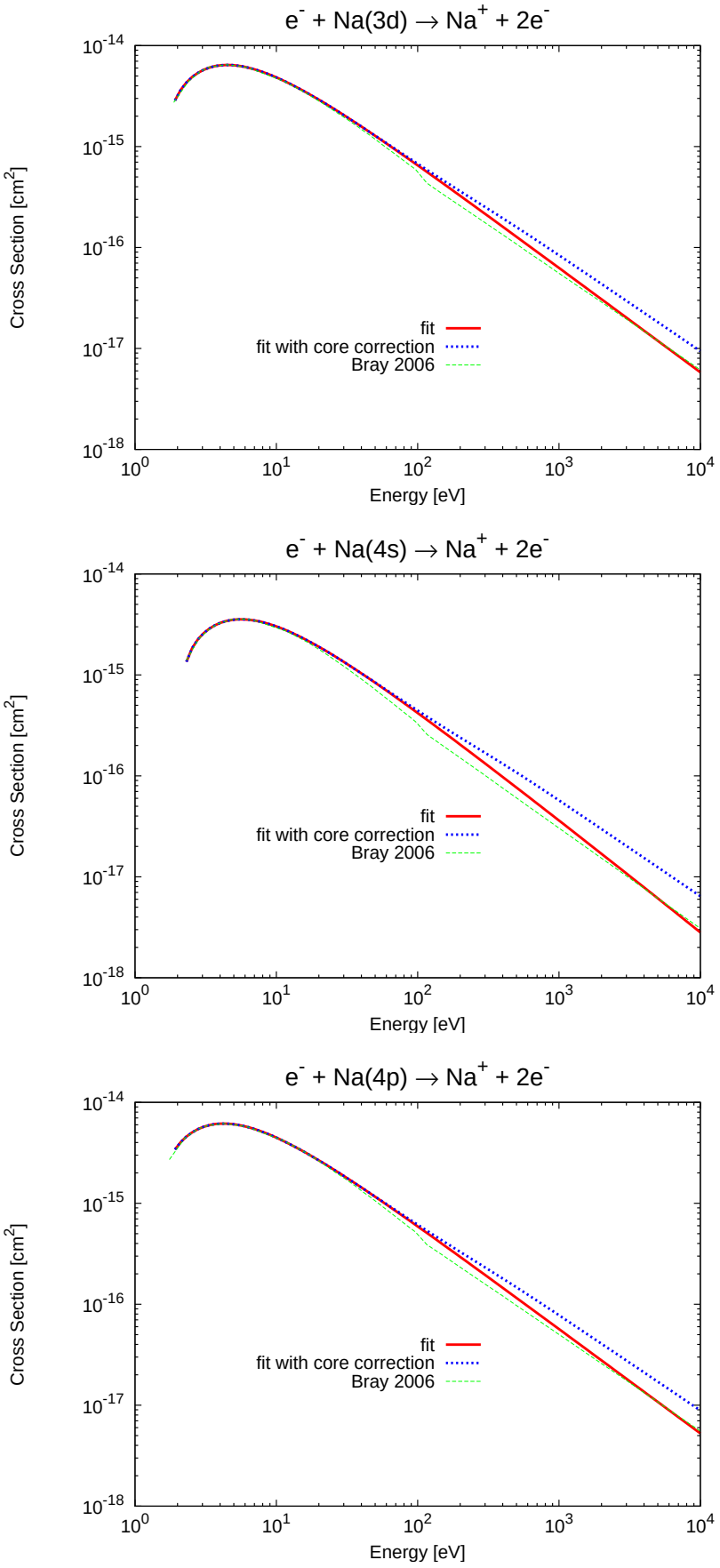

Figure 5.14: Electron-impact target ionization cross sections from Na(nl), $n = 3 - 4$

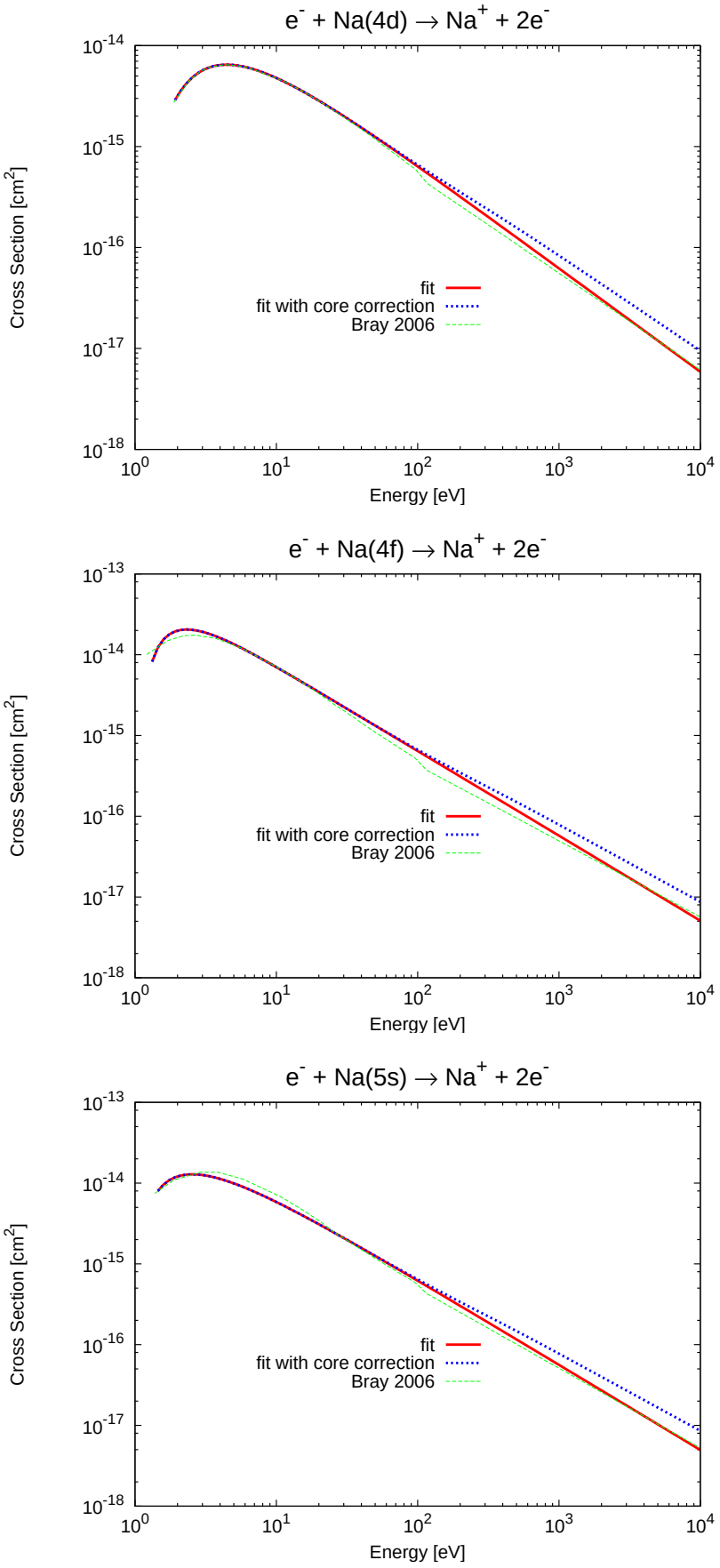

Figure 5.15: Electron-impact target ionization cross sections from Na(nl), $n = 4 - 5$

5.3.3 Proton-Impact Target Excitation Cross Sections

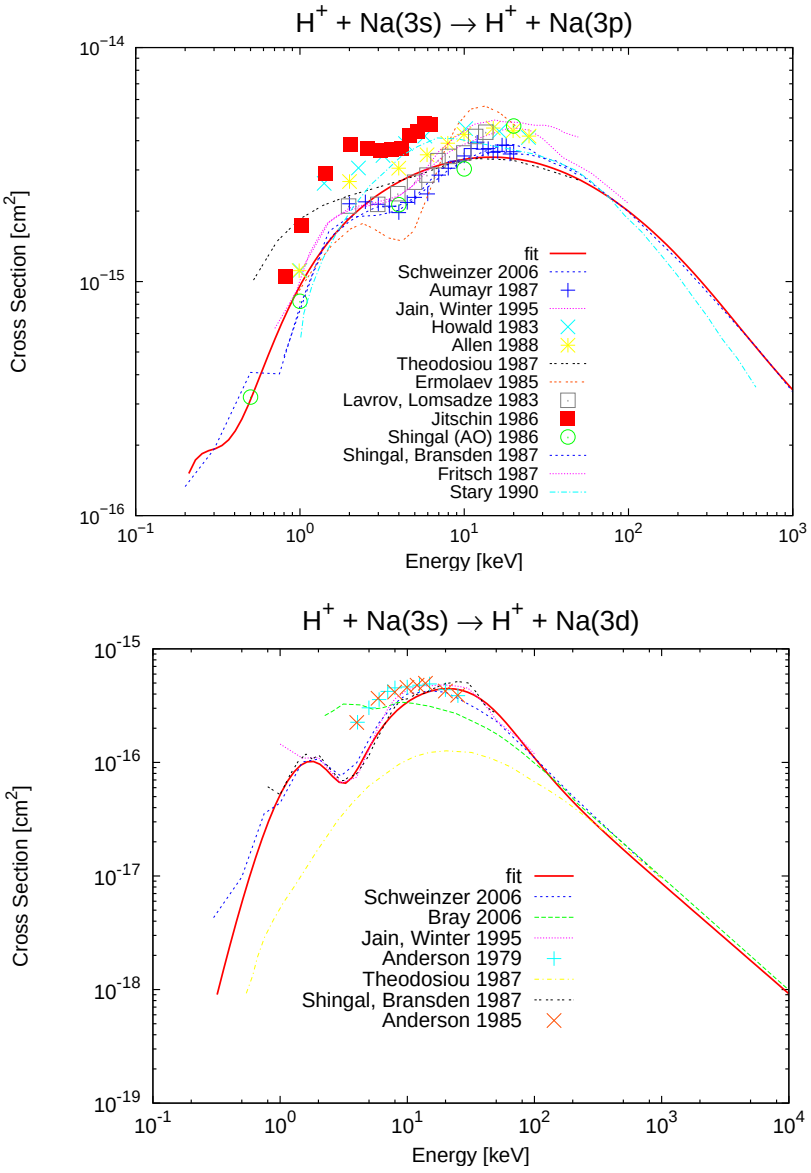

Figure 5.16: Proton-impact target excitation cross sections for 3s → n'l', $n' = 3 - 4$

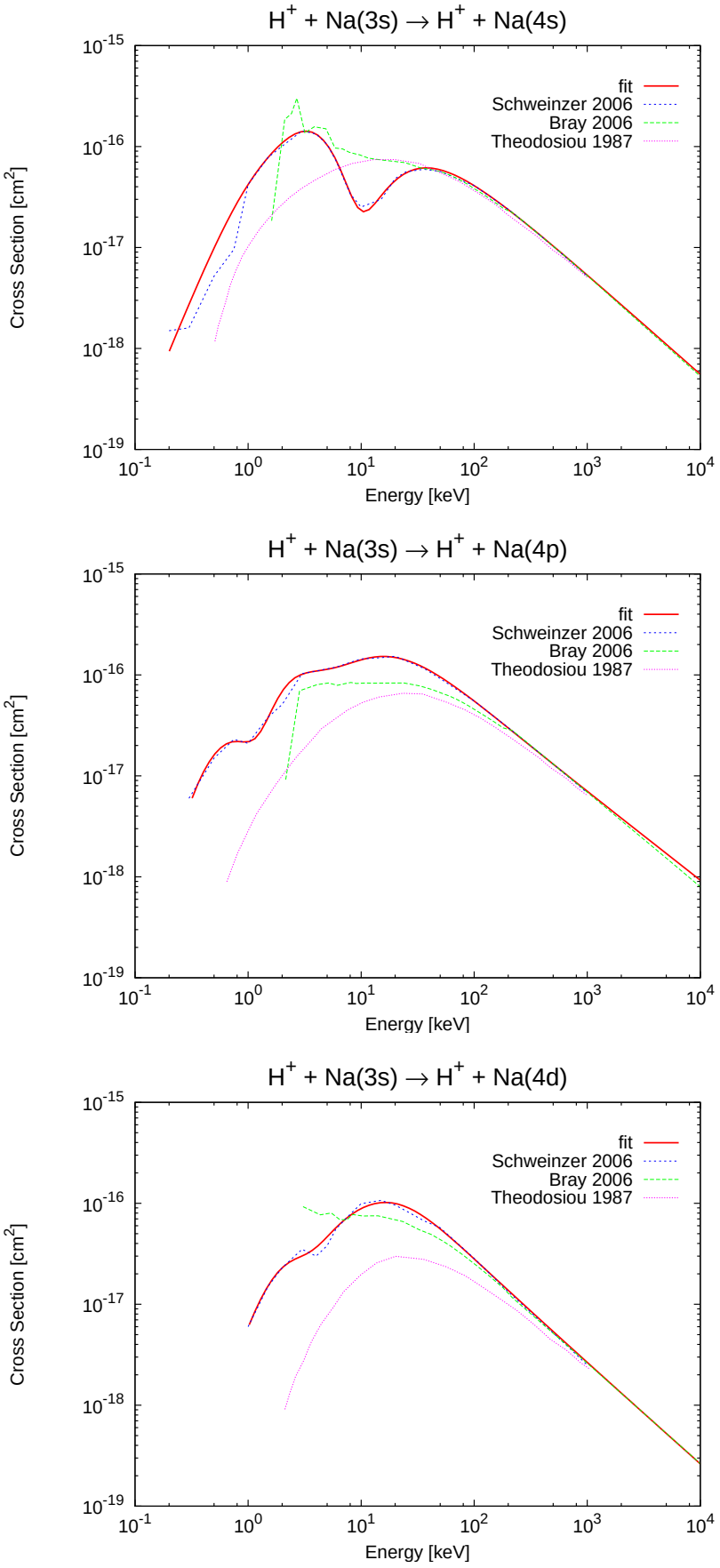

Figure 5.17: Proton-impact target excitation cross sections for 3s → n'l', $n' = 4$

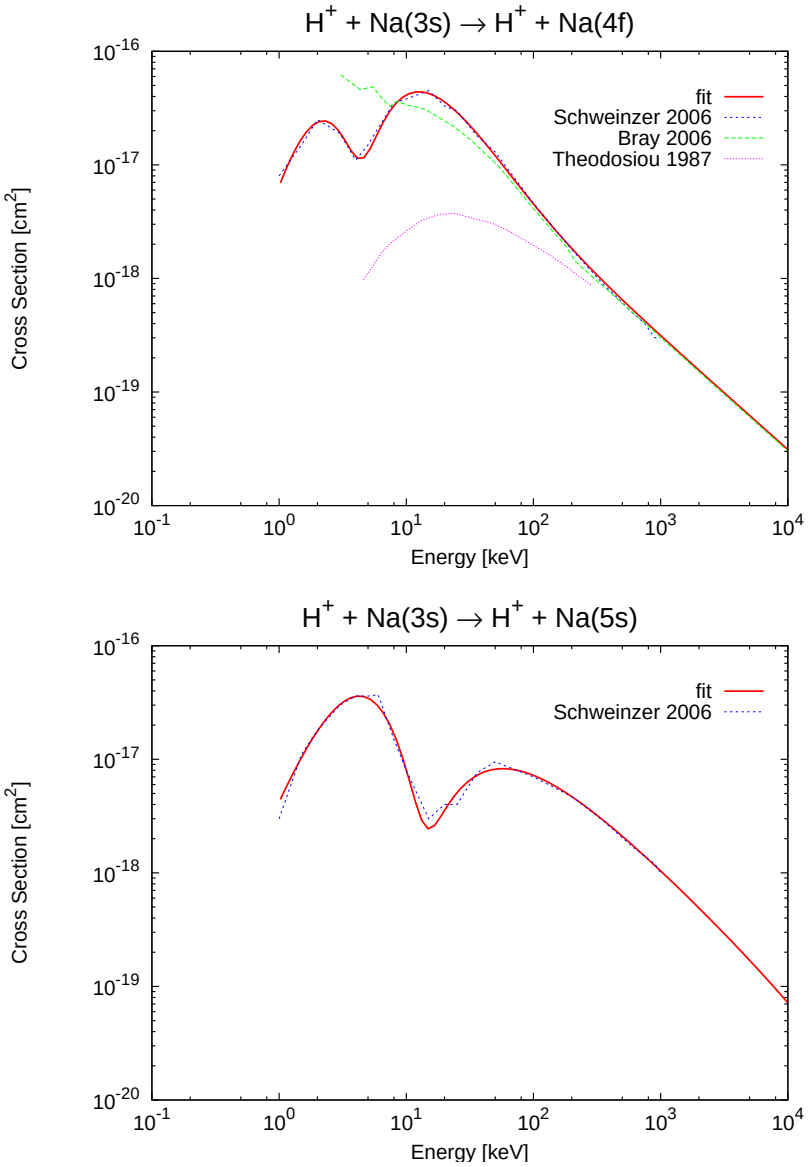

Figure 5.18: Proton-impact target excitation cross sections for 3s → n'l', $n' = 4 - 5$

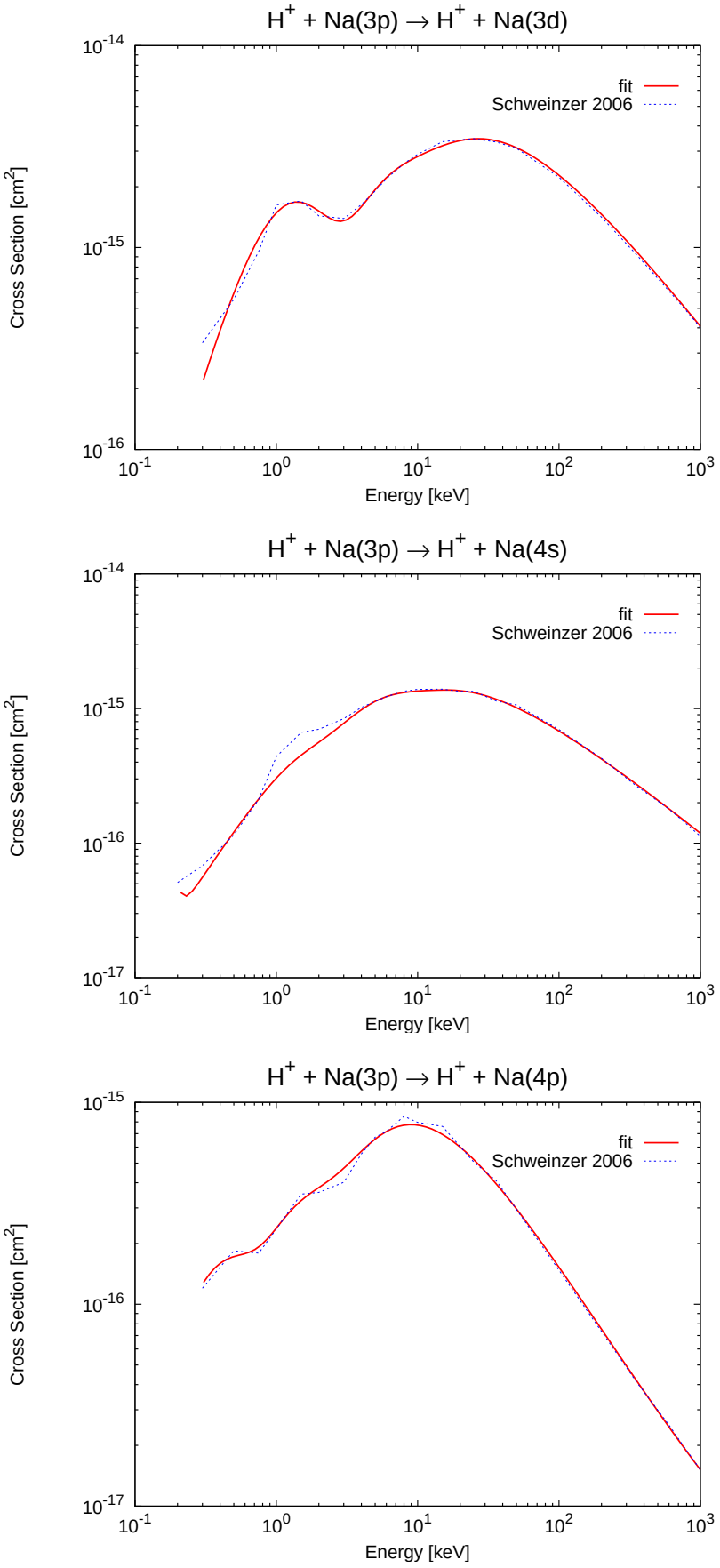

Figure 5.19: Proton-impact target excitation cross sections for 3p → n'l', $n' = 3 - 4$

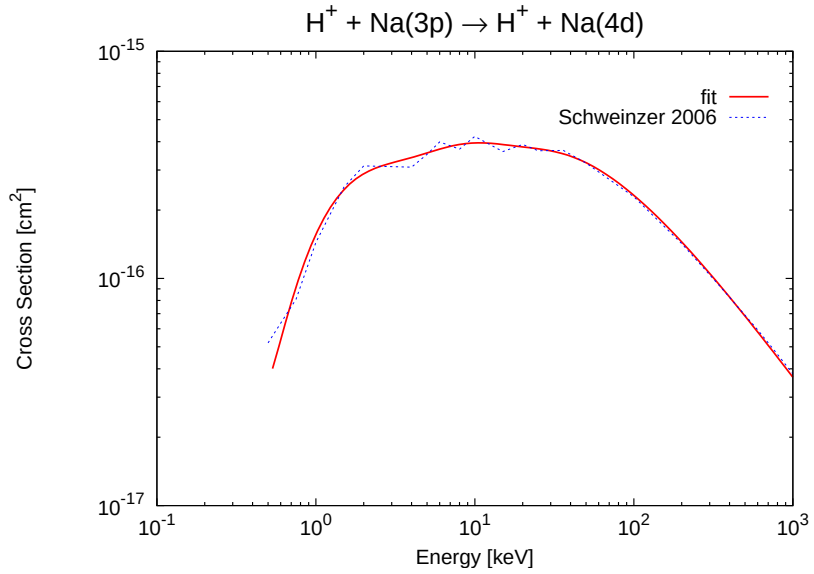
H+ + Na(3p) → H+ + Na(4d)
Cross Section [cm2]
Energy [keV]
fit
Schweinzer 2006
10-15
10-16
10-17
10-1
100
101
102
103

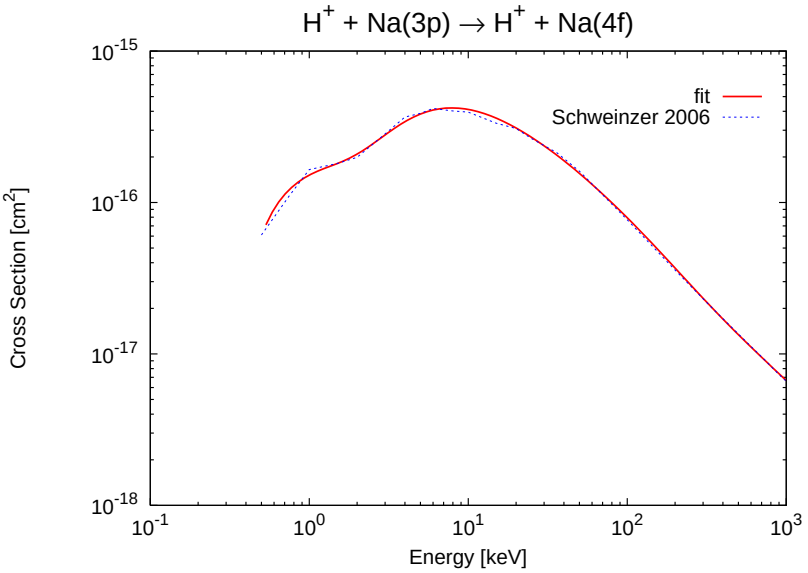
H+ + Na(3p) → H+ + Na(4f)
Cross Section [cm2]
Energy [keV]
fit
Schweinzer 2006
10-15
10-16
10-17
10-18
10-1
100
101
102
103

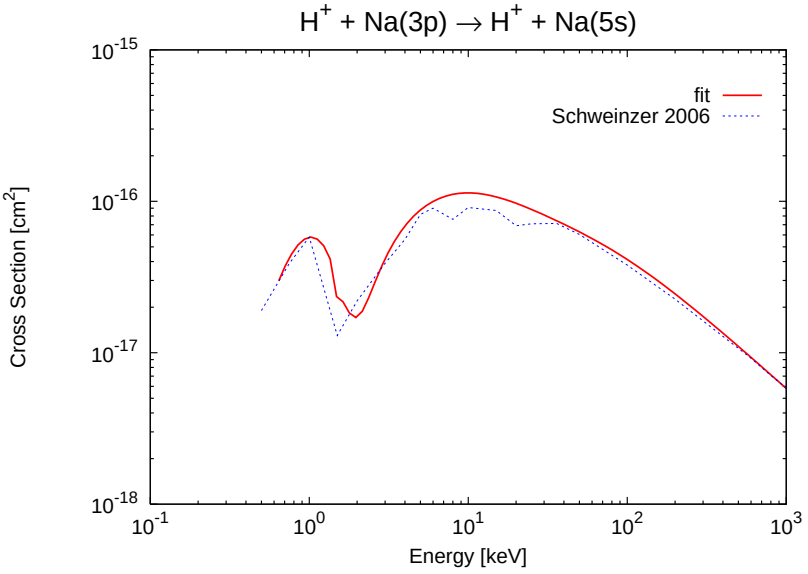
H+ + Na(3p) → H+ + Na(5s)
Cross Section [cm2]
Energy [keV]
fit
Schweinzer 2006
10-15
10-16
10-17
10-18
10-1
100
101
102
103

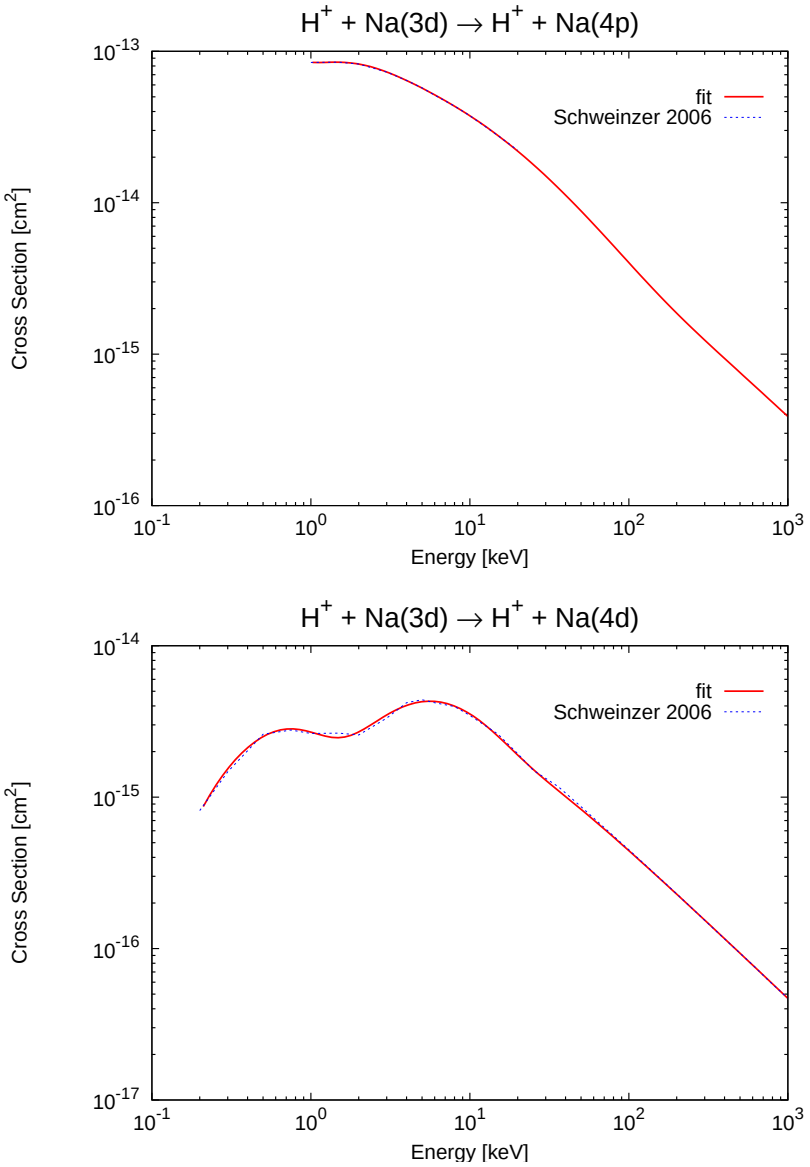

Figure 5.21: Proton-impact target excitation cross sections for 3d → n'l', $n' = 4$

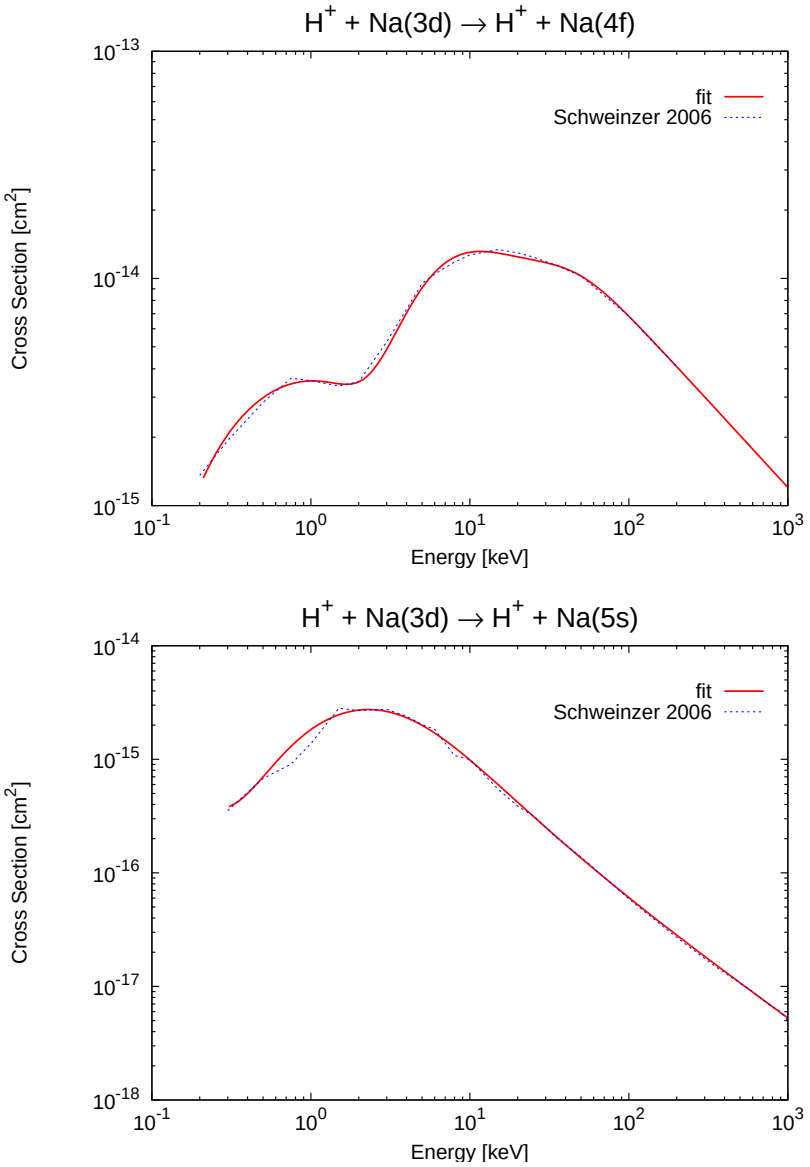

Figure 5.22: Proton-impact target excitation cross sections for 3d → n'l', $n' = 4 - 5$

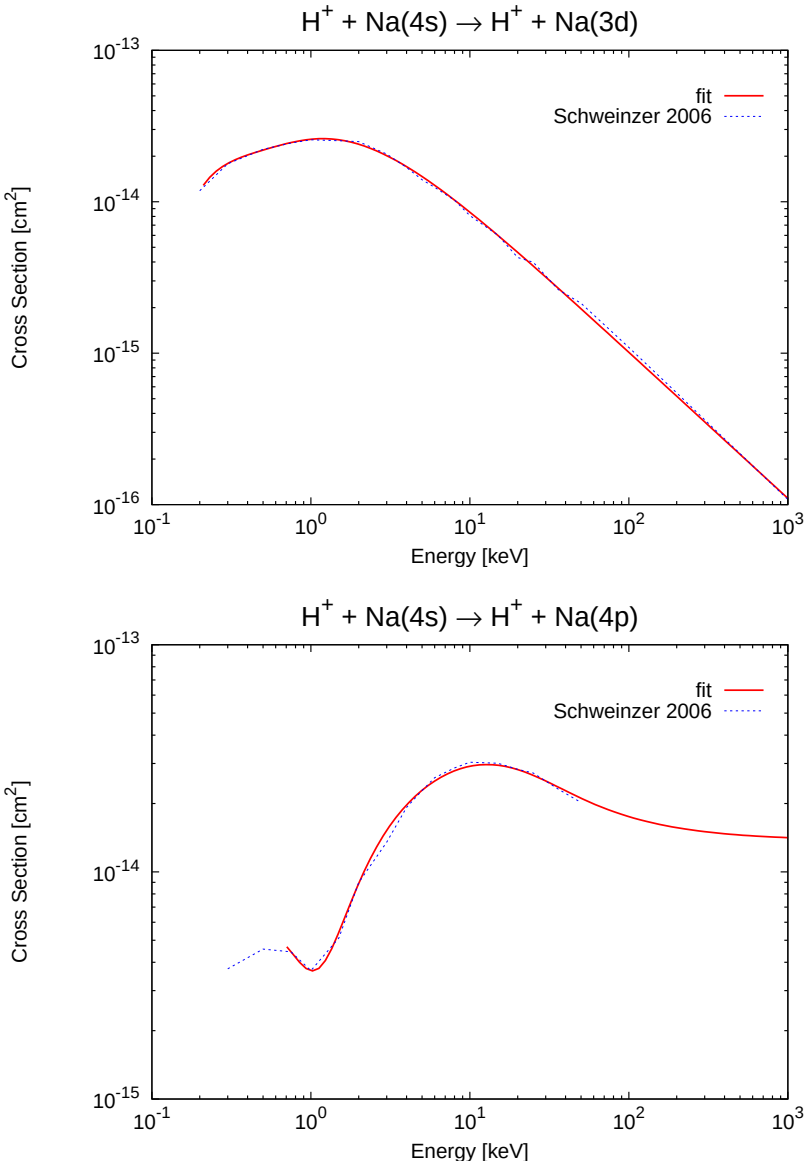

Figure 5.23: Proton-impact target excitation cross sections for 4s → n'l', $n' = 3 - 4$

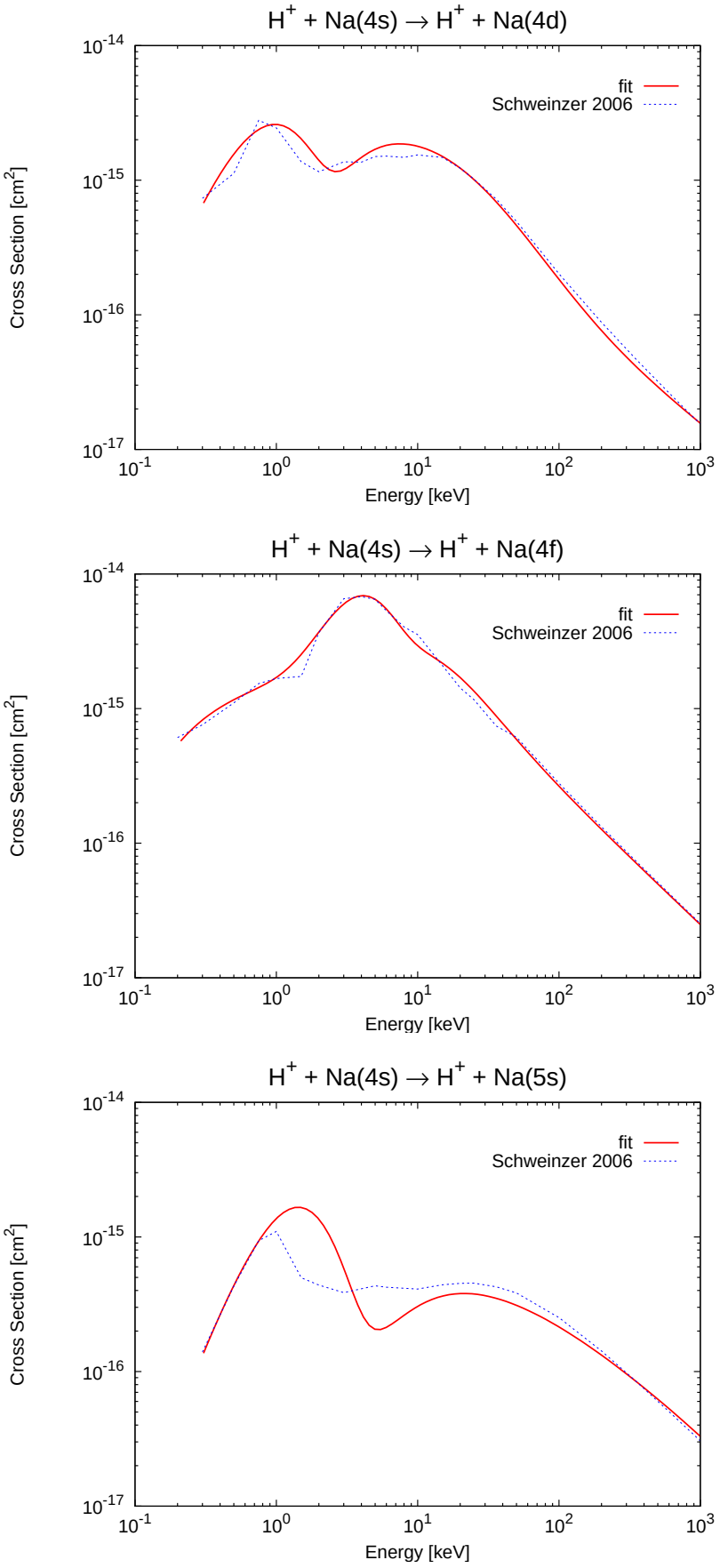

Figure 5.24: Proton-impact target excitation cross sections for 4s → n'l', $n' = 4 - 5$

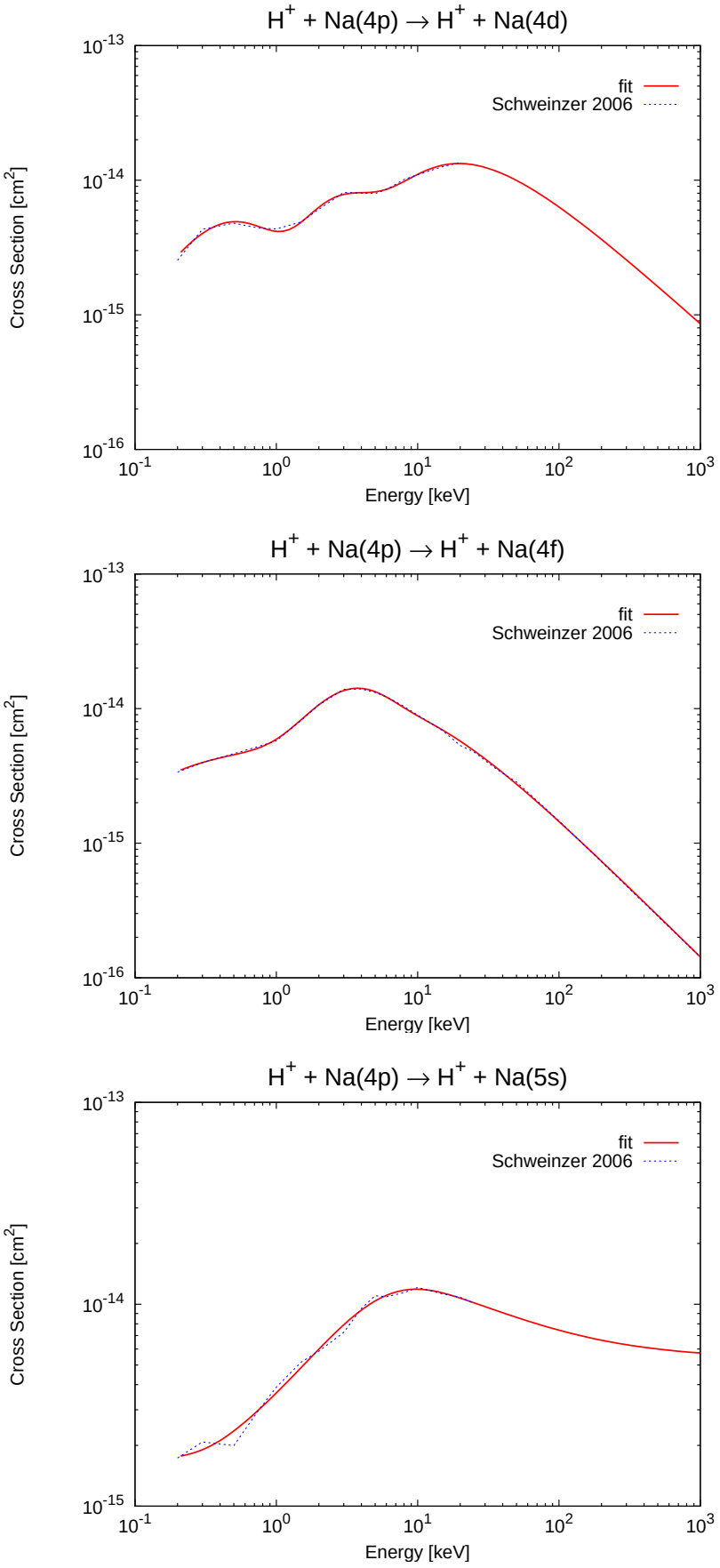

Figure 5.25: Proton-impact target excitation cross sections for 4p → n'l', $n' = 4 - 5$

5.3.4 Proton-Impact Target Electron Loss Cross Sections

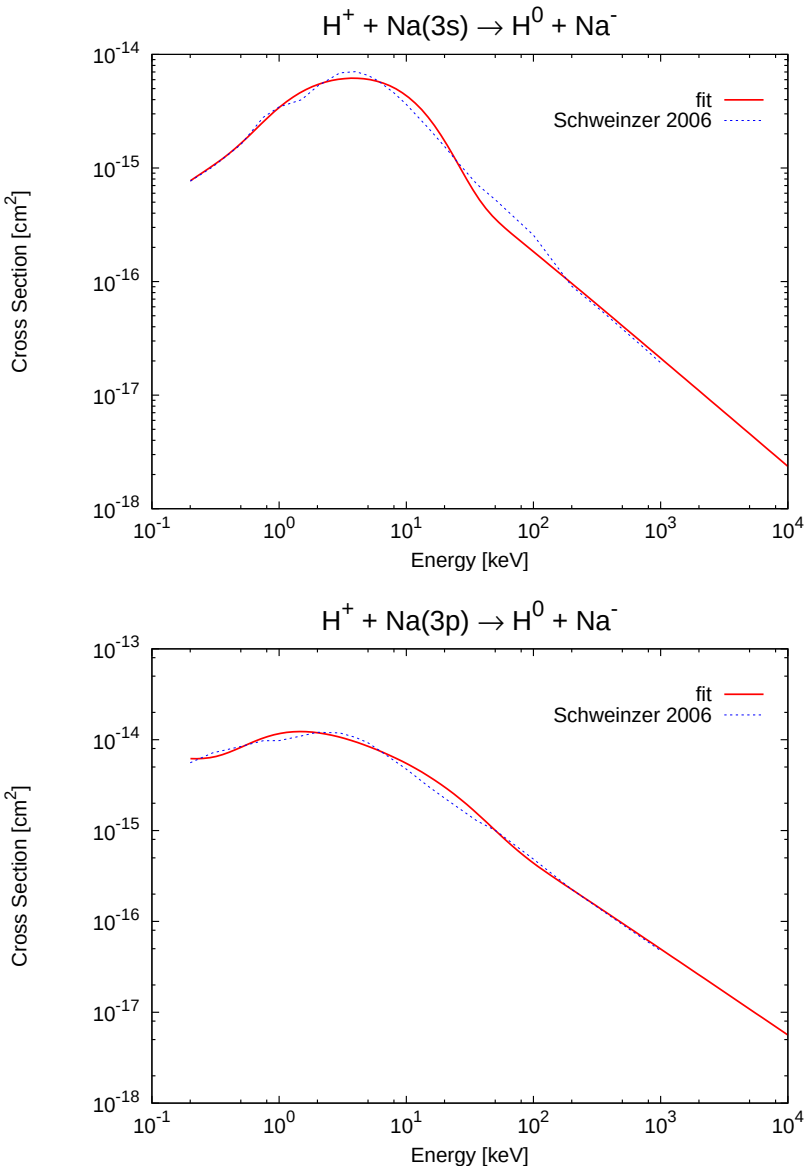

Figure 5.26: Proton-impact target electron loss cross sections from Na(nl); $n = 3$

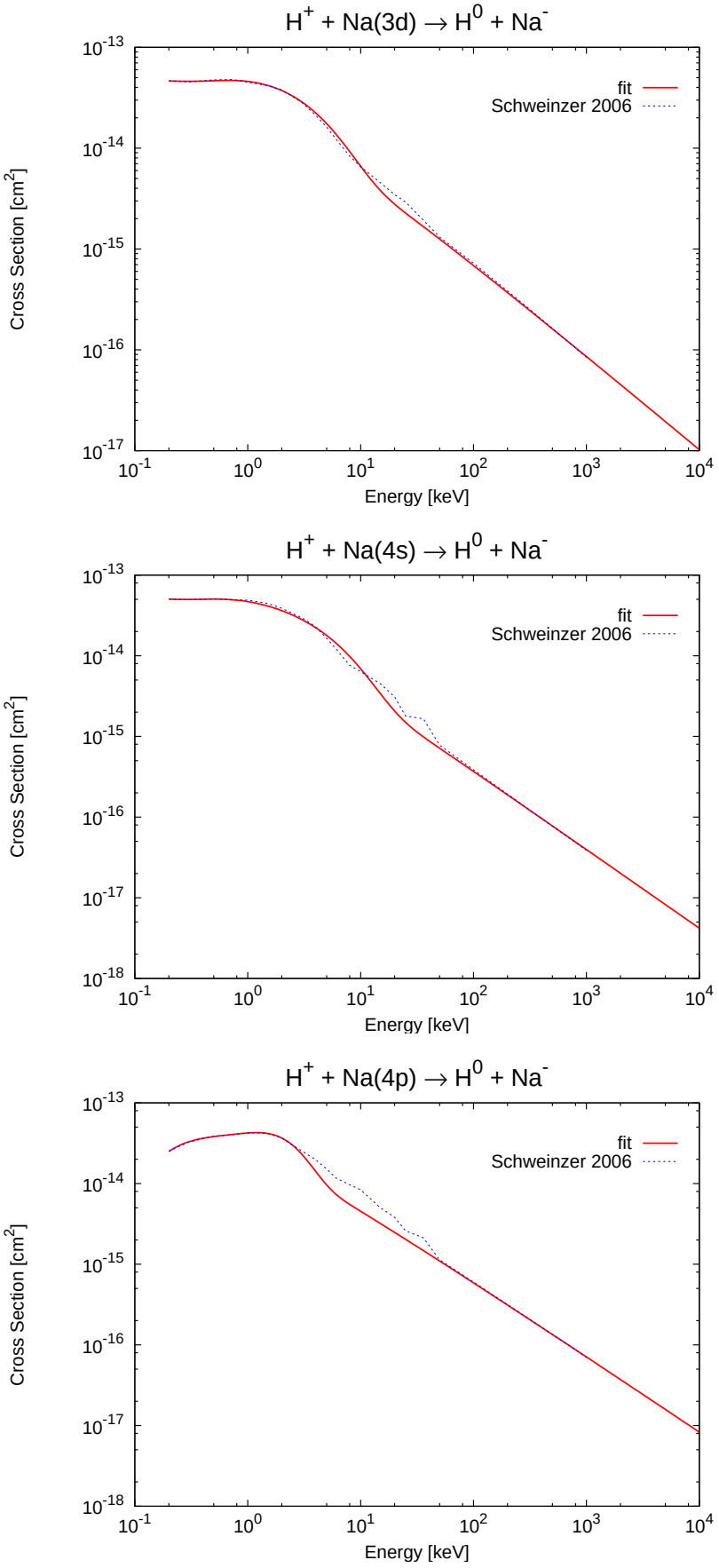

Figure 5.27: Proton-impact target electron loss cross sections from Na(nl); $n = 3 - 4$

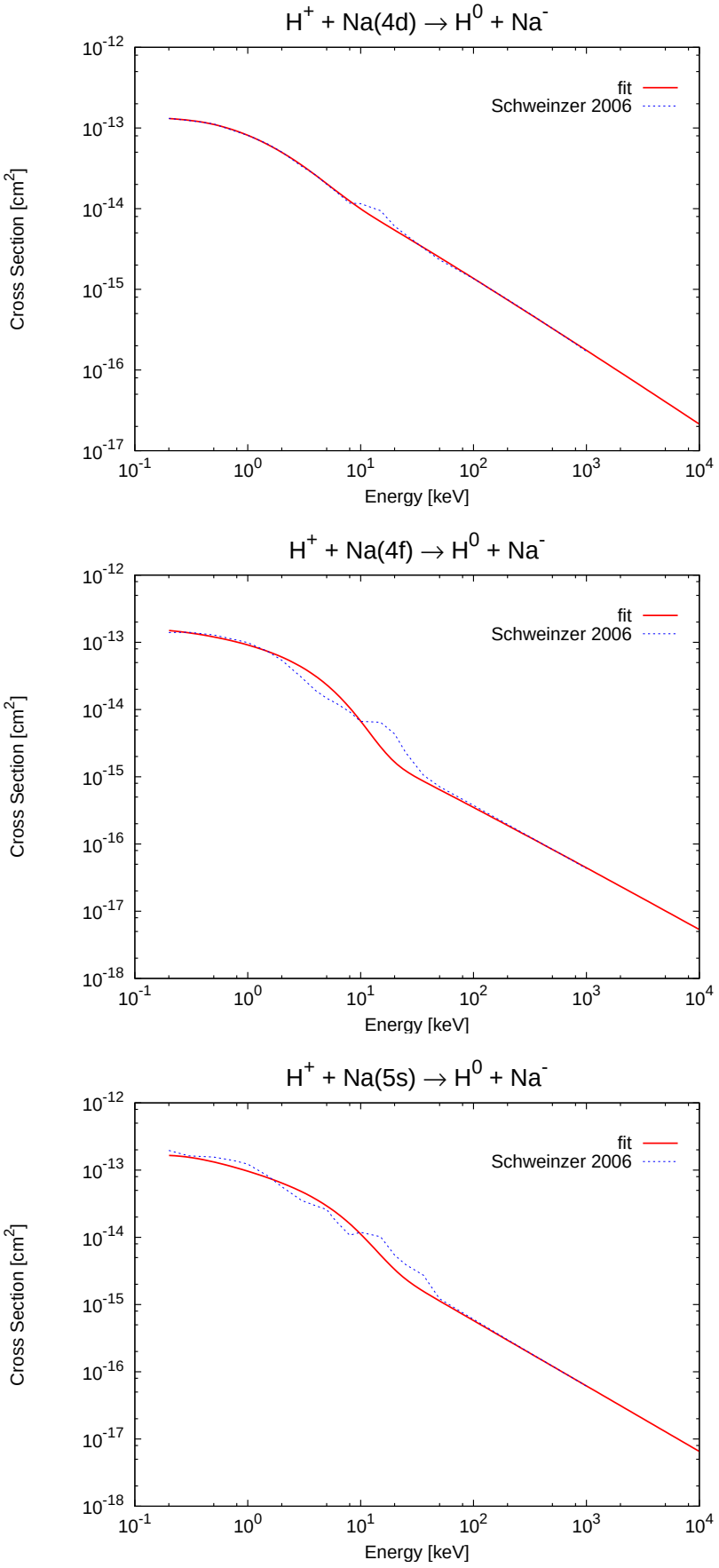

Figure 5.28: Proton-impact target electron loss cross sections from Na(nl); $n = 4 - 5$

5.4 Scaling Relations for Cross Sections of Sodium-Impurity Ion Collisions

A realistic fusion plasma is always polluted by a certain amount of impurity ions. Thus, to achieve satisfactory quality in simulations, it is necessary to include sodium - impurity ion collisions. A scaling formula with respect to the initial state electron binding energy E_b and the charge of the fully stripped projectile has been derived by Janev (1991) [104] for single electron charge transfer from excited hydrogen atoms H(n) in a wide impact energy range. The same reduced impact energy and cross section are introduced for target excitation [105]

$$E^{\mathrm{EXC}}_{\mathrm{scaled}} = \frac{E}{q}, \qquad \sigma^{\mathrm{EXC}}_{\mathrm{scaled}} = \frac{\sigma}{q} \tag{5.1}$$

and for single electron charge transfer [105]

$$E^{\mathrm{CT}}_{\mathrm{scaled}} = \frac{n^2 \cdot E}{\sqrt{q}}, \qquad \sigma^{\mathrm{CT}}_{\mathrm{scaled}} = \frac{\sigma}{n^4 q} \tag{5.2}$$

where n is the principal quantum number with respect to the binding energy ($n = 2E_b^{-1/2}$) [105]. These well approved scaling relations can be applied to the most frequent impurities (He, Be). The cross sections (not yet scaled) were calculated by J. Schweinzer [102] using the AO-CC method described in section 2.3. Fig.5.29 shows calculated cross sections of excitation of sodium (Na(3s) $\rightarrow$ Na(3p)) by impurity ion impact [102], whereas Fig.5.30 shows the corresponding reduced cross section values (by devision of q). This figure nicely and clearly demonstrates the applicability of the scaling relations of eq.(5.2). Fig.5.31 and Fig.5.32 show the same information for excitation of Na(3d) respectively Na(4s) from Na(3p).

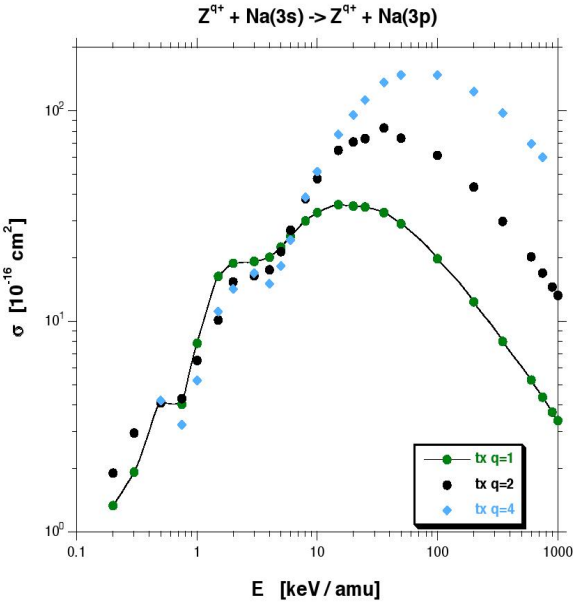

Figure 5.29: Cross sections of collisions of Na with H^+, He^{2+}, and Be^{4+} ions for the transition Na(3s) → Na(3p).

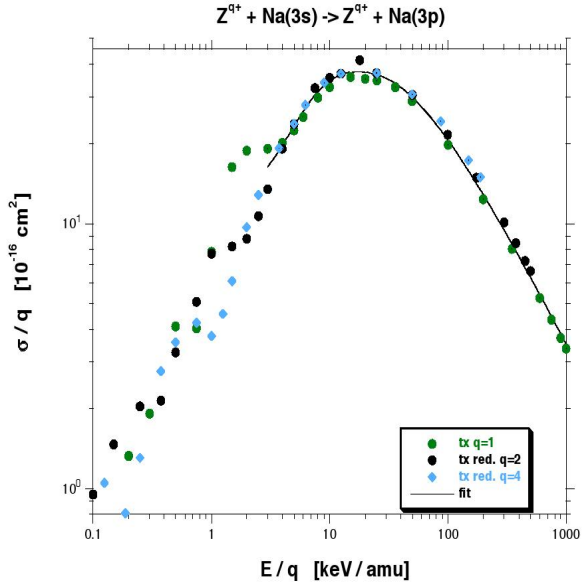

Figure 5.30: Reduced cross sections σ/q of collisions of Na with H^+, He^{2+}, and Be^{4+} ions for the transition Na(3s) → Na(3p). For reduced energies $E/q > 3\frac{\text{keV}}{\text{amu}}$, the reduced cross sections of He^{2+} and Be^{4+} follow the proton-impact cross section very well.

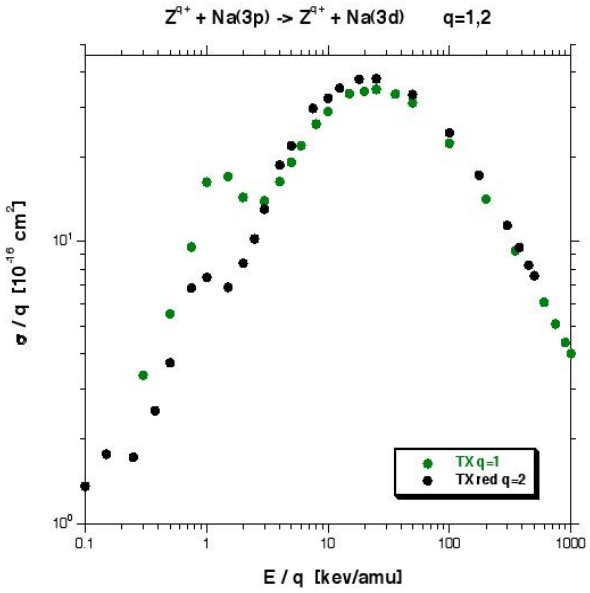

Figure 5.31: Reduced cross sections σ/q of collisions of Na with H^+ and He^{2+} ions for the transition Na(3p) → Na(3d).

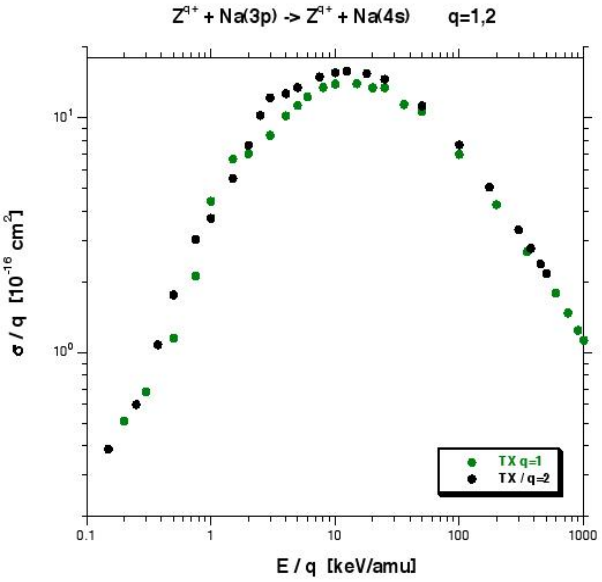

Figure 5.32: Reduced cross sections σ/q of collisions of Na with H^+, He^{2+}, and Be^{4+} impurity ions for the transition Na(3p) → Na(4s).

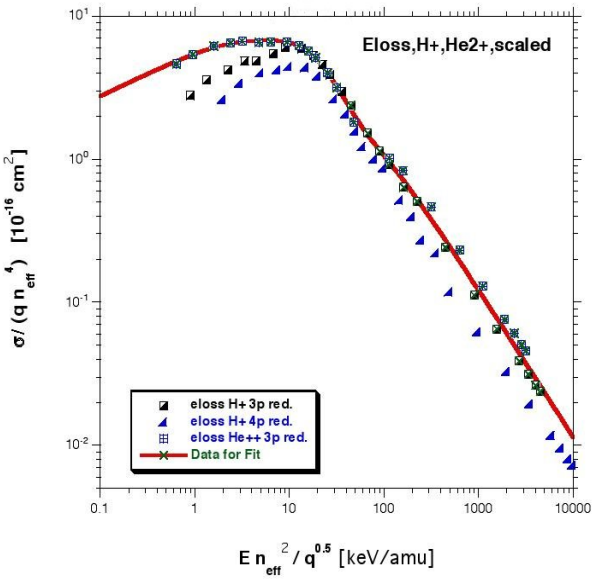

Figure 5.33: Reduced cross sections of collisions of Na(3s) with H^+ and He^{2+} ions resulting in Na electron loss

Chapter 6

Outlook

The quintessence of this thesis, the postscript plots of the data and the tables with the fit parameters, see sections 5.3 and 5.2, will be sent for publication to *Atomic Data & Nuclear Data Tables*. The publication will have the same structure as the publication of the Li databases by D. Wutte et al. in 1997 [98] and J. Schweinzer et al. in 1999 [99].

The implementation of the database in the simulation software package `Na_simula` is progressing at the moment. D. Bridi is currently at the IPP in Garching as a guest researcher to perform a series of measurements dedicated especially to sodium beam diagnostics. In the evaluation of the new experimental data, this database will be used as well as in the new enhanced simulations. Great hope is put in these investigations trying to capitalize on the advantages of sodium beam diagnostics in comparison to other neutral beam diagnostics.

To implement charge exchange processes with impurity ions for charge exchange spectroscopy in the simulation software, it needs to be evaluated in how far the sclaling relations from section 5.4 lead to correct results. It might be necessary in this context to perform more dedicated calculations of these cross sections combined with new measurements.

List of Figures

List of Tables

Appendix A

List of Acronyms & Used Constants

Acronym	Denotation
AMBDAS	Atomic and Molecular Bibliographical Database
AO-CC	Atomic-orbital close-coupling
ASDEX	Axisymmetric Divertor Experiment (Axialsymmetrisches Divertorexperiment)
AUG	ASDEX-Upgrade
CC	Close-coupling
CCC	Convergent close-coupling
COBM	Classical over-barrier model
CTMC	Classical trajectory Monte Carlo simulation
IAEA	International Atomic Energy Agency
IAP	Institut für Allgemeine Physik, Technische Universität Wien
IPP	Institut für Plasmaphysik, Max-Planck-Institut München
KFKI	Hungarian Academy of Sciences
LIA	Diagnostic Acronym used at ASDEX-Upgrade
LIC	Diagnostic Acronym used at ASDEX-Upgrade
MO-CC	Molecular-orbital close-coupling
PWBA	Plain wave Born approximation
RO	Relaxed Orbital Calculations
SP	Sudden Perturbation Calculations
VPSA	Vainshtain-Presnyakov-Sobel'man approximation

$a_0 = 5.29 \cdot 10^{-9} cm^2$	Bohr radius
$\pi = 3.1415296\ldots$	Circle constant

Appendix B

Source Code addfit

```
# include <iostream>
# include <fstream>
# include <sstream>
# include <string>
# include <list>

using namespace std;

string pia02(string inp)
{
  string::size_type loc;
  loc = inp.find(",",0);
  string tmp = inp.substr(loc+1);

  istringstream strin;
  ostringstream strout;

  strin.str(tmp);
  double d;
  strin >> d;
  d = d*3.1415296*5.2917721e-09 * 5.2917721e-09;
  strout << d;
  tmp = strout.str();
  strin.str("");
  strout.str("");

  inp.erase(loc+2);
  inp.append(tmp);
```

```
  return inp;
}

int str2int (string s)
  //converts a string s to an int i
{
  int i;
  istringstream strin;
  strin.str(s);
  strin >> i;
  return i;
}

string int2str(int i)
  //converts an int i to a string s
{
  string s;
  ostringstream strout;
  strout << i;
  s = strout.str();
  return s;
}

string write_gpl_script(string dinput, string title)
{
  string script=dinput;
  string::size_type loc, loc1;
  loc = script.find("csv",0);
  script.erase(loc);
  script.append("gpl");

  const char *cscript;
  cscript = script.c_str();

  ifstream ein;
  ein.open(cscript,ios::in);
  if (!ein.is_open()){
    cout << "write_gpl_script: Could not open file \"" << script << "\" --> ABORT" <<
        endl << endl;
    return "a";
  }
```

```
  string style;
  cout << "Choose linestyle! (points, lines, linespoints)" << endl;
  cin >> style;

  string dummy, alt="", neu, index_str;
  int index_int;
  list<string> lines;
  while (!ein.eof()){
    getline(ein,dummy);
    loc = dummy.find("x11",0); //find the first line after the plotting command
    if (loc != string::npos){
      loc1 = alt.find("index",0);
      index_str = alt.substr(loc1+6,2);
      index_int = str2int(index_str);
      index_int++;
      index_str = int2str(index_int);
      if (index_int < 10) index_str = "0" + index_str;
      alt.append(", \\");
      neu = " \"" + dinput + "\" using 1:2 index " + index_str + " with " + style + "
          title \"" + title + "\" ";
      lines.push_back(alt);
      lines.push_back(neu);
    }else{
      if (alt != "") lines.push_back(alt);
    }
    alt = dummy;
  }
  lines.push_back(dummy); //for the last line
  ein.close();

  ofstream aus;
  aus.open(cscript,ios::trunc);

  list<string>::const_iterator pos;
  for (pos = lines.begin(); pos != lines.end(); pos++) aus << *pos << endl;
  aus.close();

  return script;
}

void call_gnuplot(string script)
```

```
{
  string commandline;
  commandline = "gnuplot -persist " + script;
  system(commandline.c_str());
}

void call_kgv(string eps)
{
  string commandline;
  commandline = "kgv " + eps + " &";
  system(commandline.c_str());
}

void call_kate(string script)
{
  string commandline;
  commandline ="kate " + script + " &";
  system(commandline.c_str());
}


int main()
{
  int r=0; //return value for errors

  cout << "----------------------"<< endl << endl;
  cout << "     add2db & fit     "<< endl << endl;
  cout << "----------------------"<< endl << endl;
  cout << "Enter the name of the database file!" << endl;
  string dinput, ninput;
  cin >> dinput;
  cout << endl << "Enter the name of the file with the new data!" << endl;
  cin >> ninput;

  const char *dbfname, *nfname;

  dbfname = dinput.c_str();
  nfname = ninput.c_str();

  ofstream db;
  db.open(dbfname,ios::app);
  if (!db.is_open()){
```

```
  cout << "main: Could not open file \"" << dinput << "\" --> ABORT!" << endl << endl
      ;
  r++;
  return r;
}

ifstream neu;
neu.open(nfname,ios::in);
if(!neu.is_open()){
  cout << "main: Could not open file \"" << ninput << "\" --> ABORT!" << endl << endl
      ;
  r++;
  return r;
}

cout << endl << "Convert cross sections from units of pi*a_0^2 to cm^2? (y/n)" <<
    endl;
string conv;
cin >> conv;

//-->write new data to database file

db << endl << endl; // two empty lines in front of the new data
string firstline;
getline(neu,firstline); //reads in the first line of each new dataset
                        //this line contains the title of the dataset

string dummy;
while(!neu.eof()){
  getline(neu,dummy);
  if (conv =="y" && dummy.substr(0,1) != "#" && dummy.length() > 1) dummy = pia02(
      dummy);
  db << dummy << endl;
}
db.close();
neu.close();

//<--write new data to database file

//-->write new gnuplot script
string script;
script = write_gpl_script(dinput, firstline);
```

```
  //<--write new gnuplot script

  //-->load script in gnuplot
  call_gnuplot(script);
  //<--load script in gnuplot

  //-->call ghostview to look at the result
  string::size_type loc;
  string eps = script;
  loc = eps.find(".",0);
  eps.erase(loc);
  eps.append(".eps");

  call_kgv(eps);
  //<--call ghostview to look at the result

  return 0;
}
```

Appendix C

Source Code iap2ipp

```
#include <iostream>
#include <fstream>
#include <string>
#include <list>
#include "potenz.h"

using namespace std;

class data{
public:
  string fname, fitf, param, cnst, states, initial, final, kommas;
  int num;

  //contructor

  data (string fname = "", string fitf = "", string cnst = "", string states = "",
      string initial = "", string final = "", string kommas = "", int num =0) : fname(
      fname), fitf(fitf), cnst(cnst), states(states), initial(initial), final(final),
      kommas(kommas), num(num)
  {}

  //destructor

  ~data() {}

  //functions

  void Print2Screen()
```

```
{
  cout << "fname: " << fname << ":" << endl;
  cout << "fitf: " << fitf << endl;
  cout << "param: " << param << endl;
  cout << "cnst: " << cnst << endl;
  cout << "num: " << num << endl << endl;
  cout << states << fitf << cnst << param << kommas << endl << endl;
}

 void Print2File(string ofname, bool first) const
{
  ofstream aus;
  if (first) aus.open(ofname.c_str(), ios::trunc); else aus.open(ofname.c_str(), ios
      ::app);
  if (!aus.is_open()) cout << "Could not open file \"" << ofname << "\" --> ABORT!!"
       << endl;
  cout << "--> writing " << fname << " to file " << ofname << endl;
  aus << states << fitf << cnst << param << kommas << endl;
  aus.close();
}

void clear()
{
  fname = "";
  fitf = "";
  param = "";
  cnst = "";
  states = "";
  kommas = "";
  num = 0;
}

string find_states ()
{
  if (fname.substr(0,3) == "EXC"){
    initial = fname.substr(7,2);
    final = fname.substr(10,2);
  }

  if (fname.substr(0,3) == "ION"){
    initial = fname.substr(7,2);
    final = initial;
```

```
  }

  if (fname.substr(0,3) == "ELO"){
    initial = fname.substr(9,2);
    final = initial;
  }

//cout << "initial: " << initial << " final: " << final << endl;
  string i, f;
  if (initial=="3s") i = "1, ";
  if (initial=="3p") i = "2, ";
  if (initial=="4s") i = "3, ";
  if (initial=="3d") i = "4, ";
  if (initial=="4p") i = "5, ";
  if (initial=="5s") i = "6, ";
  if (initial=="4d") i = "7, ";
  if (initial=="4f") i = "8, ";
  if (final=="3s") f = "1, ";
  if (final=="3p") f = "2, ";
  if (final=="4s") f = "3, ";
  if (final=="3d") f = "4, ";
  if (final=="4p") f = "5, ";
  if (final=="5s") f = "6, ";
  if (final=="4d") f = "7, ";
  if (final=="4f") f = "8, ";

//cout << "inital + final = " << initial + final << endl;

  return i + f;
}

string fit_function()
{

  string::size_type loc, loc1;
  loc = fname.find("-", 0);
  if (loc == string::npos) loc = fname.find("+",0);
  string process = fname.substr(0, loc+1);
  //cout << "process: " << process << endl;
  //stop();
  string p;
```

```
  if (process == "EXC_e-") p = "\'eexc Na ";
  if (process == "ION_e-") p = "\'eion Na ";
  if (process == "EXC_H+") p = "\'hexc Na ";
  if (process == "ELOSS_H+") p = "\'heloss Na ";

  states = find_states();

  string s;
  if (initial == final) s = initial; else s = initial + final;
  return p + s + "\', ";
}

void convert_parameters()
{
  ifstream ein;
  ein.open(fname.c_str(), ios::in);
  if (!ein.is_open()) cout << "Could not open file \"" << fname << "\" --> ABORT!!"
      << endl << endl;
  string param_name, dummy, value, alt;
  //    num = 0;
  while(!ein.eof()){
    ein >> param_name >> dummy >> value;
    if (param_name == alt) break;
    value = potenz(value);
    int check=2;
    if (param_name == "d" || param_name =="I") check = 0;
    if (param_name =="t") check = 1;

    switch (check){
    case 0:
    cnst = value + ", ";
    num++;
    break;

    case 1:
    cnst = cnst + value + ", ";
    num++;
    break;

    default:
    param = param + value + ", ";
    num++;
```

```
      break;
      }
      alt = param_name;
    }
    param = param.substr(0, param.length()-2);
  }

  void add_kommas(int nr)
  {
    int i;

    for (i=0; i<(nr-num); i++){
      kommas = kommas + ", ";
    }
  }

};


int main()

{
  cout << "   ---------------------" << endl;
  cout << "   |   iap -> ipp    |" << endl;
  cout << "   ---------------------" << endl << endl;

  //-->open file with filenames
  ifstream files;
  string names[2] = {"e-_iapfiles.txt", "H+_iapfiles.txt"}; //filenames of e- and H+
      impact parameter files

  int i;
  list<data> eminus, Hplus;
  for (i=0; i<2; i++){
    ifstream iap;
    iap.open(names[i].c_str(), ios::in);
    if (!iap.is_open()){
      cout << "Could not open file \"" << names[i] << "\" --> ABORT!!" << endl << endl;
      return 1;
    }

    data entry; // making object entry of class data
```

```
  while(!iap.eof()){
    entry.clear();
    iap >> entry.fname;
    if ((entry.fname).length() < 2) break;
    cout << "--> processing " << entry.fname << endl;
    entry.states = entry.find_states();
    //cout << "states: " << entry.states << endl;
    //      stop();
    entry.fitf = entry.fit_function();
    //cout << "fitf: " << entry.fitf << endl;

    //      stop();
    entry.convert_parameters();
    switch (i){
    case 0:
  eminus.push_back(entry);
  break;

    case 1:
  Hplus.push_back(entry);
  break;

    default:
  cout << "Major problem occured! -->ABORT!!" << endl << endl;
  return 1;
    }
  }
}

list<data>::const_iterator pos;
int nr1=0, nr2=0;
for (pos = eminus.begin(); pos != eminus.end(); pos++) {
  if ((*pos).num > nr1) nr1 = (*pos).num;
  cout << (*pos).fname << ": " << (*pos).num << " : " << nr1 << endl;
}
for (pos = Hplus.begin(); pos != Hplus.end(); pos++) if ((*pos).num > nr2) nr2 = (*
    pos).num;

//cout << "nr1: " << nr1 << " nr2: " << nr2 << endl << endl;
//--> haengt sich zwischen hier und stop auf!
string ofname = "e-_param.ipp";
```

```
  data entry;
  for (pos = eminus.begin(); pos != eminus.end(); pos++){
    entry = *pos;
    if (entry.num < nr1) entry.add_kommas(nr1);
    //    entry.Print2Screen();
    //stop();
    if (pos == eminus.begin()) entry.Print2File(ofname, true); else entry.Print2File(
        ofname,false);
  }
  //stop();
  ofname = "H+_param.ipp";
  for (pos = Hplus.begin(); pos != Hplus.end(); pos++){
    entry = *pos;
    if (entry.num < nr2) entry.add_kommas(nr2);
    if (pos == Hplus.begin()) entry.Print2File(ofname, true); else entry.Print2File(
        ofname, false);
  }

  cout << "   ---------------------------------------" << endl << endl;
  cout << "   |      Conversion IAP --> IPP      |" << endl;
  cout << "   |         was successfull          |" << endl << endl;
  cout << "   ---------------------------------------" << endl << endl;

  return 0;
}
```

C.1 Source Code potenz.h

```
#include <string>
#include <sstream>
#include <iostream>
#include <cmath>

using namespace std;

void stop()
{
  cout << "STOP!! Press any key to continue!" << endl;
  string s;
  cin >> s;
}
```

```
double str2dbl(string s)
  //converts a string s to a double d;
{
  double d;
  istringstream strin;
  strin.str(s);
  strin >> d;
  return d;
}

int str2int(string s)
  //converts a string s to an int i;
{
  int i;
  istringstream strin;
  strin.str(s);
  strin >> i;
  return i;
}

string dbl2str(double d)
  //converts a double d to a string s
{
  string s;
  ostringstream strout;
  strout << d;
  s = strout.str();
  return s;
}

string int2str(int d)
  //converts an int i to a string s
{
  string s;
  ostringstream strout;
  strout << d;
  s = strout.str();
  return s;
}

double int2dbl(int i)
     //converts an int i to a double
```

```
{
  string istr = int2str(i);
  istr = istr + ".0";
  return str2dbl(istr);
}

string potenz(string inp)
{
  double dinp = str2dbl(inp);

  if(abs(dinp) < 1000 && abs(dinp) > 0.01) return dbl2str(dinp);

  if(abs(dinp)>=1e6 || abs(dinp) <=1e-5) return dbl2str(dinp);

  int p=0;
  double z;
  bool minus=false;
  if (dinp < 0){
    dinp = -1*dinp;
    minus = true;
  }

  if (dinp >=1000){
    while(true){
      p++;
      if ((dinp/pow(10.,int2dbl(p)))<10) break;
    }
    z = dinp/pow(10., int2dbl(p));
    if (!minus) return dbl2str(z) + "e+" + int2str(p); else return "-" + dbl2str(z) + "
        e+" + int2str(p);
  }

  p=0;
  if (dinp < 0.01){
    while(true){
      p++;
      if ((dinp * pow(10.,int2dbl(p))) > 1) break;
    }
    z = dinp * pow(10.,int2dbl(p));
    if (!minus) return dbl2str(z) + "e-" + int2str(p); else return "-" + dbl2str(z) + "
        e-" + int2str(p);
  }
```

```
}

string potenzlatex(string inp)
{
  string ret;
  inp = potenz(inp);

  string::size_type loc;

  loc = inp.find("e", 0);

  if(loc != string::npos){
    ret = inp.substr(0,loc-1) + "$\\cdot 10^{" + int2str(str2int(inp.substr(loc+1))) +
        "}$";
  }else{
    ret = inp;
  }

  return ret;

}
```

Appendix D

Commented Exemplary Gnuplot Script

```
# Gnuplot 4.0 script that produces a plot of fitted data
# for electron-impact excitation of Na(3s) to Na(3p)
# change terminal to postscript
  set terminal postscript eps enhanced "Helvetica" 10 landscape color
# filename of the output file
  set output "EXC_e-_3s_3p.eps"
# load start parameters from corresponding file
  load "EXC_e-_3s_3p.param"
# define analytic fitting function
  f(x) = A7*1E-16/x*(((x-d)/x)**A6)*(A1/((x/d)**0)+A2/((x/d)**1)+ \
    A3/((x/d)**2) + A4/((x/d)**3) + A5*log(x/d))
# fitting command
  fit f(x) "EXC_e-_3s_3p.csv" using 1:2:3 via A1, A2, A3, A4, A5, A6, A7
# size of the plot
  set size 1.0, 1.0
# define the plot title
# {/Symbol=24 \256} is a long arrow from left to right, see [106]
# {/=24 ...} sets the fontsize to 24
  set title '{/=24 e^- + Na(3s) {/Symbol=24 \256} e^- + Na(3p)}'
# set both axes to logarithmic scale
  set logscale xy
# define the location and the length of the symbols of the key
  set key graph 0.95, graph 0.97 samplen 2

# define the labels of the x- and the y-axis
  set xlabel "{/=18 Energy [eV]}"
  set ylabel "{/=18 Cross Section [cm^2]}"
# define the range of the x-axis
```

```
  set xrange [1:1e4]
# define the format of the axis inscriptions
  set format xy "10^{%T}"
# enlarge the data points
  set pointsize 2
# plot the fit and the used data
   plot f(x) linetype 1 linewidth 3 title "fit", \
     "EXC_e-_3s_3p.csv" using 1:2 index 00 with lines title "Bray 2006", \
     "EXC_e-_3s_3p.csv" using 1:2 index 01 with points title "Phelps, Lin 1981", \
     "EXC_e-_3s_3p.csv" using 1:2 index 02 with lines title "Kim 2001" , \
     "EXC_e-_3s_3p.csv" using 1:2 index 03 with points title "Zapesochnyi 1976" , \
     "EXC_e-_3s_3p.csv" using 1:2 index 04 with points title "Enemark, Gallagher 1972" , \
     "EXC_e-_3s_3p.csv" using 1:2 index 05 with points title "Moores, Norcross (2CC) 1972" , \
     "EXC_e-_3s_3p.csv" using 1:2 index 06 with points title "Moores, Norcross (4CC) 1972" , \
     "EXC_e-_3s_3p.csv" using 1:2 index 07 with points title "Karule 1970" , \
     "EXC_e-_3s_3p.csv" using 1:2 index 08 with lines title "Gould 1970" , \
     "EXC_e-_3s_3p.csv" using 1:2 index 09 with lines title "Mitroy 1987" , \
     "EXC_e-_3s_3p.csv" using 1:2 index 10 with points title "Buckman, Teubner 1979" , \
     "EXC_e-_3s_3p.csv" using 1:2 index 11 with points title "Srivastava, Vuskovic 1980"
# return to "normal" terminal
  set terminal x11
# set print output to the parameter file
  set print "EXC_e-_3s_3p.param"
# print the newly calculated fitting parameters to this file
  print "d = ", d
  print "A1 = ", A1
  print "A2 = ", A2
  print "A3 = ", A3
  print "A4 = ", A4
  print "A5 = ", A5
  print "A6 = ", A6
  print "A7 = ", A7
  print "t = ", t
# exit the script
  quit
```

Appendix E

Postscript Editing

The following steps need to be followed to manually change the postscript code to implement more than nine line styles.

1. Open the ∗.eps file in an ordinary text editor.
2. Find the definitions of the line styles. The default definition is the following:

   /LTw { PL [] 1 setgray } def
   /LTb { BL [] 0 0 0 DL } def
   /LTa { AL[1 udl mul 2 udl mul] 0 setdash 0 0 0 setrgbcolor } def
   /LT0 { PL [] 1 0 0 DL } def
   /LT1 { PL [4 dl 2 dl] 0 1 0 DL } def
   /LT2 { PL [2 dl 3 dl] 0 0 1 DL } def
   /LT3 { PL [1 dl 1.5 dl] 1 0 1 DL } def
   /LT4 { PL [5 dl 2 dl 1 dl 2 dl] 0 1 1 DL } def
   /LT5 { PL [4 dl 3 dl 1 dl 3 dl] 1 1 0 DL } def
   /LT6 { PL [2 dl 2 dl 2 dl 4 dl] 0 0 0 DL } def
   /LT7 { PL [2 dl 2 dl 2 dl 2 dl 2 dl 4 dl] 1 0.3 0 DL } def
   /LT8 { PL [2 dl 2 dl 2 dl 2 dl 2 dl 2 dl 2 dl 4 dl] 0.5 0.5 0.5 DL } def
3. Add the wanted linestyles. For example

   /LT9 {PL [1 dl 2 dl 3 dl ...] 1 0 0.5 DL } def

   /LT9: line no. [1 dl 2 dl 3 dl ...]: defines the pattern. 1 0 0.5: defines the line color

   The line's patters is defined within the squared brackets. The first number is the length of a line (1 being a dot). This is followed by "dl". The next number is the length of the gap, followed again by "dl" and then again by a number which defines the length of the next line. In that way, any arbitrary pattern can be constructed.
   The three numbers following the closing]-bracket define the line color in terms of RGB numbers. These numbers have values between 0 and 1. The first number defines the amount of red, the second the amount of green, and the third the amount of blue in the color. For example, 1 0 0 is red, 0 0 0 black, and 0 0 1 blue.
4. Find the data that should be plotted using the newly defined line styles. Much further down in the postscript text, lines like

   LT1
   LTb 3266 1499 M

[[(Helvetica) 120.0 0.0 true true 0 (Stumpf, Gallagher 1985)]

] -40.0 MRshow

LT1

occur. The name of the dataset is inside the round brackets (). In this example "Stumpf, Gallagher 1985". Find the right dataset and change the numbers after each of the two occurrences of "LT".

Bibliography

[1] Homepage of the ITER Project. online: http://www.iter.org.

[2] M. Reich: *A new diagnostic for ASDEX Upgrade edge ion temperatures by lithium-beam charge exchange recombination spectroscopy.* PhD Thesis. Ludwig-Maximilians-Universität München. 2004.

[3] Homepage of the Institut für Plasmaphysik of the Max-Planck-Gesellschaft. online: http://www.ipp.mpg.de.

[4] M. Schneider: Beiträge zur Untersuchung von Tokamak-Randschichtplasmen mittels aktiver Li-Atomstrahlen. Master Thesis. Technische Universität Wien. 1990.

[5] F. Aumayr, H. Winter: Plasmadiagnostik mit Lithiumatomstrahl aktivierter Umladungsspektroskopie. *Ann. d. Physik.* 1985. Vol.42, p.228–238.

[6] R.P. Schorn, E. Hintz, D. Rusbüldt, F. Aumayr, M. Schneider, E. Unterreiter, H. Winter: Absolute concentrations of light impurity ions in tokamak discharges measured with Lithium beam-activated charge exchange spectroscopy. *J. Appl. Phys. B.* 1991. Vol.52, p.71–78.

[7] F. Aumayr, R.P. Schorn, M. Pöckl, J. Schweinzer, E. Wolfrum, K. McCormick, E. Hintz, H. Winter: Tokamak edge plasma densities measured by means of active Lithium beam diagnostics. *J. Nucl. Mat.*. 1992. Vol.196-198, p.928–932.

[8] R.P. Schorn, E. Wolfrum, F. Aumayr, E. Hintz, D. Rusbüldt, H. Winter: Radial temperature distributions of C6+ - ions in the TEXTOR edge plasma measured with Li-CXS. *Nuclear Fusion.* 1992. Vol.32, p.351–359.

[9] J. Schweinzer, E. Wolfrum, F. Aumayr, M. Pöckl, H. Winter, R.P. Schorn, E. Hintz, A. Unterreiter: Reconstruction of plasma edge density profiles from LiI(2s-2p) emission profiles. *Plasma Physics and Controlled Fusion.* 1992. Vol.34, p.1173–1183.

[10] E. Wolfrum, F. Aumayr, D. Wutte, HP. Winter, E. Hintz, D. Rusbüldt, R.P. Schorn: Fast lithium - beam spectroscopy of tokamak edge plasmas. *Rev. Sc. Instr.*. 1993. Vol.64, p.2285–2292.

[11] R. Brandenburg, J. Schweinzer, S. Fiedler, F. Aumayr, HP. Winter: Modelling of fast neutral Li beams for fusion edge plasma diagnostics. *Plasma Physics and Controlled Fusion*. 1999. Vol.41, p.471–484.

[12] S. Fiedler, R. Brandenburg, J. Baldzuhn, K. McCormick, F. Aumayr, J. Schweinzer, HP. Winter, W7AS & ASDEX Upgrade team: Edge Plasma Diagnostics on W7-AS and ASDEX Upgrade using fast Li Beams. *J. Nucl. Mat.*. 1999. Vol.266–269, p.1279–1284.

[13] M. Proschek: *Towards fast He beam edge plasma diagnostics*. PhD Thesis. Technische Universität Wien. 2001.

[14] S. Menhart: *On the applicability of fast neutral He beams for fusion plasma diagnostics*. PhD Thesis. Technische Universität Wien. 2000.

[15] E. Galutschek: *Development of a 14.5 GHz All-Permanent Magnet Multicharged ECR Ion Source for Remote Operation*. PhD Thesis. Technische Universität Wien. 2005.

[16] H. D. Falter, M. Proschek, S. Menhart, et al.: Helium doped hydrogen or deuterium beam as cost effective and simple tool for plasma spectroscopy. *Rev. Sc. Instr.*. 2000. Vol.71, p.3723–3727.

[17] H.-D. Falter, M. Proschek, S. Menhart, F. Aumayr, HP.Winter, D. A. Dines, D. Godden, T.C.Jones: Helium doped hydrogen or deuterium beam as cost effective and simple tool for plasma spectroscopy. *Fusion Engineering & Design*. 2001. Vol.56–57, p.941–946.

[18] S. Menhart, M. Proschek, H.-D. Falter, et al.: Explorative studies for the development of fast He beam diagnostics. *J. Nucl. Mat.*. 2001. Vol.290–293, p.673–677.

[19] J.O. Phelps, C.C. Lin: Electron-impact excitation of the sodium atom. *Phys. Rev. A*. 1981. Vol.24, p.1299–1326.

[20] F. Aumayr, D. Bridi, A. El-Said, et al.: Edge Plasma Diagnostics and Modelling. Annual EURATOM Report. 2006.

[21] Thomas Williams, Colin Kelley: gnuplot 4.0. online: http://www.gnuplot.info. 1986 - 1993, 1998, 2004.

[22] H. Goldstein: *Klassische Mechanik*. Akademische Verlagsgemeinschaft, Frankfurt am Main. 1963.

[23] K.R. Symon: *Mechanics*. Addison-WeslePublishingng Company. 1971.

[24] J. Mitroy, I.E. McCarthy, A.T. Selbovics: Electron scattering from sodium at intermediate energies. *J. Phys. B: At. Mol. Phys.*. 1987. Vol.20, p.4827–4850.

[25] AMBDAS - Atomic and Molecular Bibliographical Database. online: http://www-amdis.iaea.org/AMBDAS/.

[26] Google Scholar. online: http://scholar.google.com.

[27] Igor Bray, Andris T. Stelbovics: Convergent close-coupling calculations of electron-hydrogen scattering. *Phys. Rev. A*. 1992. Vol.46, p.6995–7011.

[28] I. Bray, A.T. Stelbovics: Explicit Demonstration of the Convergence of the Close-Coupling Method for a Coulomb Three-Body Problem. *Phys. Rev. Lett.*. 1992. Vol.69, p.53–56.

[29] I.C. Percival, M.J. Seaton: Partial wave theory of electron - hydrogen atom collisions. *Proc. Philosophical Soc. Cambridge*. 1957. Vol.53, p.654.

[30] J. Schweinzer: *Ein- und Zweielektronenprozesse beim Einelektroneneinfang von Alkaliatomen in doppelt geladene Edelgasionen*. PhD Thesis. Technische Universität Wien. 1990.

[31] J. Schweinzer, H. Winter: Single electron capture from alkali atoms by slow doubly charged ions: I. He^{2+} (0.5–6 keV)–Li, Na, K – one-electron processes. *J. Phys. B: At. Mol. Phys.*. 1990. Vol.23, p.3881–3898.

[32] A.N. Perumal, D.N. Tripathi: Charge Transfer and Ionization in Proton-Alkali Atoms Collisions with and without Electric Field. *J. Phys. Soc. of Japan*. 1997. Vol.66, p.3783–3789.

[33] H.S.W. Massey, R.A. Smith: The Passage of Positive Ions through Gases. *Proc. Royal Soc. London, Series A*. 1933. Vol.142, p.142–172.

[34] A. Jain, T.G. Winter: Electron transfer, target excitation, and ionization in H^++Na(3s) and H^++Na(3p) collisions in the coupled-Sturmian-pseudostate approach. *Phys. Rev. A*. 1995. Vol.51, p.2963–2973.

[35] A.E.S. Green, D.L. Sellin, A.S. Zachor: Analytic Independent-Particle Model for Atoms. *Phys. Rev.*. 1969. Vol.184, p.1–9.

[36] R. Shingal, B.H. Bransden, A.M. Ermolaev, D.R. Flower, C.W. Newby, C.J. Noble: Charge transfer in H^+-Na^0 collisions: atomic orbital calculations. *J. Phys. B: At. Mol. Phys.*. 1986. Vol.19, p.309 – 320.

[37] J. Burgdörfer, R. Morgenstern, A. Niehaus: Angular momentum distribution in the classical over-barrier model for electron capture into highly charged slow projectiles. *J. Phys. B: At. Mol. Phys.*. 1986. Vol.19, p.L507–L513.

[38] William H. Press: *Numerical recipes in C - the art of scientific computing*. ch. 15.5, p.681–688. Cambridge University Press. 1992.

[39] S. Verma, R. Srivastava: Electron impact excitation of the 3^2D states of lithium, sodium and potassium atoms. *J. Phys. B: At. Mol. Phys.*. 1996. Vol.29, p.3215–3234.

[40] C.E. Theodosiou: Theoretical verification of the differences between excitation of Na $3p$ and Na $3d$ by H^+ and H^- impact. *Phys. Rev. A*. 1988. Vol.38, p.4923–4926.

[41] N. Rakštikas, A. Kupliauskienė: The Influence of Valence Electron State on the 2p Ionization of Atomic Sodium by Electrons. *Physica Scripta*. 2001. Vol.64, p.230–236.

[42] A. Messiah: *Quantenmechanik*. de Gruyter. 1990.

[43] Constantine E. Theodosiou: Excitation of atomic hydrogen by protons and helium ions. *Phys. Rev. A*. 1980. Vol.22, p.2556–2571.

[44] F. Aumayr, M. Fehringer, H. Winter: Inelastic H^+–Li(2s) collisions (2–20kev): I. Experimental methods and Li(2p) excitation. *J. Phys. B: At. Mol. Phys.*. 1984. Vol.17, p.4185–4199.

[45] S.K. Srivastava, L. Vušković: Elastic and inelastic scattering of electrons by Na. *J. Phys. B: At. Mol. Phys.*. 1980. Vol.13, p.2633–2643.

[46] A.M. Howald, R.E. Miers, J.S. Allen, L.W. Anderson, C.C. Lin: Excitation of the Na(3p) level by H^+, H_2^+, or H_3^+ ions. *Physics Letters A*. 1982. Vol.92A, p.328.

[47] B. Stumpf, A. Gallagher: Electron excitation of Na(3S) and Na(3P) atoms to the Na(3D) state. *Phys. Rev. A*. 1985. Vol.32, p.3344–3353.

[48] E.A. Enemark, A. Gallagher: Electron Excitation of the Sodium D Lines. *Phys. Rev. A*. 1972. Vol.6, p.192–205.

[49] I.P. Zapesochnyi, L.L. Shimon: Effective excitation cross sections of alkali metal atoms colliding with slow electrons. II - Potassium. *Opt. i Spektroskopiya*. 1965. Vol.19, p.480–484.

[50] E.M. Karule, R.K. Peterkop: in: V.Ya. Veldre (ed.): *Atomic Collisions* . Vol.3, p.3. Akademiya Nauk Latvovskoi SSR Institute Fizika, Riga. 1965.

[51] P.S. Ganas: Excitation of sodium atoms by electron impact. *J. Appl. Phys.*. 1985. Vol.57, p.154–156.

[52] H. Bethe: The theory of the passage of rapid neutron radiation through matter. *Ann. d. Phys.*. 1930. Vol.5, p.325-400.

[53] I.P Zapesochnyi, E.N. Postoi, I.S. Aleksakhin: *Sov. Phys. JETP*. 1976. Vol.41, p.865.

[54] A.R. Johnston, P.D. Burrow: Electron-impact ionization of Na. *Phys. Rev. A*. 1995. Vol.51, p.R1735–R1737.

[55] Y.-K. Kim: Scaling of plane-wave Born cross sections for electron-impact excitation of neutral atoms. *Phys. Rev. A*. 2001. Vol.64, p.032713.

[56] E.J. McGuire: Inelastic Scattering of Electrons and Protons by the Elements He to Na. *Phys. Rev. A*. 1971. Vol.3, p.267–279.

[57] A. Burgess, J.A. Tully: On the Bethe approximation. *J. Phys. B: At. Mol. Phys.*. 1978. Vol.11, p.4271–4282.

[58] E.J. McGuire: Systematics of *ns* subshell electron ionization cross sections. *J. Phys. B: At. Mol. Phys.*. 1997. Vol.30, p.1563–1587.

[59] S.J. Buckman, P.J.O. Teubner: Differential cross sections for the electron impact excitation of the $3^2P_{1/2,3/2}$ resonance levels of sodium. *J. Phys. B: At. Mol. Phys.*. 1979. Vol.12, p.1741–1750.

[60] D.L. Moores, D.W. Norcross: The scattering of electrons by sodium atoms. *J. Phys. B: At. Mol. Phys.*. 1972. Vol.5, p.1482–1505.

[61] G. Gould: *Atomic beam measurements of some sodium excitation functions.* PhD Thesis. University of New South Wales. 1970.

[62] K. Omidvar, H.L. Kyle, E.C. Sullivan: Ionization of Multielectron Atoms by Fast Charged Particles. *Phys. Rev. A*. 1972. Vol.5, p.1174–1187.

[63] D.R. Bates, A.H. Boyd, S.S. Prasad: Impact ionization of sodium. *Proc. Phys. Soc. London.* 1965. Vol.85, p.1121–1126.

[64] W.S. Tan, Z. Shi, C.H. Ying, Vušković: Electron-impact ionization of laser-excited sodium atom. *Phys. Rev. A*. 1996. Vol.54, p.R3710–R3713.

[65] I.P. Zapesochnyi, I.S. Aleksakhin: Ionization of alkali-metal atoms by slow electrons. *Zh. Eksp. Teor. Fiz.*. 1968. Vol.55, p.76–85.

[66] R.J. Allan: Charge transfer in H^+ - Na^0 collisions: molecular orbital calculations. *J. Phys. B: At. Mol. Phys.*. 1986. Vol.19, p.321-334.

[67] R.W. McCullough: unpublished results quoted by Kubach, Sidis (1981). 1978.

[68] F. Aumayr, G. Lakits, H. Winter: Charge transfer and target excitation in H^+-Na(3s) collisions ($2 - 20$ keV). *J. Phys. B: At. Mol. Phys.*. 1987. Vol.20, p.2025–2030.

[69] G.V. Avakov, L.D. Blokhintsev, A.S. Kadyrov, A.M. Mukhamedzhanov: Electron capture in proton collisions with alkalatomsos as a three-body problem. *J. Phys. B: At. Mol. Phys.*. 1992. Vol.25, p.213–219.

[70] R.N. Il'in, V.A. Oparin, E.S. Solov'ev, N.V. Fedorenko: Charge transfer of protons in alkali metal vapors with the formation of highly excited hydrogren atoms. *Zh. Tekh. Fiz.*. 1966. Vol.36, p.1241–1250.

[71] K. Basu Choudhury, D.P. Sural: Electron capture in ground and excited states in proton-alkali-metal-atom collisions. *J. Phys. B: At. Mol. Phys.*. 1992. Vol.25, p.853–867.

[72] K. Basu Choudhury, D.P. Sural: *Ind. J. Phys. B*. 1983. Vol.57, p.20.

[73] R. Daniele, G. Ferrante, E. Fiordilino: *Nuovo Cimento B*. 1979. Vol.54, p.185.

[74] R.D. DuBois: Charge transfer leading to multiple ionization of neon, sodium, and magnesium. *Phys. Rev. A*. 1986. Vol.34, p.2738–2745.

[75] R.D. DuBois, L.H. Toburen: Electron capture by protons and helium ions from lithium, sodium, and magnesium. *Phys. Rev. A*. 1985. Vol.31, p.3603–3611.

[76] C.F. Barnett, J.A. Ray, E. Ricci, M.I. Wilker, E.W. McDaniel, E.W. Thomas, H.B. Gilbody: Report No. ORNL-5206. *Oak Ridge National Laboratory*. 1977. Vol.1. unpublished; tabulated data prior to 1977.

[77] F. Ebel, E. Salzborn: Charge transfer of $0.2 - 5.0$ keV protons and hydrogen atoms in sodium-, potassium- and rubidium-vapour targets. *J. Phys. B: At. Mol. Phys.*. 1987. Vol.20, p.4531–4542.

[78] C. Kubach, V. Sidis: Theoretical study of near-resonant charge-exchange collisions of H^+ with alkali atoms. *Phys. Rev. A*. 1981. Vol.23, p.110–118.

[79] M. Kimura, R.E. Olson, J. Pascale: Molecular treatment of electron capture by protons from ground and excited states of alkali-metal atoms. *Phys. Rev. A*. 1982. Vol.26, p.3113–3124.

[80] A.M. Ermolaev: Charge transfer in collisions between protons and lithium atoms. *J. Phys. B: At. Mol. Phys.*. 1984. Vol.17, p.1069–1082.

[81] W. Fritsch: Atomic-basis study of electron transfer in H^+ + Na and H^+ + K collisions. *Phys. Rev. A*. 1984. Vol.30, p.1135–1138.

[82] W. Grüebler, P.A. Schmelzbach, V. König, P. Marmier: Charge Exchange Collisions between Hydrogen Ions and Alkali Vapour in the Energy Range of 1 to 20 keV. *Helv. Phys. Acta*. 1970. Vol.43, p.254–270.

[83] C.J. Anderson, A.M. Howald, L.W. Anderson: Charge transfer cross sections and equilibrium fractions for 1–25 keV H^+ ions incident of a Na vapor target. *Nucl. Instrum. Meth.*. 1979. Vol.165, p.583–587.

[84] J.S. Allen, L.W. Anderson, C.C. Lin: Cross section for excitation of sodium by impact of H^+, H_2^+, H_3^+, and H^- ions. *Phys. Rev. A*. 1988. Vol.37, p.349–355.

[85] W. Fritsch: Theoretical study of Na excitation and ionization in H^+ + Na collisions. *Phys. Rev. A*. 1987. Vol.35, p.2342–2344.

[86] W. Jitschin, S. Osimitsch, D.W. Mueller, H. Reihl, R.J.Allan, O. Schöller, H.O. Lutz: Excitation of the Na 3p state by proton impact. *J. Phys. B: At. Mol. Phys.*. 1986. Vol.19, p.2299–2309.

[87] C.J. Lundy, R.E. Olson: A classical analysis of proton collisions with ground-state and excited, aligned sodium targets. *J. Phys. B: At. Mol. Phys.*. 1996. Vol.29, p.1723–1736.

[88] T. Nagata: Charge Changing Collisions of Atomic Beams in Alkali-Metal Vapors. IV. Total Cross Sections for Single-Electron Capture by H^+ Ion and H(1s) Atom. *J. Phys. Soc. of Japan*. 1980. Vol.48, p.2068 – 2075.

[89] B.G. O'Hare, R.W. McCullough, H.B. Gilbody: Ionization of sodium and potassium vapour by $20 - 100$ keV H^+ and He^+ ions. *J. Phys. B: At. Mol. Phys.*. 1975. Vol.8, p.2968–2978.

[90] J.D. Garcia, E. Gerjuoy, J.E. Welker: Classical Approximation of Ionization by Proton Impact. *Phys. Rev.*. 1968. Vol.165, p.66–71.

[91] D.R. Bates, A.E. Kingston: Vol.6, p.269. Academic Press New York. 1970.

[92] F. Sattin: Further study of the over-barrier model to compute charge-exchange processes. *Phys. Rev. A*. 2001. Vol.64, p.034704.

[93] J. W. Thomsen, N. Andersen, D. Dowek, et al.: Orbital alignment dependence of electron transfer cross sections. *Z. Phys. D*. 1996. Vol.37, p.133–139.

[94] R. Shingal, B.H. Bransden: Charge transfer, target excitation and ionisation in H^+ + Na(3s) collisions. *J. Phys. B: At. Mol. Phys.*. 1987. Vol.20, p.4815–4825.

[95] L.W. Anderson, J.S. Allen, C.C. Lin, R.E. Miers: in: M.J. Coggiola al. (ed.): *Proc. 14th Int. Conf. on Physics of Electronic and Atomic Collisions* . , p.385. North Holland, Amsterdam. 1985.

[96] A.N. Tripathi, K.C. Mathur, S.K. Joshi: Impact ionization of Na, K, Rb and Cs by electron and proton impacts. *J. Phys. B: At. Mol. Phys.*. 1969. Vol.2, p.155-158.

[97] M. Gryziski: Classical Theory of Electronic and Ionic Inelastic Collisions. *Phys. Rev.*. 1959. Vol.115, p.374–383.

[98] D. Wutte, R.K. Janev, F. Aumayr, M. Schneider, J. Schweinzer, J.J. Smith, HP. Winter: Cross Sections for Collision Processes of Li Atoms Interacting With Electrons, Protons, Multiply Charged Ions, And Hydrogen Molecules. *Atomic Data & Nuclear Data Tables*. 1997. Vol.65, p.155–180. Article No. DT970736.

[99] J. Schweinzer, R. Brandenburg, I. Bray, R. Hoekstra, F. Aumayr, R.K. Janev, HP. Winter: Database for Inelastic Collisions of Lithium Atoms With Electrons, Protons, And Multiply Charged Ions. *Atomic Data & Nuclear Data Tables*. 1999. Vol.72, p.239–273. Article ID adnd. 1999.0815.

[100] W. Lotz: Electron-Impact Ionization Cross-Sections and Ionization Rate Coefficients for Atoms and Ions from Hydrogen to Calcium. *Zeitschrift für Physik*. 1968. Vol.216, p.241–247.

[101] W. Lotz: Subshell Binding Energies of Atoms and Ions from Hydrogen to Zinc. *J. Opt. Soc. Am.*. 1968. Vol.58, p.915–921.

[102] J. Schweinzer: Atomic-Orbital Close-Coupling Calculations of Proton-Impact Cross Sections. Private communication. 2006.

[103] Thomas Williams, Colin Kelley: *gnuplot - An Interactive Plotting Program*. 2004.

[104] R.K. Janev: Unified cross section scaling for electron capture from excited hydrogen atoms by multicharged ions. *Physics Letters A*. 1991. Vol.160.

[105] J. Schweinzer, D. Wutte, H.P. Winter: A study of electron capture and excitation processes in collisions of multiply charged ions with lithium atoms. *J. Phys. B: At. Mol. Phys.*. 1994. Vol.27, p.137–153.

[106] David Denholm, Matt Heffron, Dick Crawford: *Syntax for postscript enhanced option*. ps_guide.ps.

Acknowledgements

I like to dedicate this thesis to the memory of Prof. Dr. Hannspeter Winter. With his support and connections to fusion research groups he provided an excellent initial position for first my project work and then my diploma thesis. His sudden and unexpected death was an incredible loss.

My special thanks belong to Prof. Dr. Friedrich Aumayr for his continuous support of my diploma work. Without his knowledge on all matters surrounding the topic and without his expertise in evaluating the credibility of the collected cross section data this whole thesis would not have been possible.

Furthermore, I'd like to thank Mag. Dorian Bridi for two years of collaboration and common problem solving. Due to his enormous effort, I was lucky to get the best working infrastructure.

Dr. Josef Schweinzer was a great help assisting me via e-mail and several meetings. His atomic-orbital calculations improved the quality of the database to an enormous degree. He also made the connection to Prof. Dr. Igor Bray of the Murdoch University, Australia, who calculated the electron-impact cross sections.

My parents and my sister deserve great thanks for the incredible support throughout my studies. What started with supporting my decision to study in Vienna in every way resulted in proof-reading my thesis and giving many great and useful remarks.

My friends Hannah Satlow, Kristin Nickel, and Johannes Feist all made their very own contributions. Hannah with her continuous support, pushing me further whenever I caved, for "dona nobis pacem" and for keeping my social life alive. Kristin who could not be stopped by the very late hours and proofread my introduction nevertheless. Johannes who would always have an open ear for all kinds of problems and who made the suggestion to use `kubuntu` as opperating system which proved to be an excellent choice.

Last but not least, I want to give my thanks to stella, lilla, and stora, my computers. They worked properly through all heights and depths without recking my nerves too often.